XIII Workshop di Geofisica
e
IV Giornata di Formazione

Fondazione Museo Civico di Rovereto

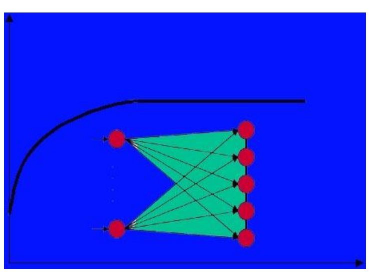
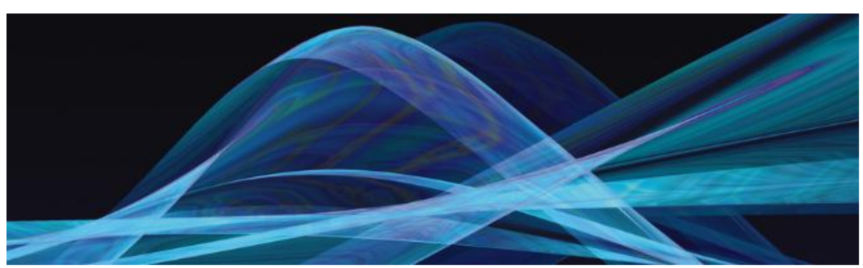
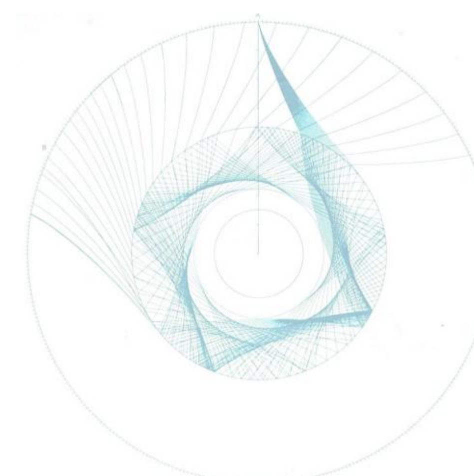

GeoNeurale

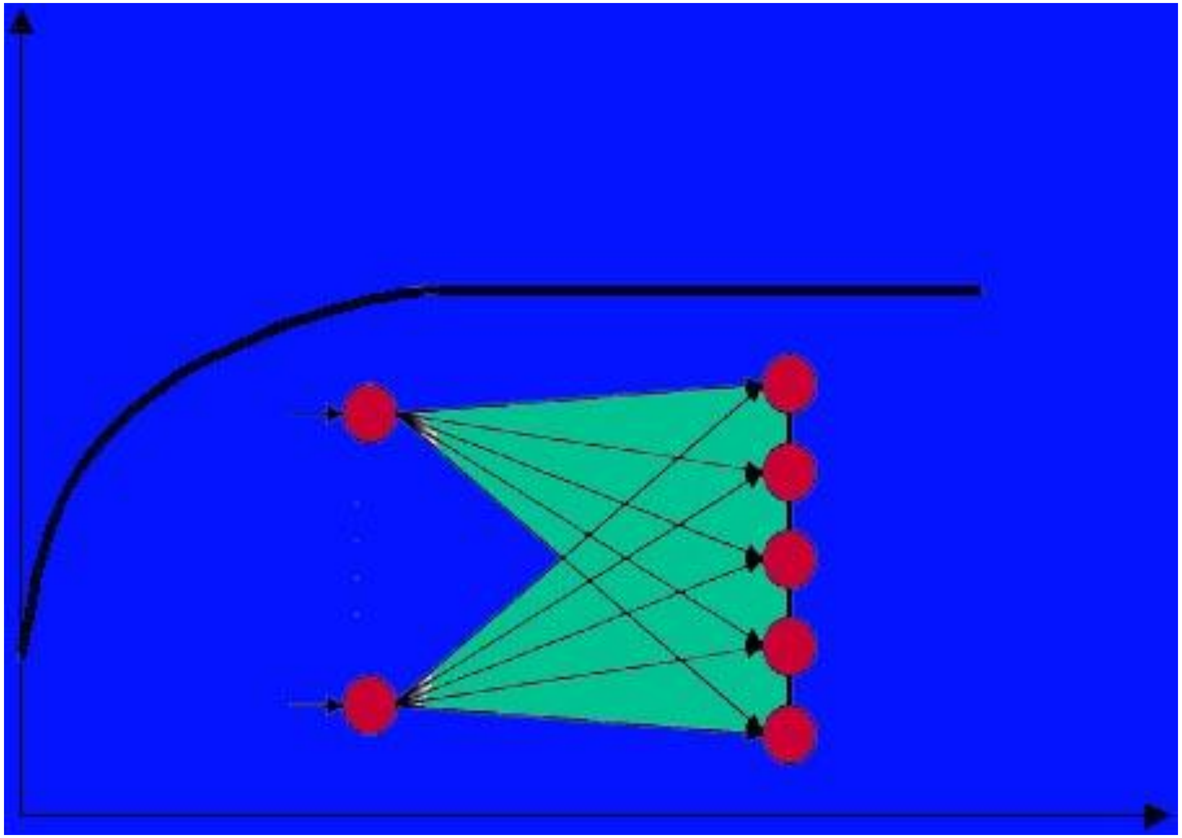

Wavefields

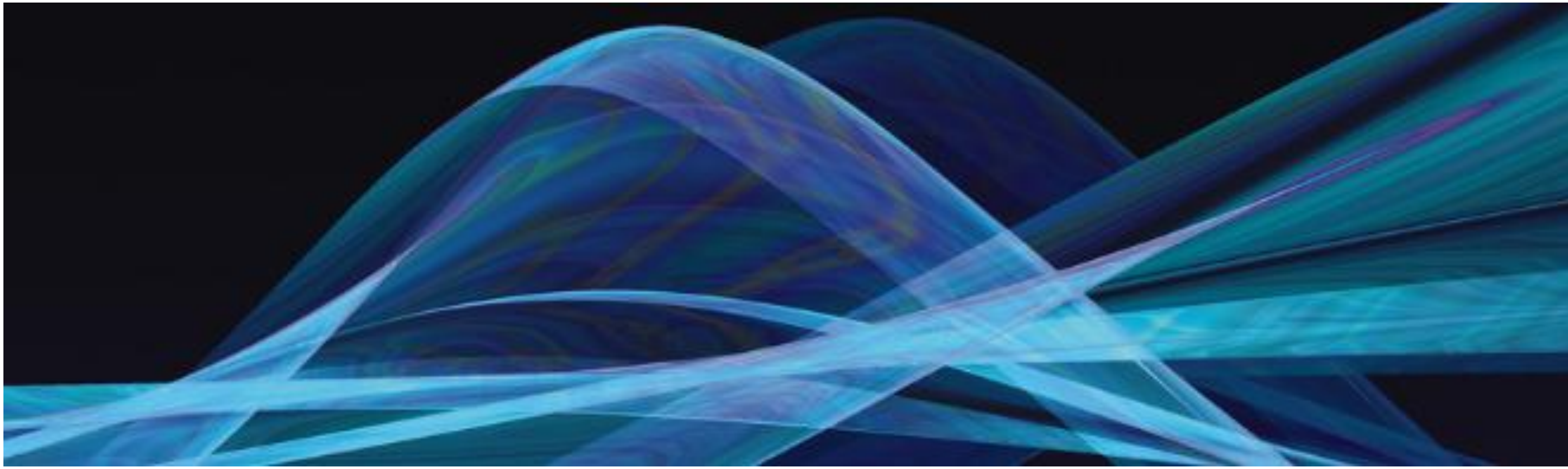

Petrophysic-Consultants

Geosystems Engineering

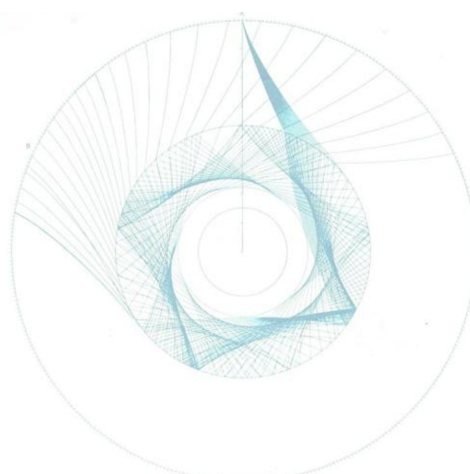

DALL’ESPLORAZIONE GEOTERMICA IN BAVIERA (CASE STUDY DI FATTIBILITA´ IN KOENIGSDORF) ALLE POTENZIALITA´ DI SVILUPPO DELLA GEOTERMIA PROFONDA IN ITALIA

Angelo Piasentin
GeoNeurale/Wavefields

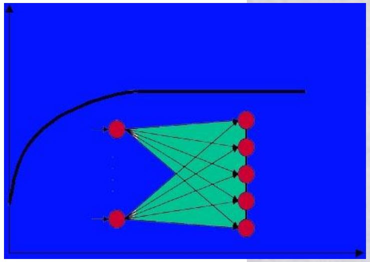

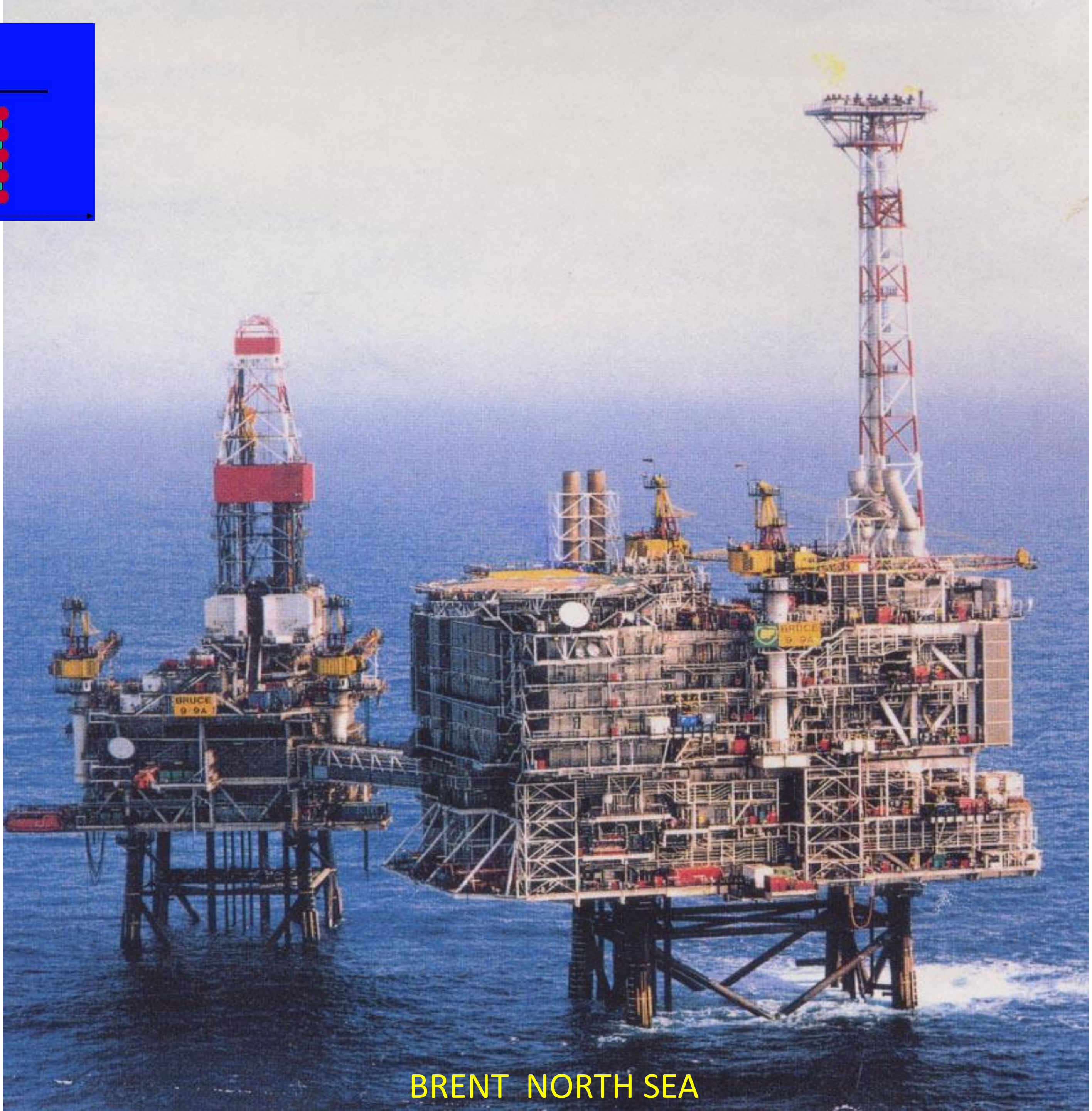
BRUCE
9-9A
BRENT NORTH SEA

WYTCH FARM

The longest ''Extended-Reach Drilling'' well worldwide MD > 11 Km

(Dorset – Poole Harbous, England)

The field sits near a nature preserve and is in an area of outstanding natural beauty

WYTCH FARM

COMPARISON : Conventional Directional DRILLING (CDD) – ERD
95⁄8-in. casing to a departure beyond 8000 m (Casing flotation technology)

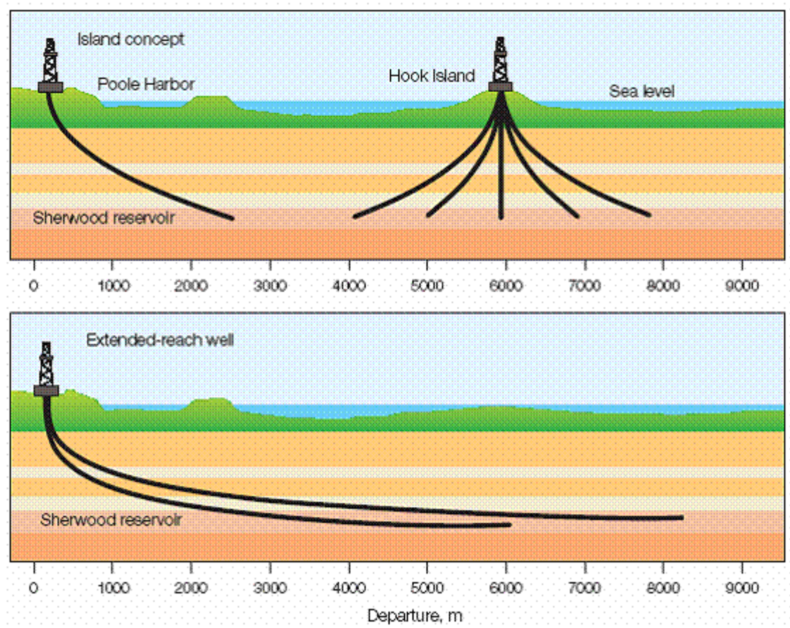

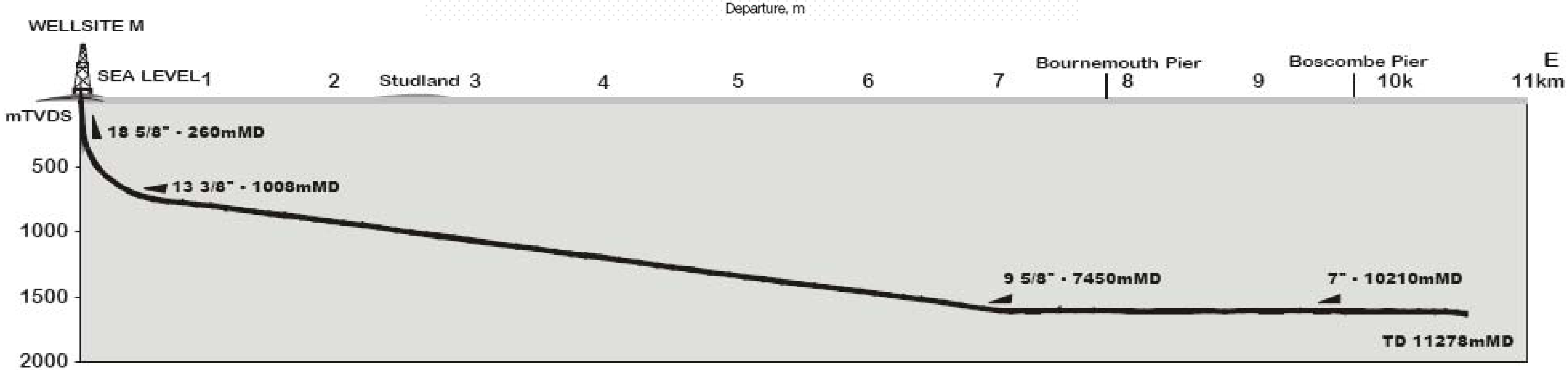

M16 Well Trajectory

TEST RIG AT HALLIBURTON

Halliburton – Dallas Research Rig - Downhole log tools testing facility

FIRST GEOSTEERING PROJECTS – SOLTAU GERMANY

Horizontal Drilling

EWR Resistivity Navigation – Forward Modeling

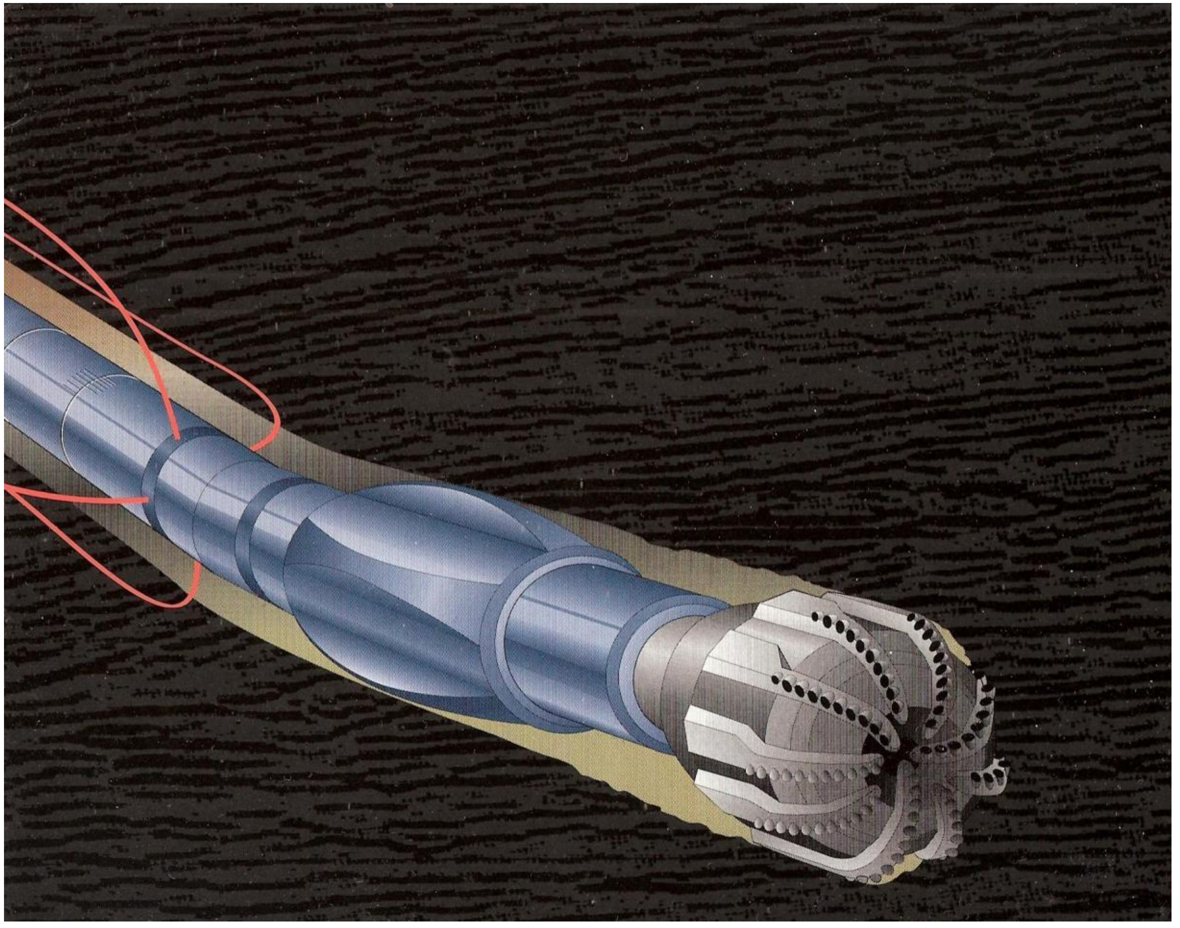

MWD / LWD STEERABLE SYSTEMS – T LOG , P LOG

GeoNeurale / Wavefields

THE FIRST ADVANCED SCHOOL FOR OIL EXPLORATION SCIENCES IN GERMANY (PETROPHYSICS, 3D SEISMIC, MULTICOMPONENT SEISMIC, GEOSTATISTICS)

THE FIRST SEISMIC PROCESSING LAB IN BAVARIA

THE FIRST MULTICOMPONENT SEISMIC INVERSION LAB IN BAVARIA

EXPLORATION OPERATIONS – PETROPHYSICS / GEOMECHANICS RESEARCH

(Schlumberger, Halliburton, Baker-Hughes, TerraTek

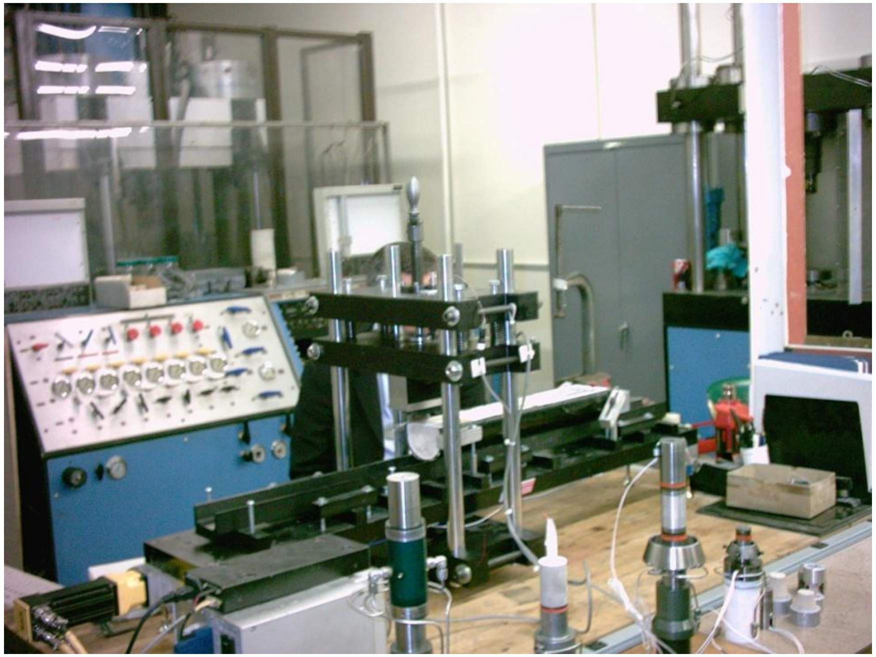

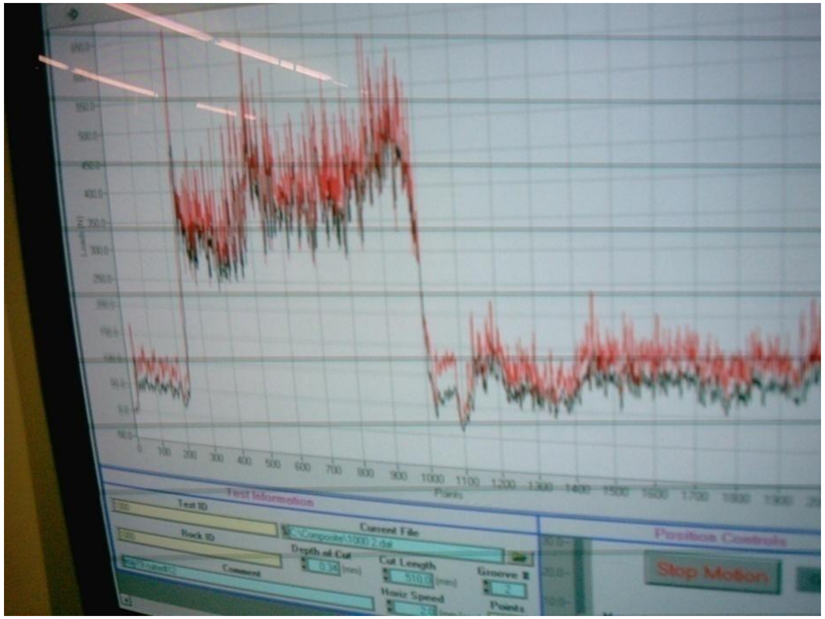

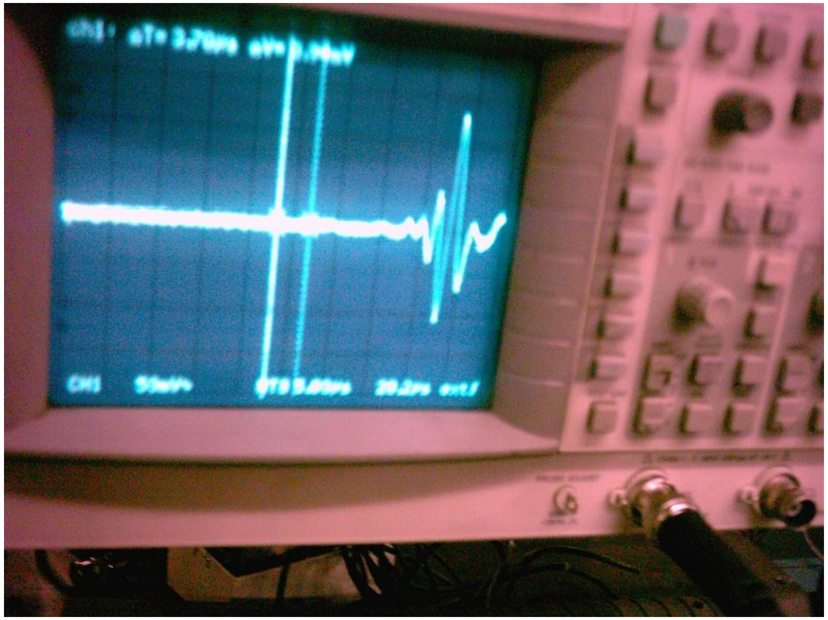

DRILLING DYNAMICS - REALTIME MECHANICAL EFFICIENCY

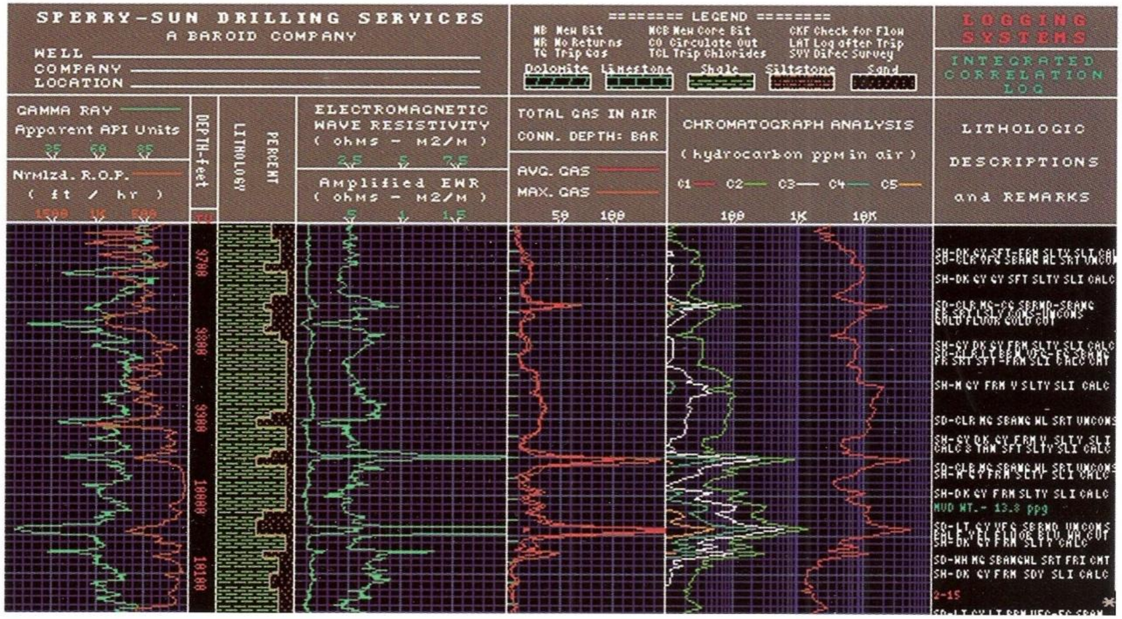

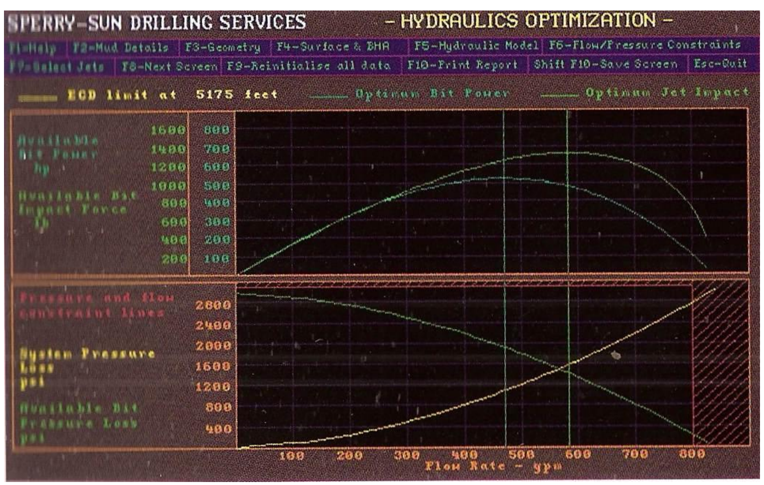

OUTPUT PROGRAMS PROCESS-DIAGNOSTICS ´´HYDRAULICS´´

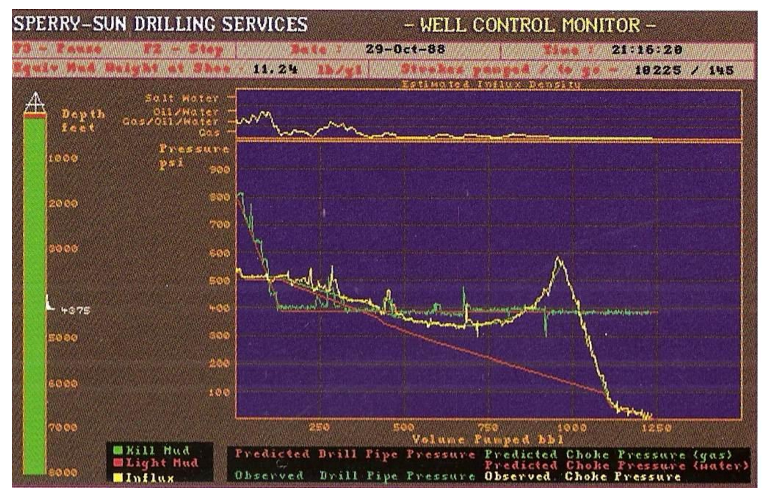

OUTPUT PROGRAMS PROCESS-DIAGNOSTICS ´´KILL MONITOR´´

REALTIME PETROPHYSICS

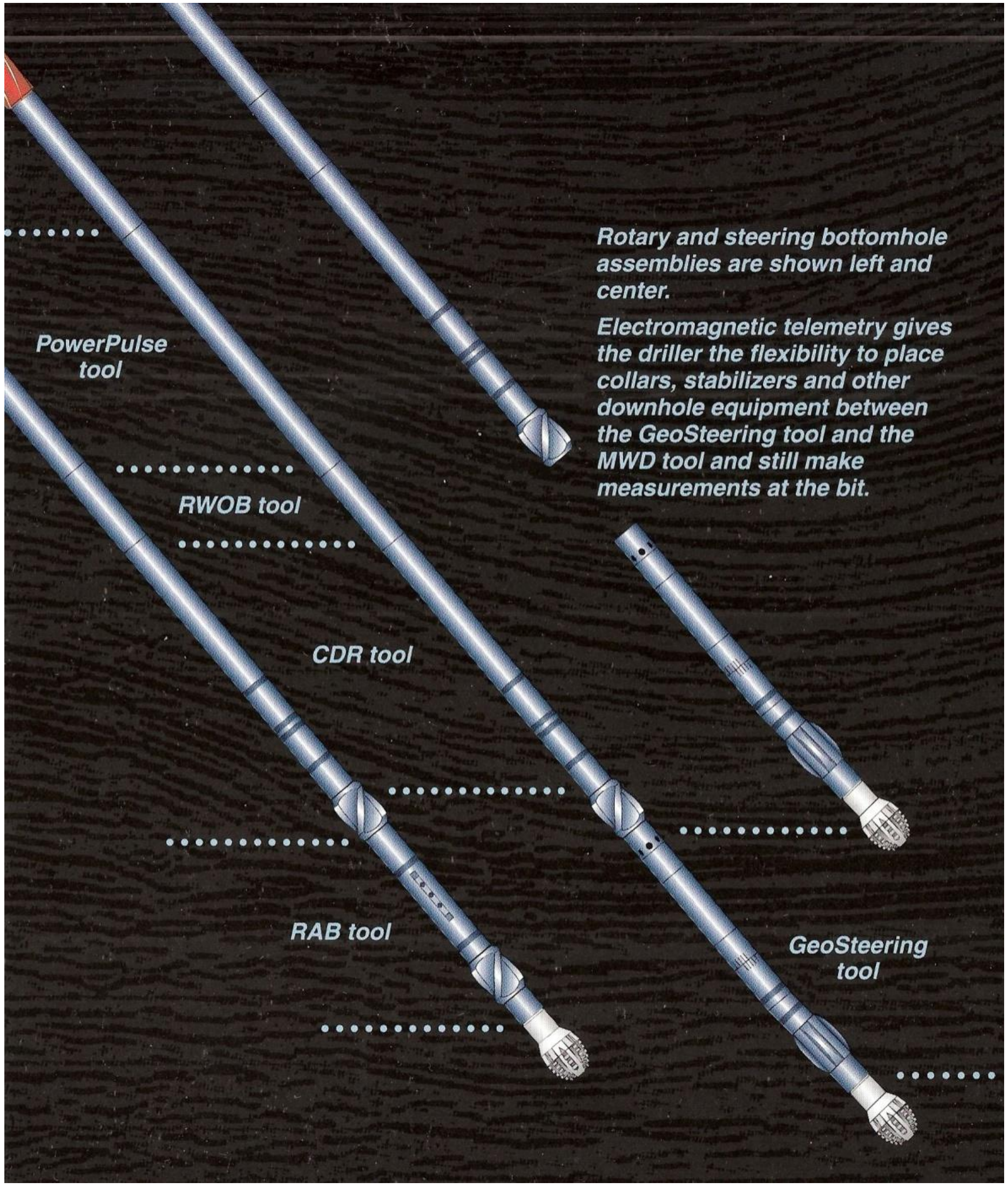

MWD / LWD ASSEMBLY

CDR – CDN – DIPOLE/DIPOLE SONIC
Realtime Log Interpretation

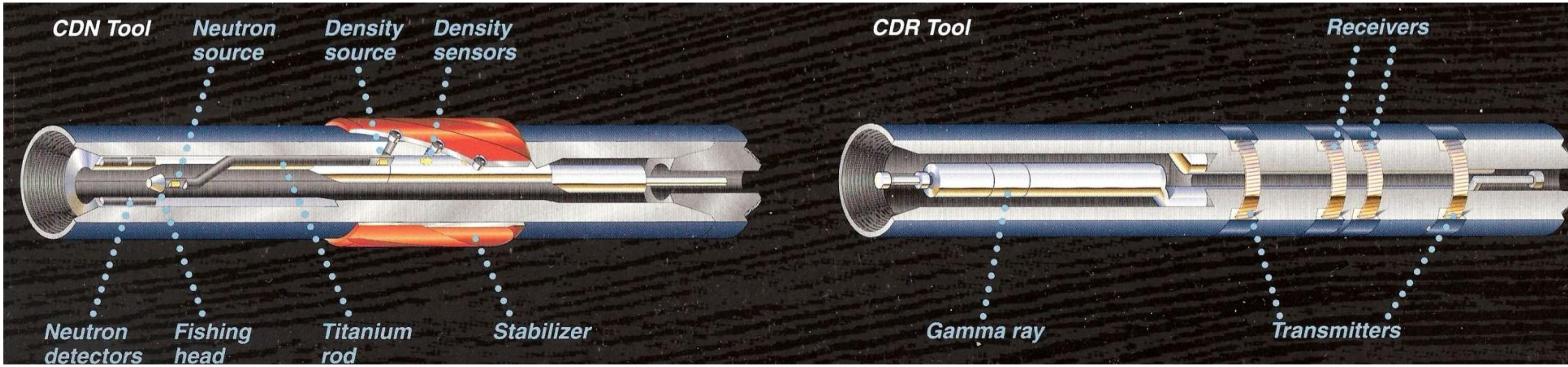

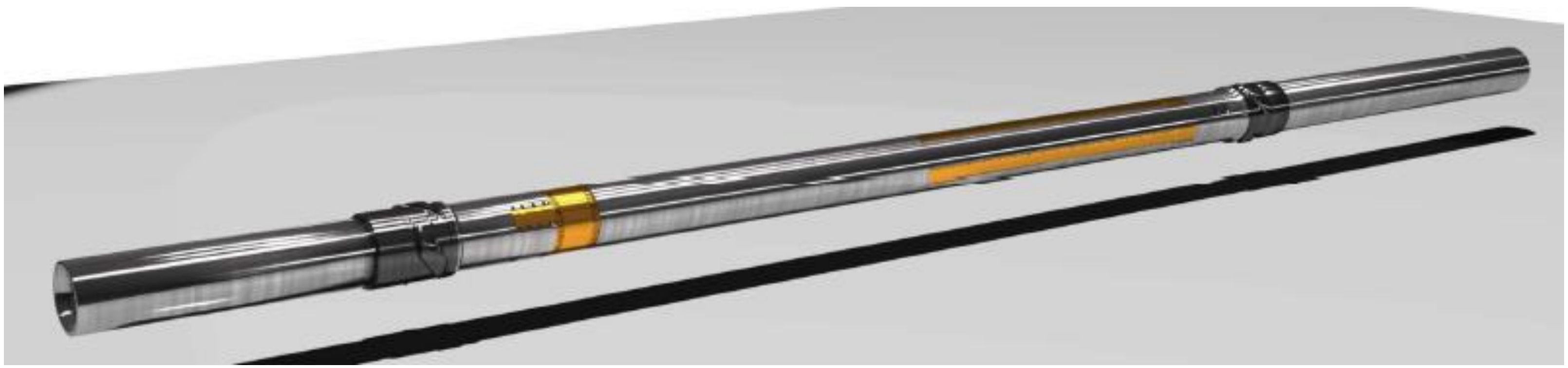

MWD / LWD SYSTEMS : TRIPLE COMBO ASSY

Dipole-Dipole Sonic P-S Waves, S-Polarization, Elastic Parameters
Gamma-Gamma (Electron-Density)
Neutron-Gamma (Hydrogen-Index)
Electromagnetic Resistivity (Amplitude, Phase Delay)
Natural Gammay Ray (Clay Index)

Petrophysics

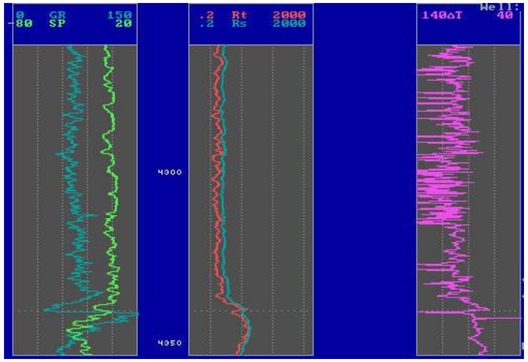

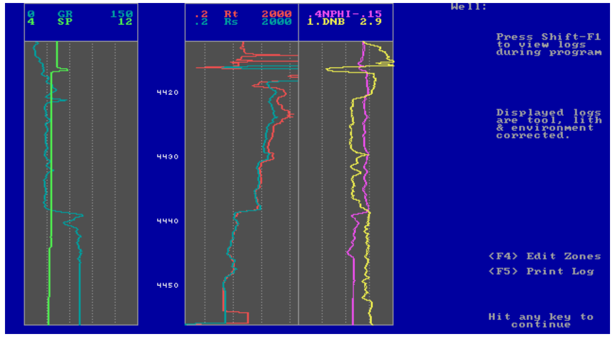

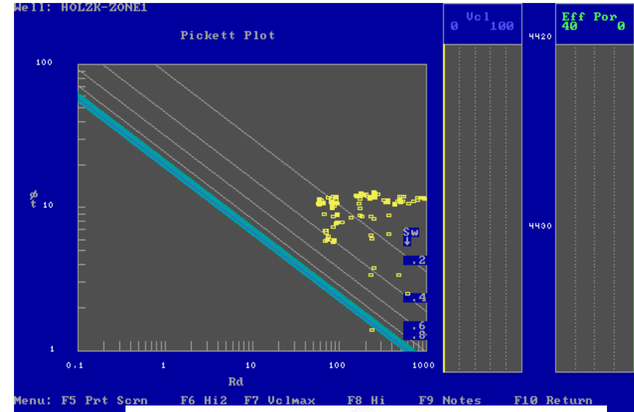

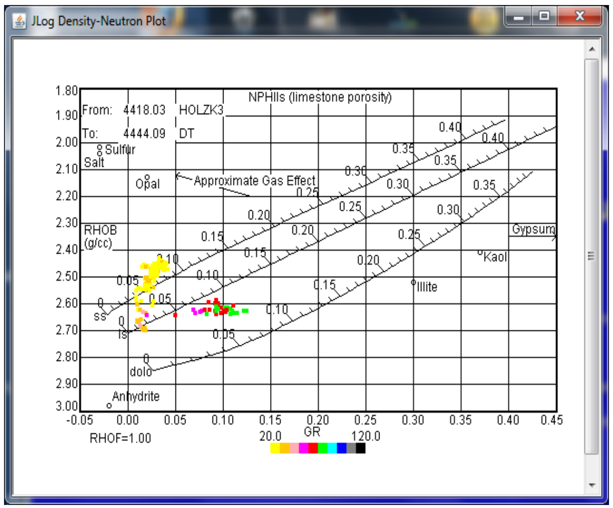

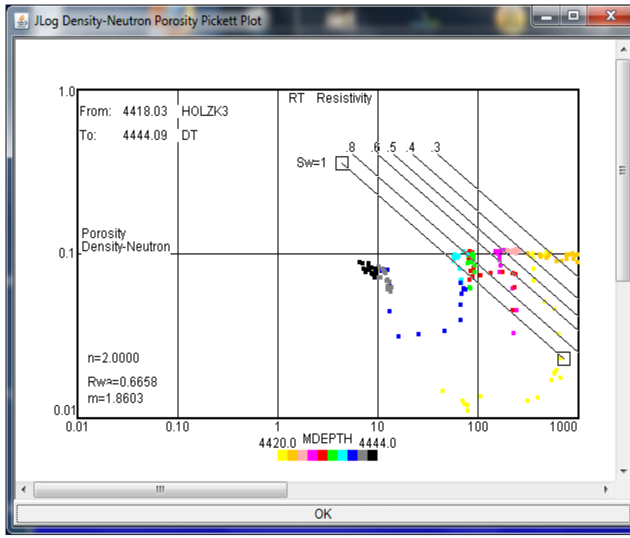

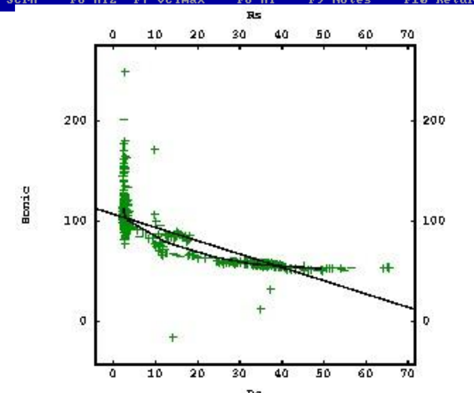

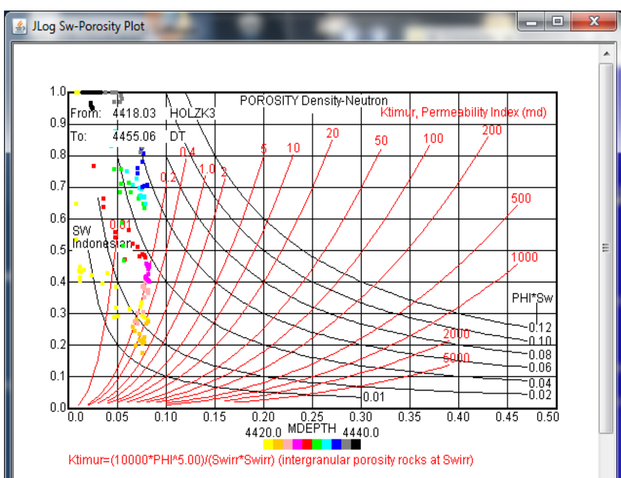

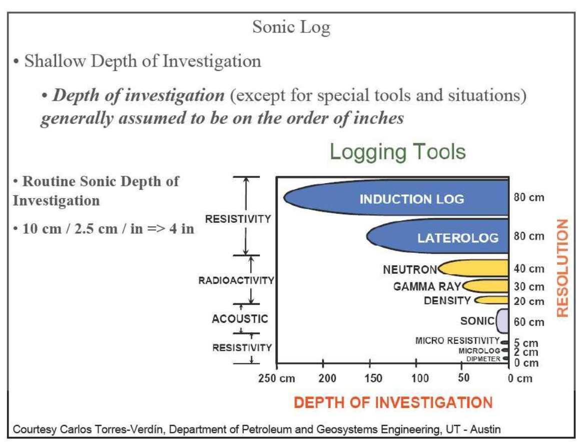

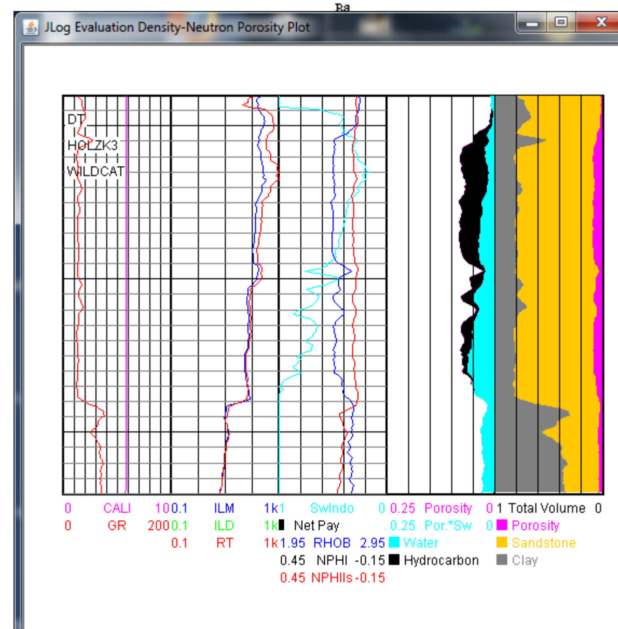

Seismic

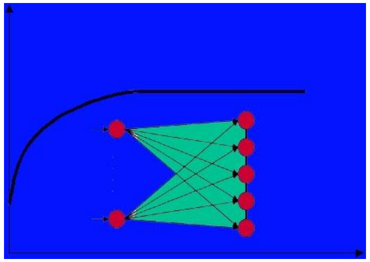

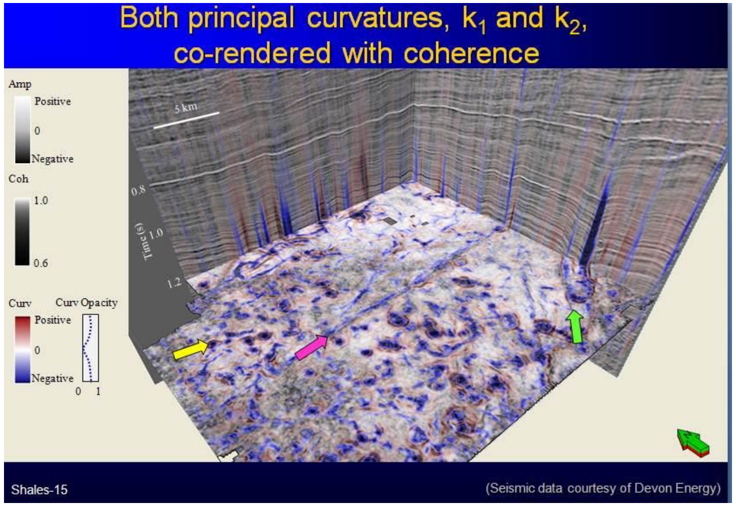

Both principal curvatures, k_1 and k_2, co-rendered with coherence
Amp
Positive
0
Negative
Coh
1.0
0.6
Curv
Positive
0
Negative
Curv Opacity
0 1
5 km
0.8
1.0
1.2
Time(s)
Shales-15
(Seismic data courtesy of Devon Energy)

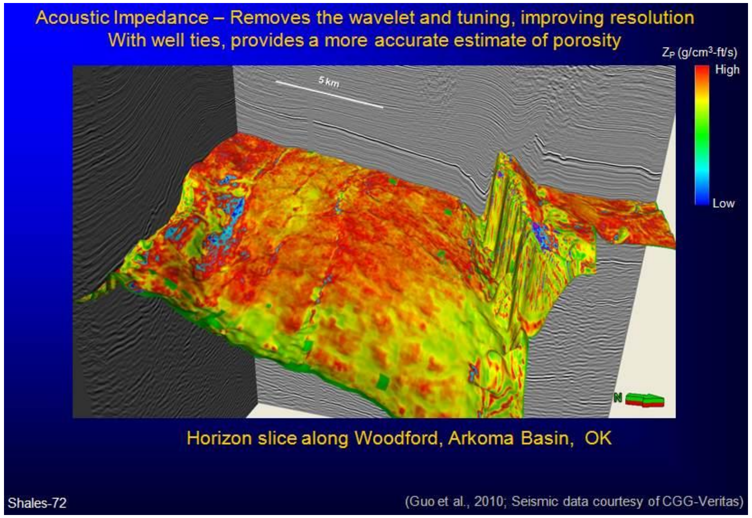

Acoustic Impedance – Removes the wavelet and tuning, improving resolution
With well ties, provides a more accurate estimate of porosity
Z_P (g/cm³-ft/s)
High
Low
5 km
Horizon slice along Woodford, Arkoma Basin, OK
Shales-72
(Guo et al., 2010; Seismic data courtesy of CGG-Veritas)

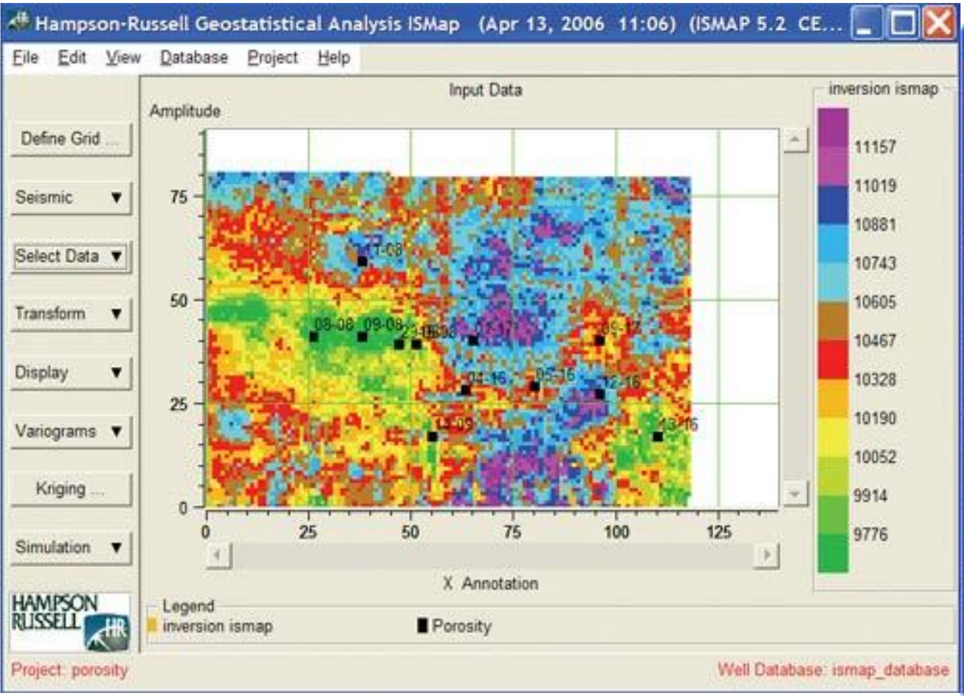

Hampson-Russell Geostatistical Analysis ISMap (Apr 13, 2006 11:06) (ISMAP 5.2 CE...
File Edit View Database Project Help
Define Grid ...
Seismic
Select Data
Transform
Display
Variograms
Kriging ...
Simulation
Input Data
Amplitude
inversion ismap
11157
11019
10881
10743
10605
10467
10328
10190
10052
9914
9776
0
25
50
75
100
125
X Annotation
Legend
inversion ismap
Porosity
HAMPSON RUSSELL
Project: porosity
Well Database: ismap_database

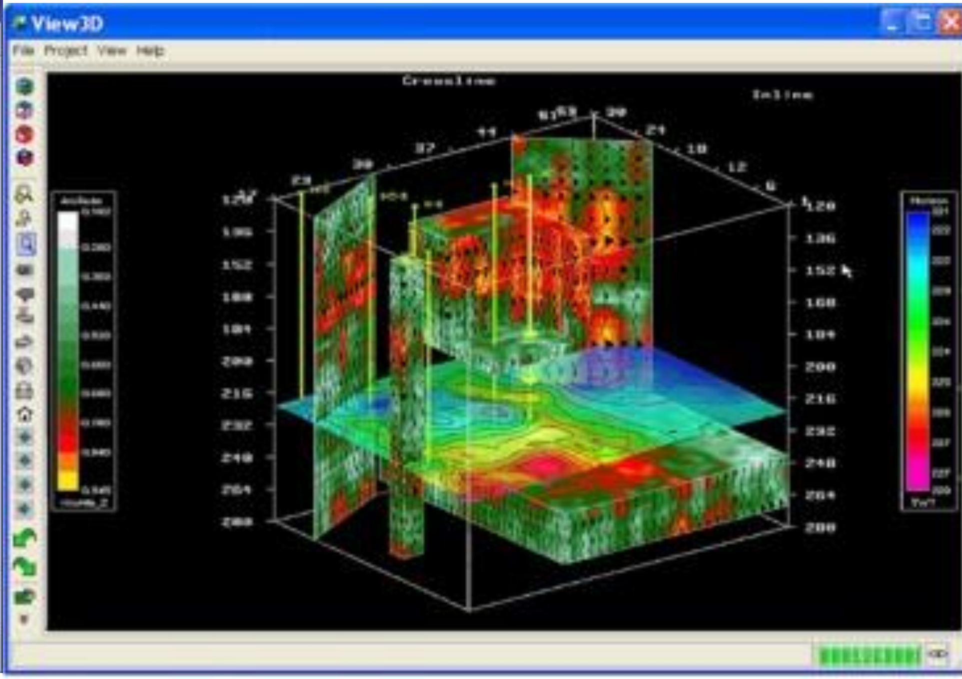

View3D
File Project View Help

WHAT MAKES THE DIFFERENCE IN GEOTHERMAL PROJECTS

GeoNeurale / Wavefields
Petrophysic-Consultants

Activity start

TECHNOLOGY	YEAR
Micro/Macrosystems Theory	2014
Seismic/Petrophysics Integr.	2013
Seismic Processing	2013
Seismic Inversion	2006
Static Modeling	2005
Advanced Rock Mechanics	2005
Seismic Attribute Analysis	2004
Geostatistics	2005
Seismic Interpretation	2004
Advanced Petrophysics	2003
Frac-operations	1992
Petrophysics	1991
Log Analysis	1991
LWD Technology	1990
MWD Technology	1989
Sigma-Log / IDEL	1988
Pore Pressure Evaluation	1988
MEL	1987
Drilling Dynamics	1986
Drilling Technology	1985
Data Logging	1985

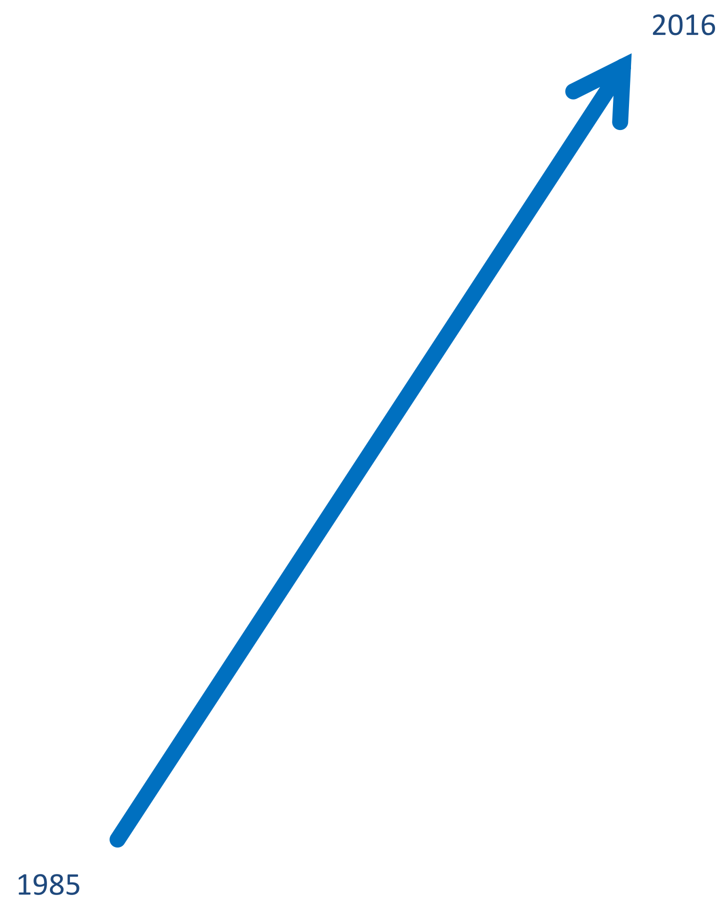

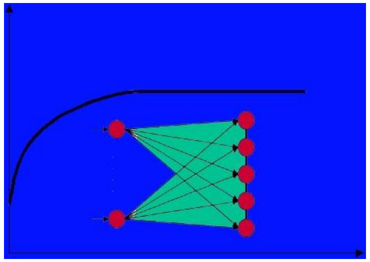

THE BAVARIAN MALM

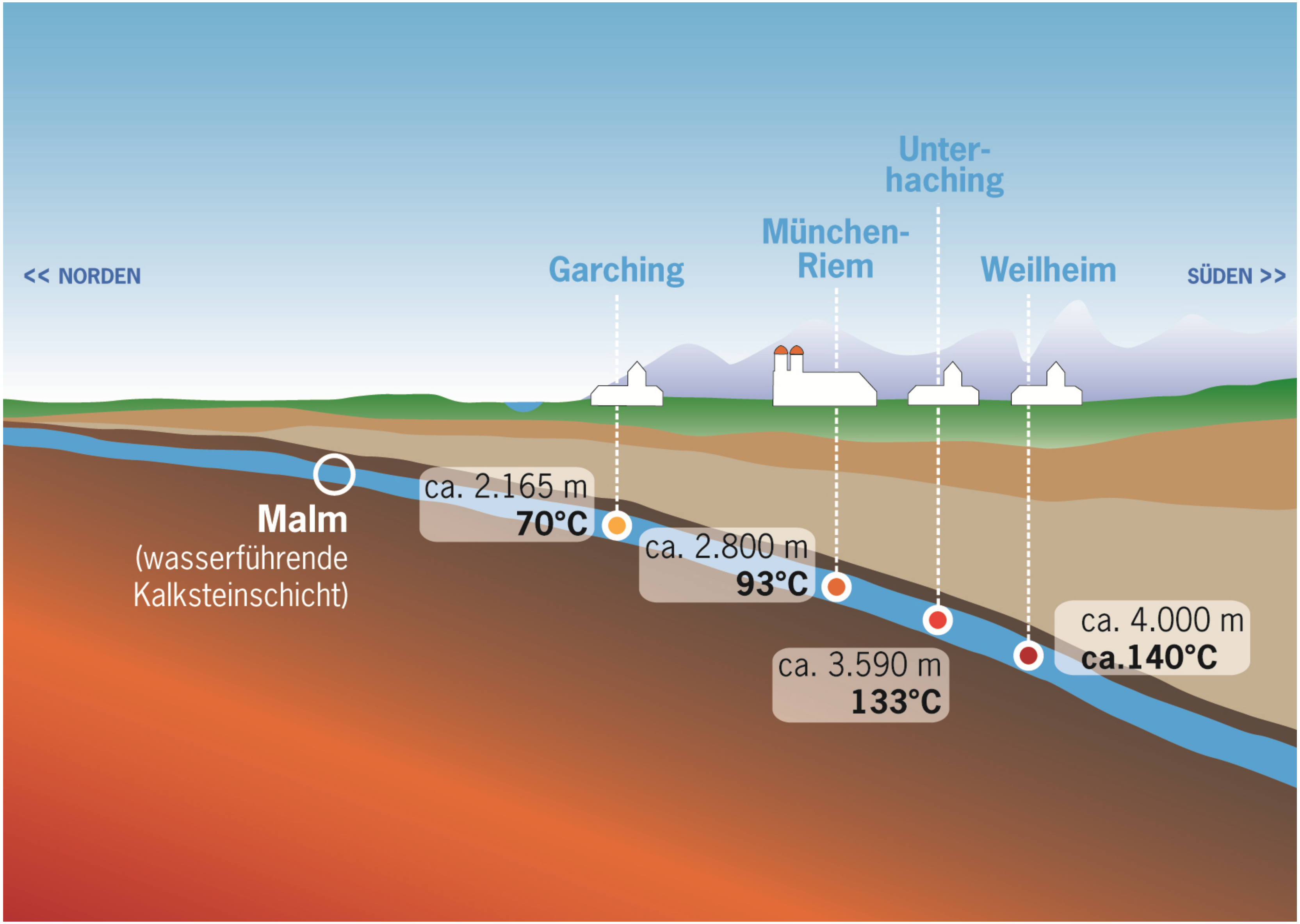

<< NORDEN
SÜDEN >>
Garching
München-
Riem
Unter-
haching
Weilheim
Malm
(wasserführende
Kalksteinschicht)
ca. 2.165 m
70°C
ca. 2.800 m
93°C
ca. 3.590 m
133°C
ca. 4.000 m
ca.140°C

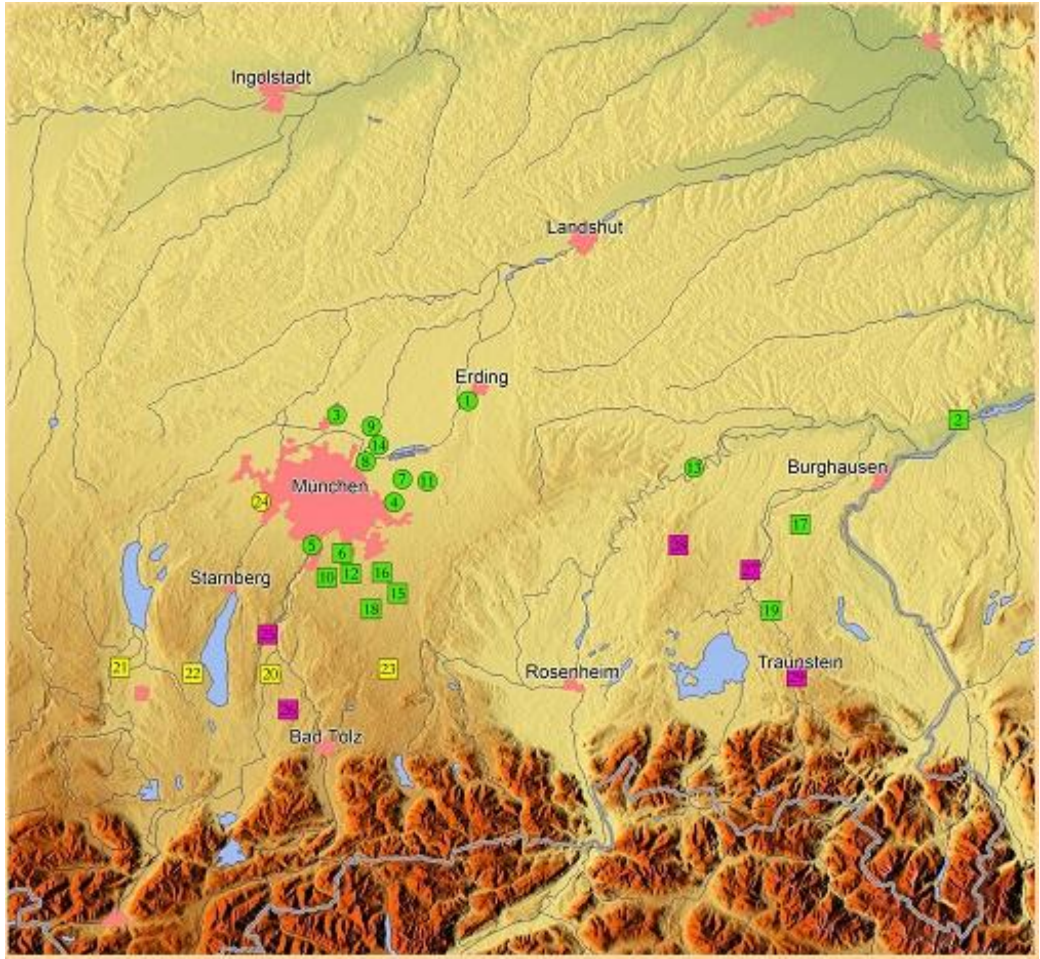
Ingolstadt
Landshut
Erding
München
Burghausen
Starnberg
Rosenheim
Traunstein
Bad Tölz

DOWNHOLE PUMPS

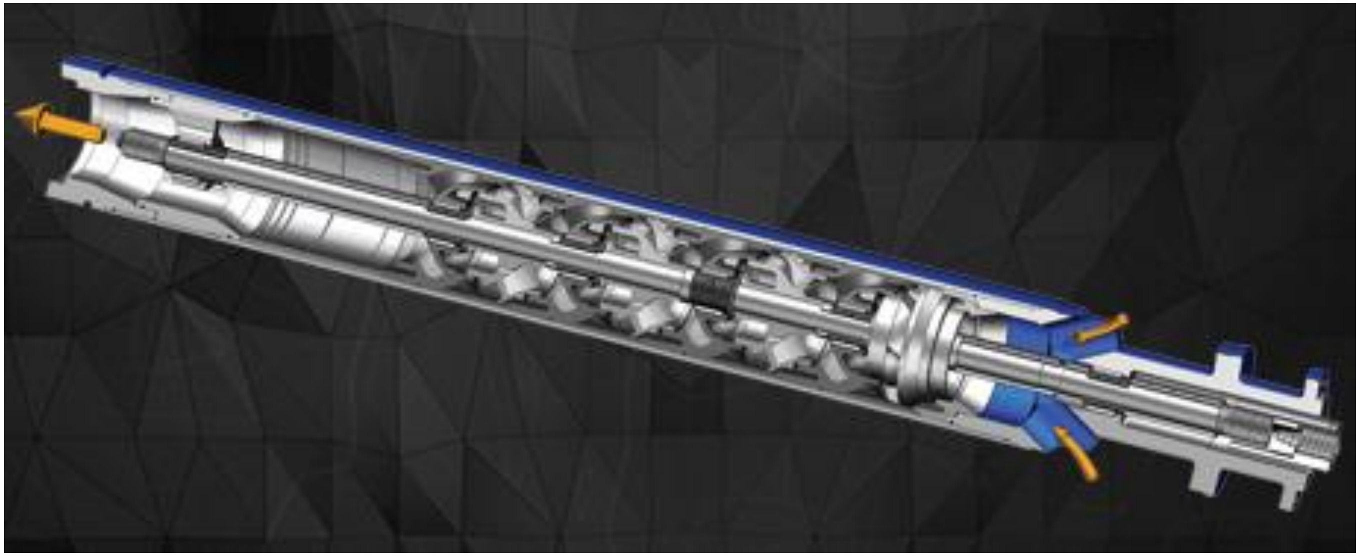

DOUBLETTE PRODUCTOR - INJECTOR

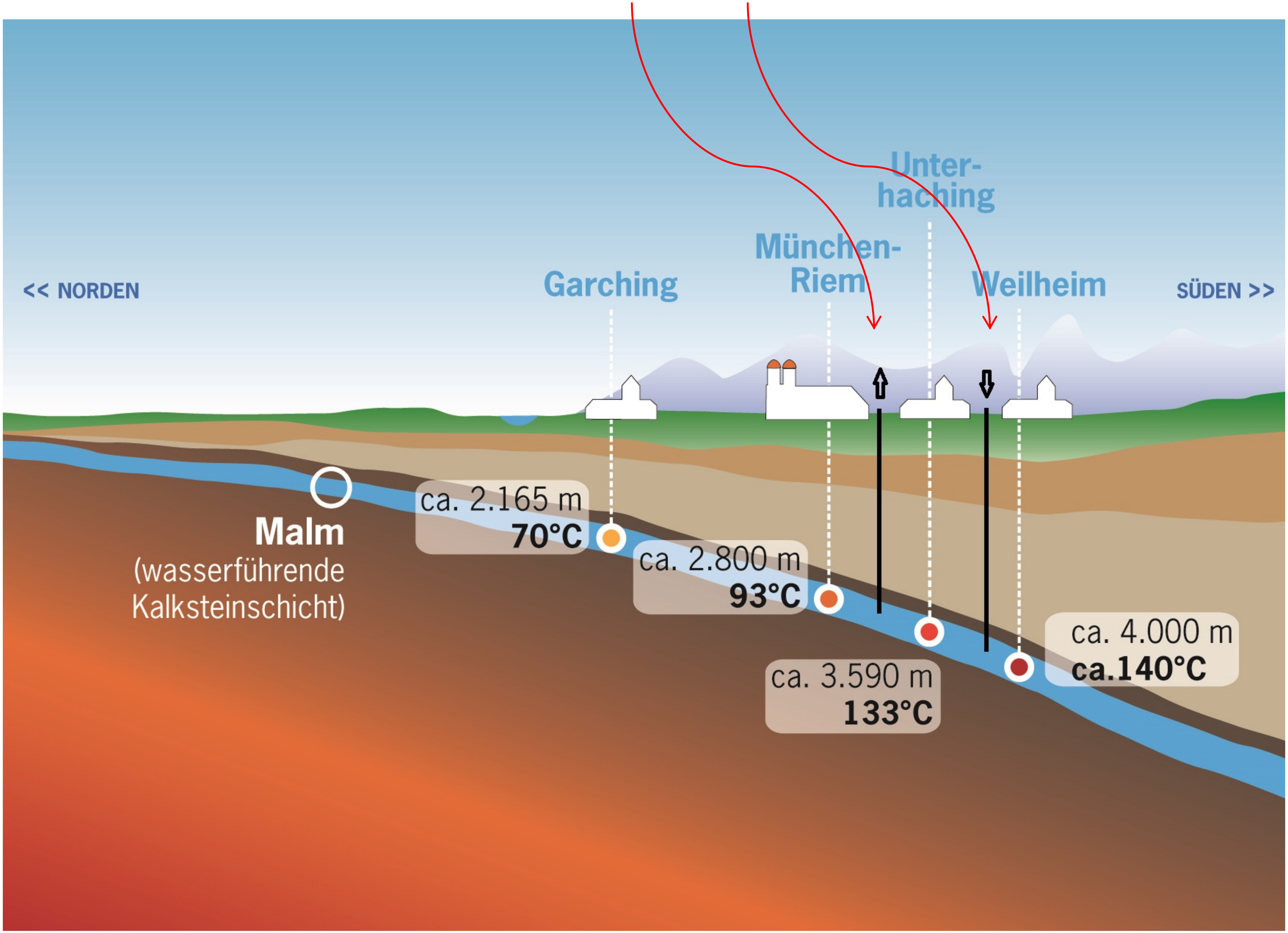

TYPICAL DIRECTIONAL WELLS FOR HYDROGEOTHERMAL PROJECTS

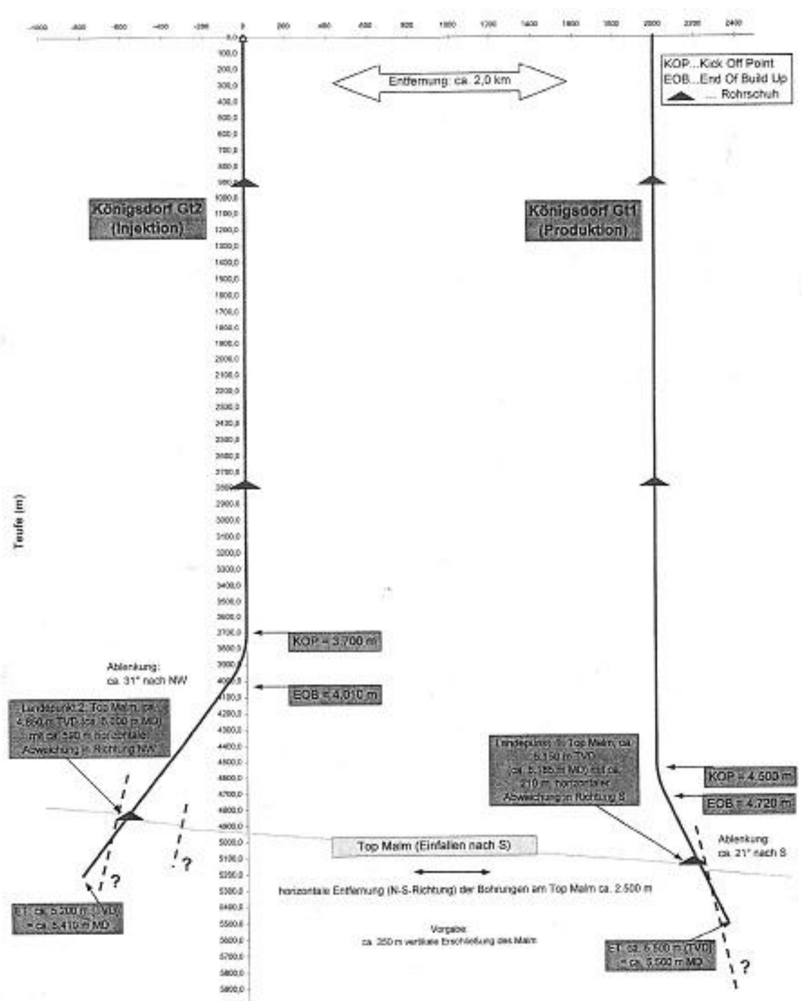

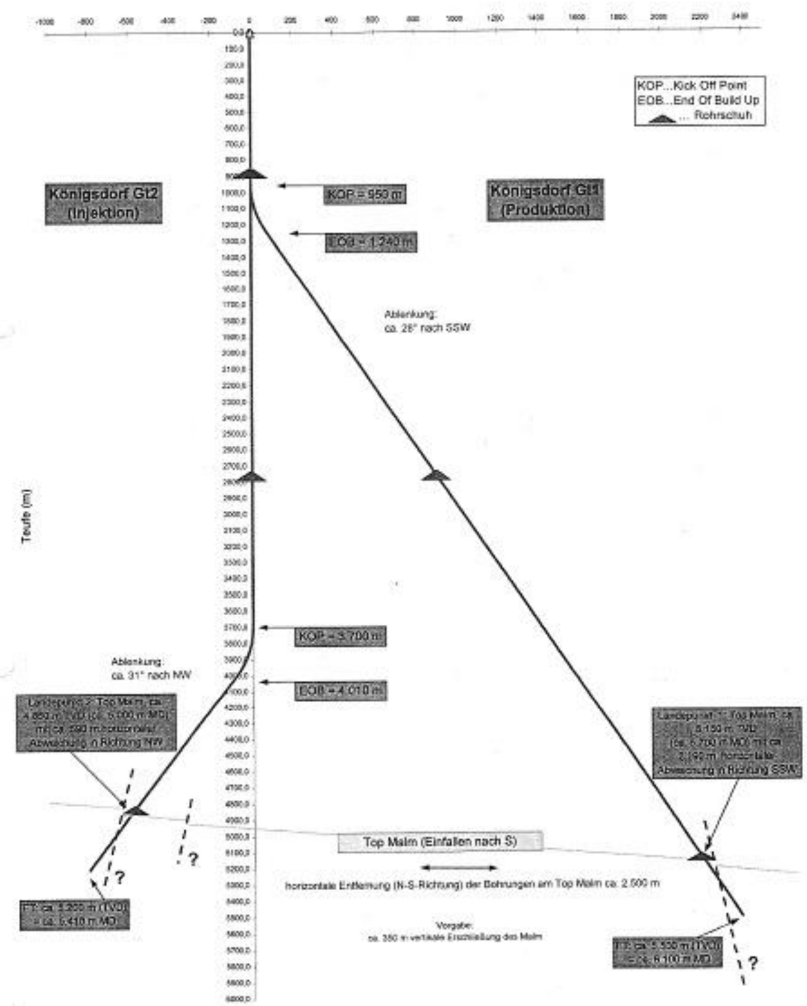

KÖNIGSDORF FEASIBILITY STUDY

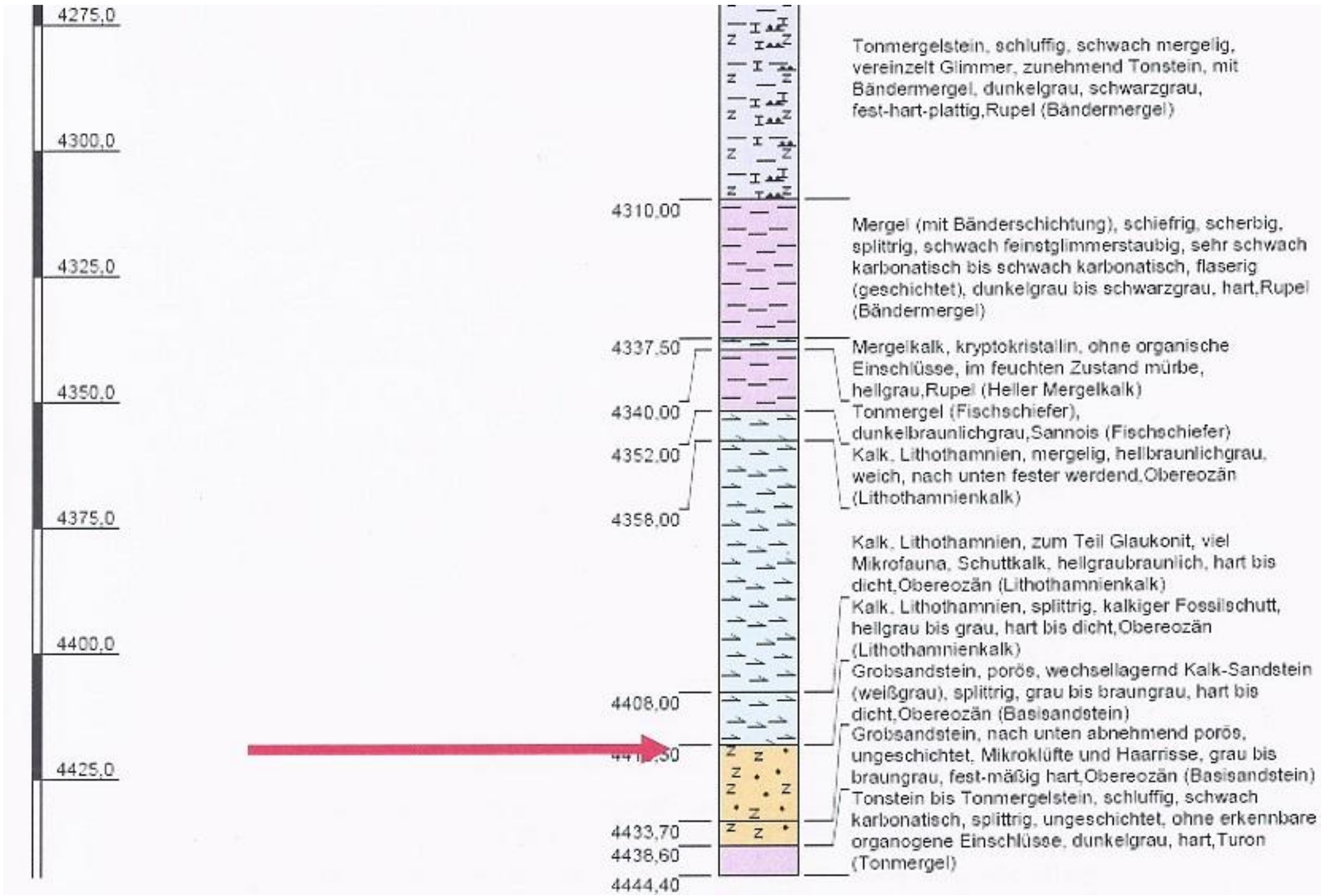

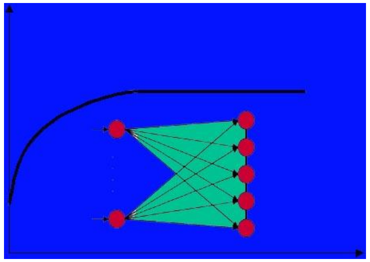

KÖNIGSDORF: THE PETROPHYSICS ANALYSIS PHASE

RESOLUTION

Sonic Log

- Shallow Depth of Investigation
  - ***Depth of investigation*** (except for special tools and situations) ***generally assumed to be on the order of inches***

Logging Tools

- **Routine Sonic Depth of Investigation**
- **10 cm / 2.5 cm / in => 4 in**

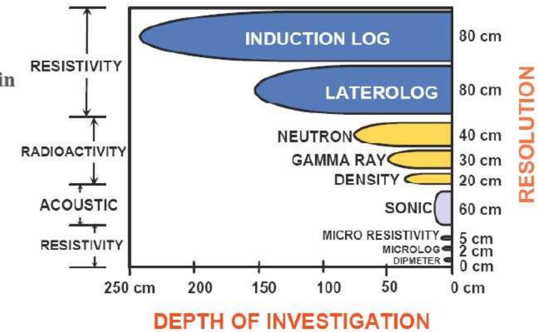

Courtesy Carlos Torres-Verdín, Department of Petroleum and Geosystems Engineering, UT - Austin

Sw Equations for Shaley-Sand Analysis

- Indonesia

$$S_w = \frac{1}{\frac{V_{cl}^{\left(1-\frac{V_{cl}}{2}\right)}}{\sqrt{R_{cl}}} + \frac{\phi_e}{\sqrt{R_w}}} * \frac{1}{\sqrt{R_t}}$$

- Nigeria

$$\frac{1}{R_t} = \left(\frac{V_{cl}^{1.4}}{\sqrt{R_{cl}}} + \frac{\phi_e^{m/2}}{\sqrt{aR_w}}\right)^2 S_w^n$$

- Waxman-Smits

$$\frac{1}{R_t} = \frac{S_w^2}{F^* R_w} + \frac{BQ_v S_w}{F^*}$$

- Dual Water

$$C_t = \frac{\phi_t^m S_{wt}^n}{a}\left[C_w + \frac{S_{wb}}{S_{wt}}\left(C_{wb} - C_w\right)\right]$$

Vcl Analysis

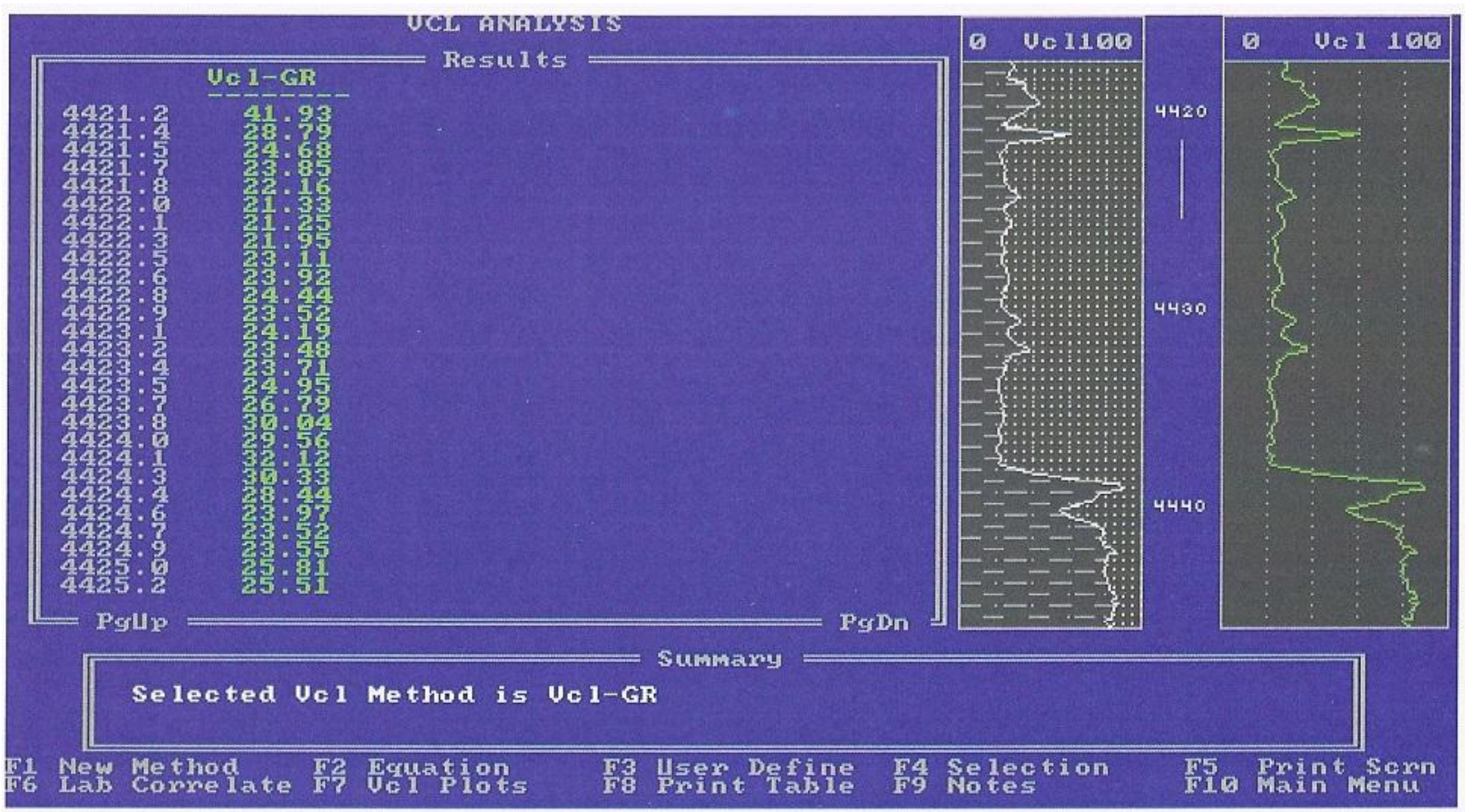

NPHI POReff Analysis

POROSITY ANALYSIS

Results

	Por Tot	Por Eff
4425.2	8.82	8.03
4425.3	8.46	7.59
4425.5	8.08	7.19
4425.6	8.05	7.19
4425.8	8.40	7.62
4426.0	8.40	7.66
4426.1	8.47	7.69
4426.3	8.55	7.73
4426.4	8.21	7.33
4426.6	8.16	7.31
4426.7	8.10	7.27
4426.9	8.46	7.67
4427.0	8.46	7.68
4427.2	8.49	7.70
4427.3	8.46	7.70
4427.5	8.85	8.09
4427.6	8.83	8.06
4427.8	8.47	7.64
4427.9	8.46	7.64
4428.1	8.45	7.62
4428.2	8.42	7.60
4428.4	8.36	7.61
4428.5	7.92	7.20
4428.7	7.50	6.84
4428.9	6.69	6.03
4429.0	6.21	5.69
4429.1	4.14	3.78

PgUp PgDn

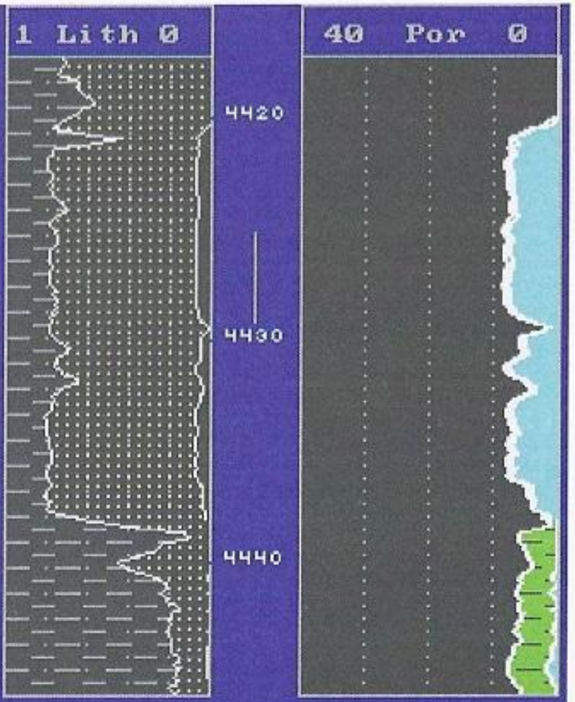

Summary

Selected Vcl Method is Vcl-GR
Selected Por Method is Density-Neutron

F1 New Method F2 Equation F4 Print Table F5 Print Scrn
F7 QPlot F8 DN Xplot F9 Notes F10 Main Menu

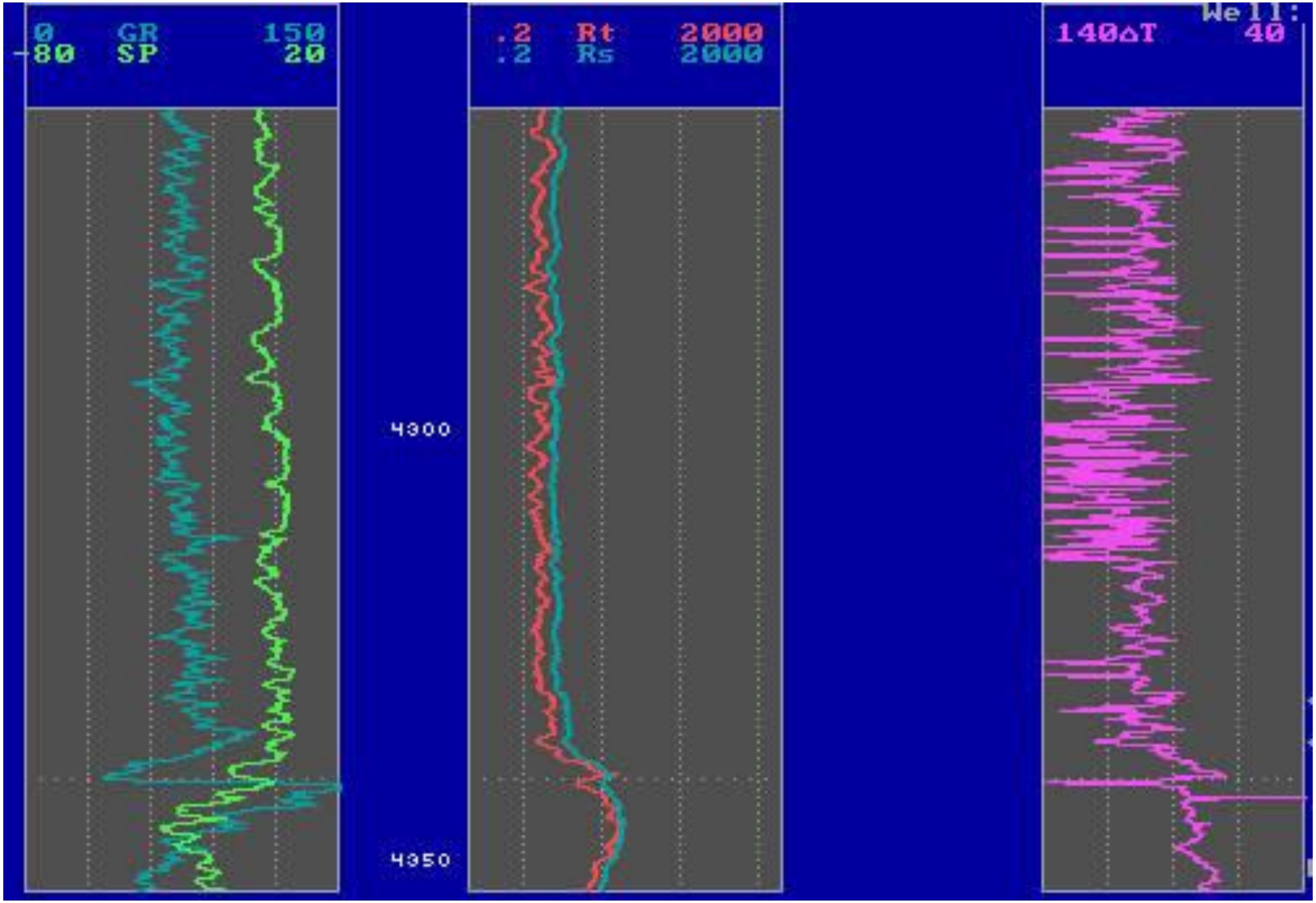
0 GR 150
-80 SP 20
.2 Rt 2000
.2 Rs 2000
140 ΔT 40
Well:
4300
4350

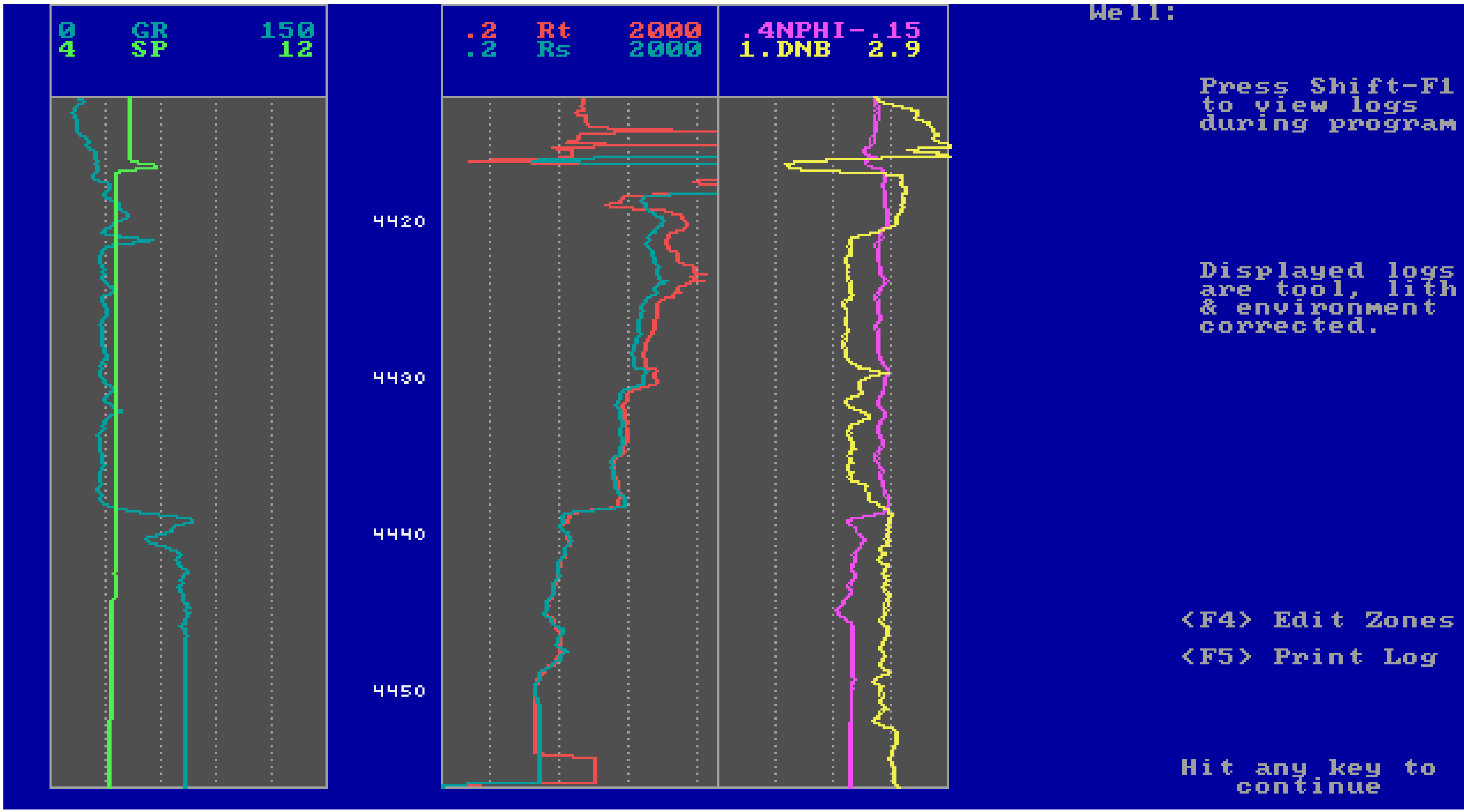
Well:
0 GR 150
4 SP 12
.2 Rt 2000
.2 Rs 2000
.4NPHI-.15
1.DNB 2.9
4420
4430
4440
4450
Press Shift-F1 to view logs during program
Displayed logs are tool, lith & environment corrected.
<F4> Edit Zones
<F5> Print Log
Hit any key to continue

RHOB-NPHI Xplot Analysis

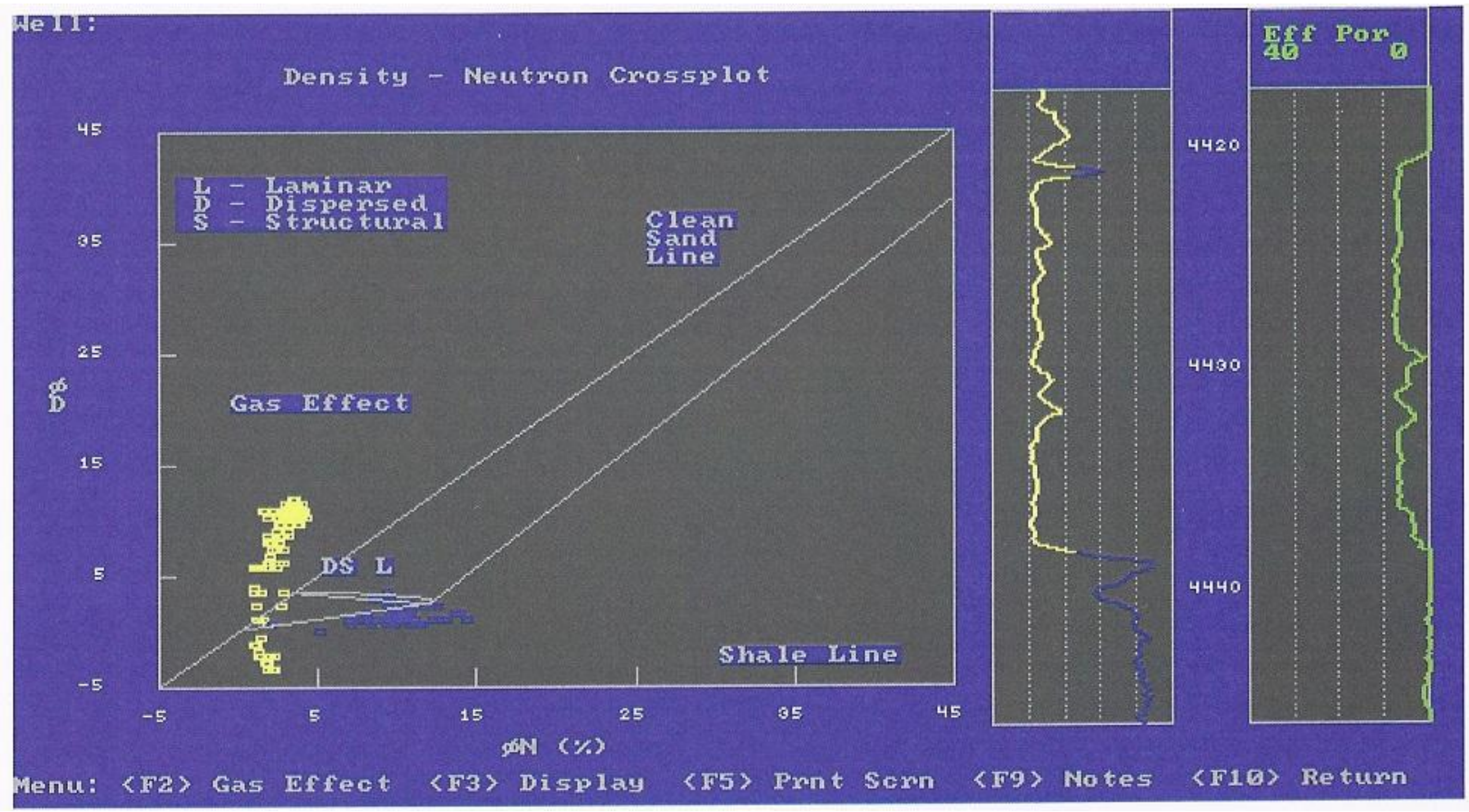

RHOB-NPHI Xplot Analysis theory

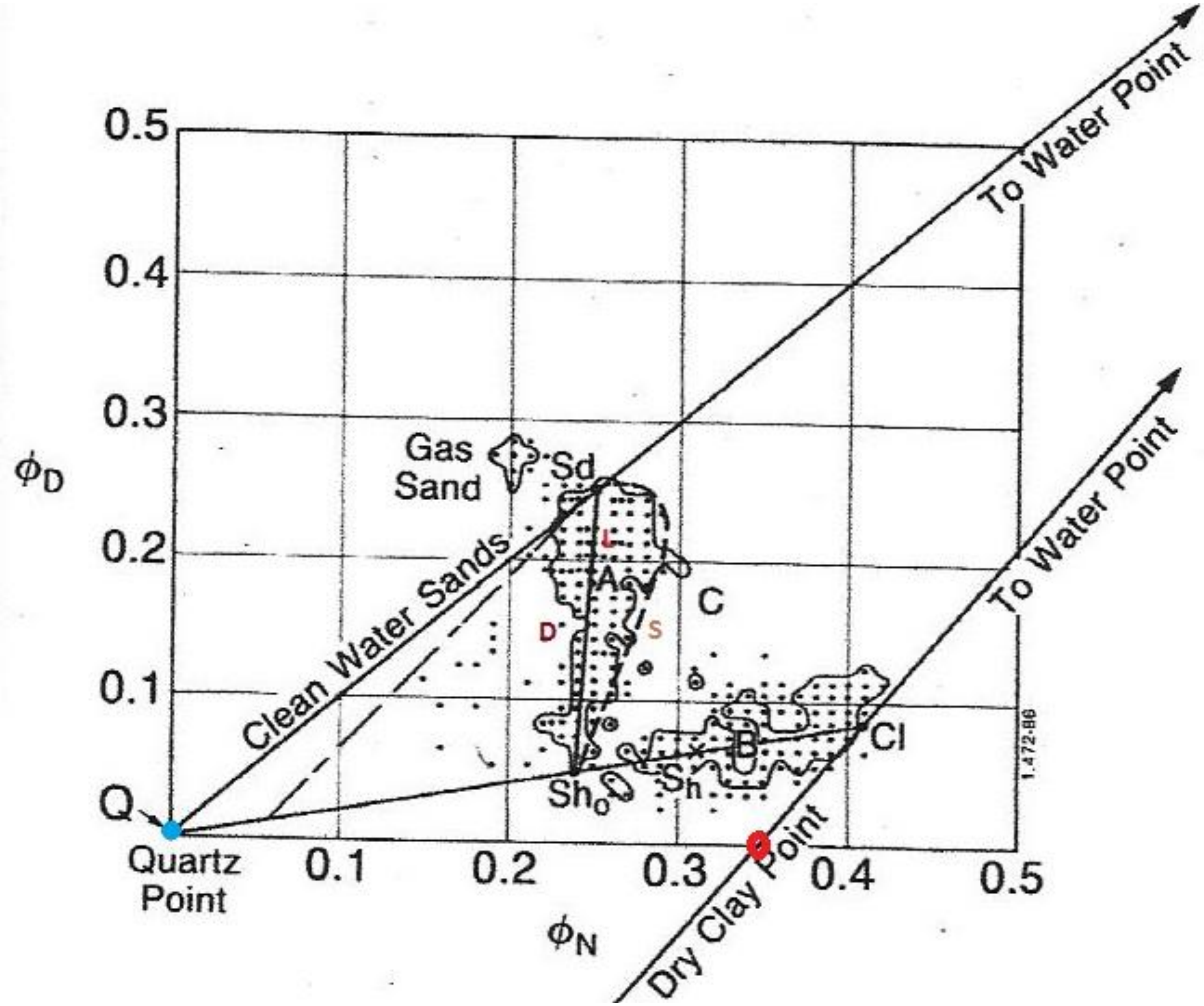

Courtesy Schlumberger

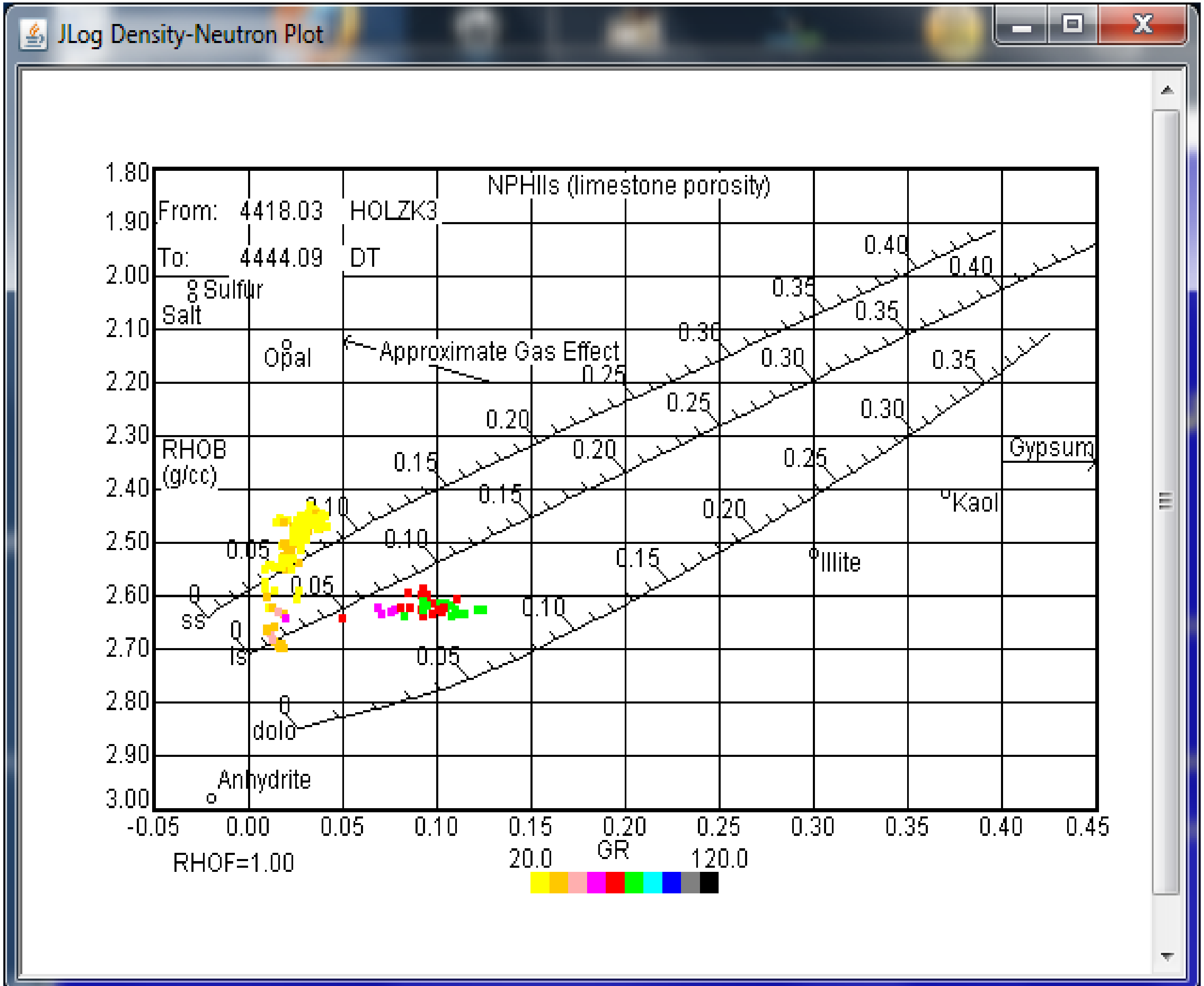
JLog Density-Neutron Plot
NPHIls (limestone porosity)
From: 4418.03 HOLZK3
To: 4444.09 DT
Sulfur
Salt
Opal
Approximate Gas Effect
RHOB (g/cc)
Gypsum
Kaol
Illite
ss
ls
dolo
Anhydrite
RHOF=1.00
GR
20.0
120.0

BVW Analysis on Buckle Plot

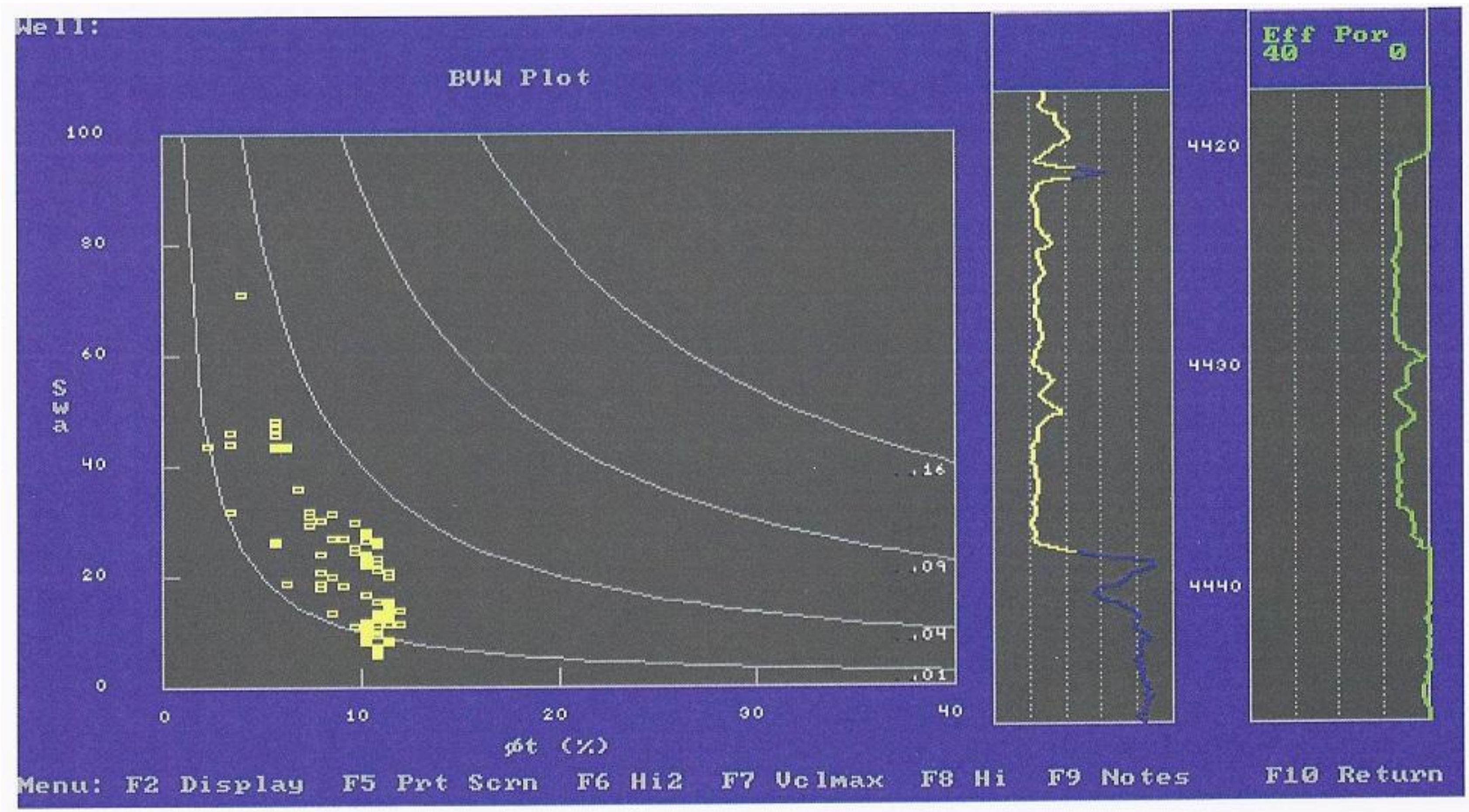

BVW Analysis on Buckle Plot PHI-K Plot

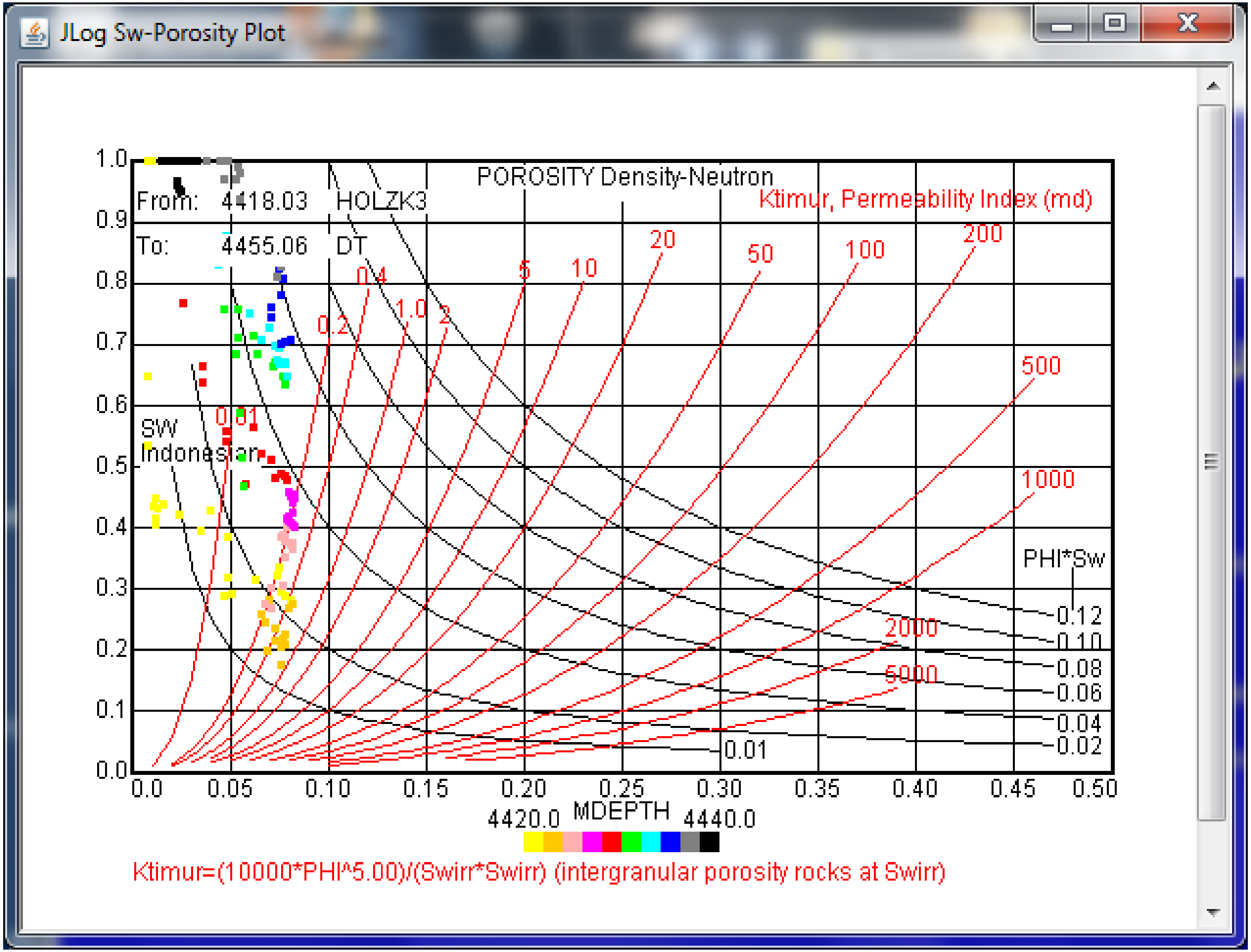

Pickett Plot

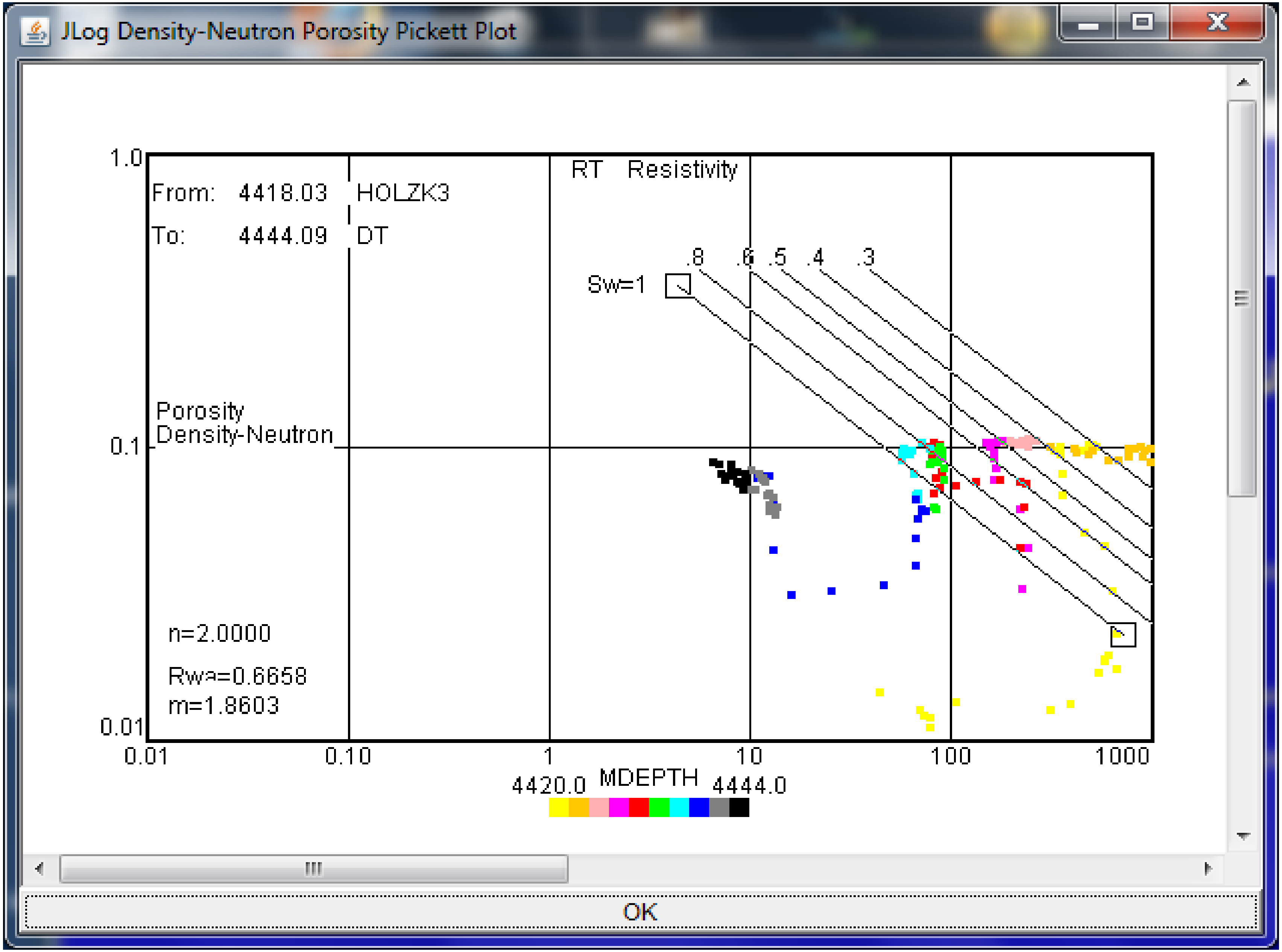

LOG TRIPLE COMBO

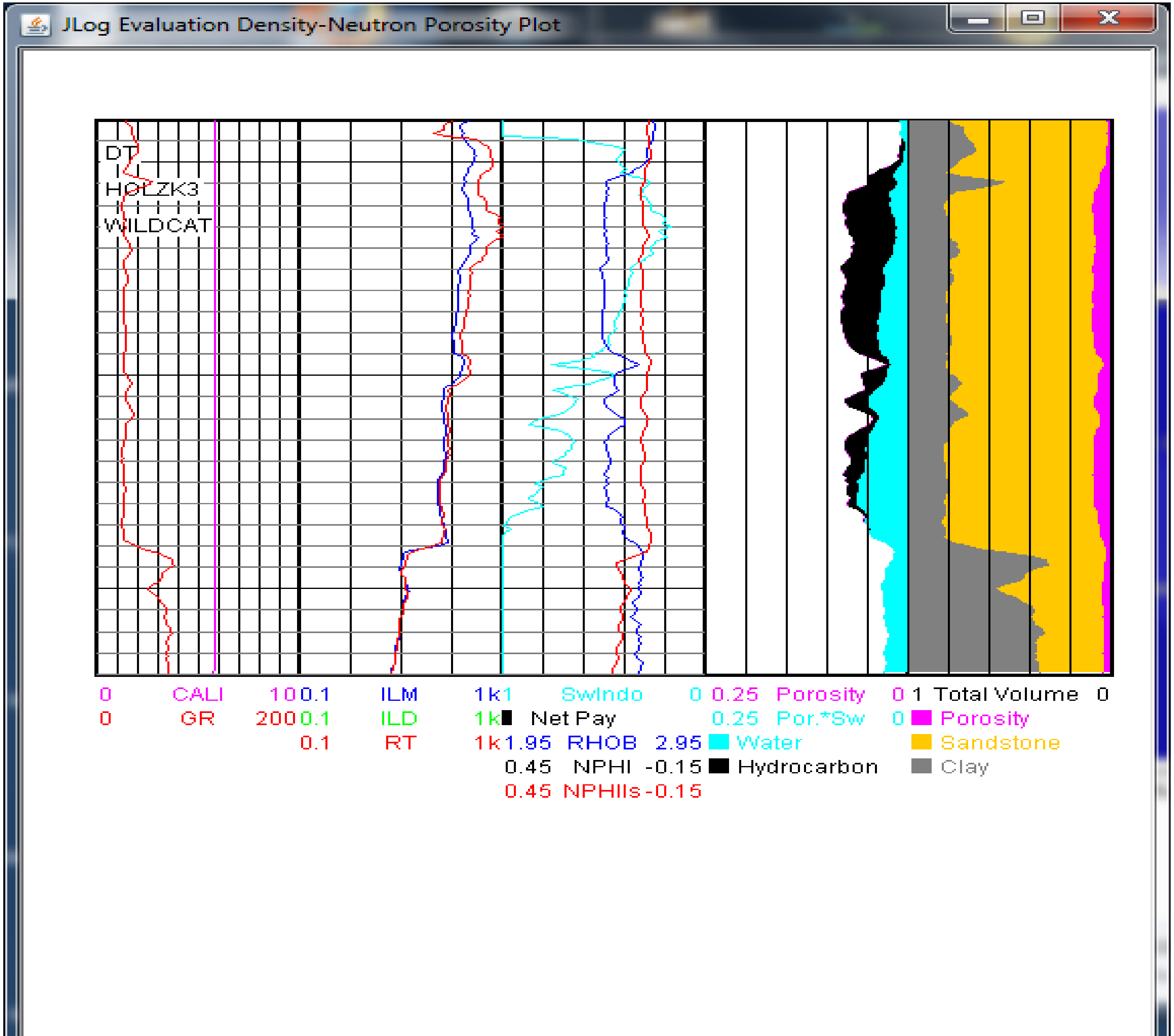

JOINT VARIOGRAPHIC ANALYSIS

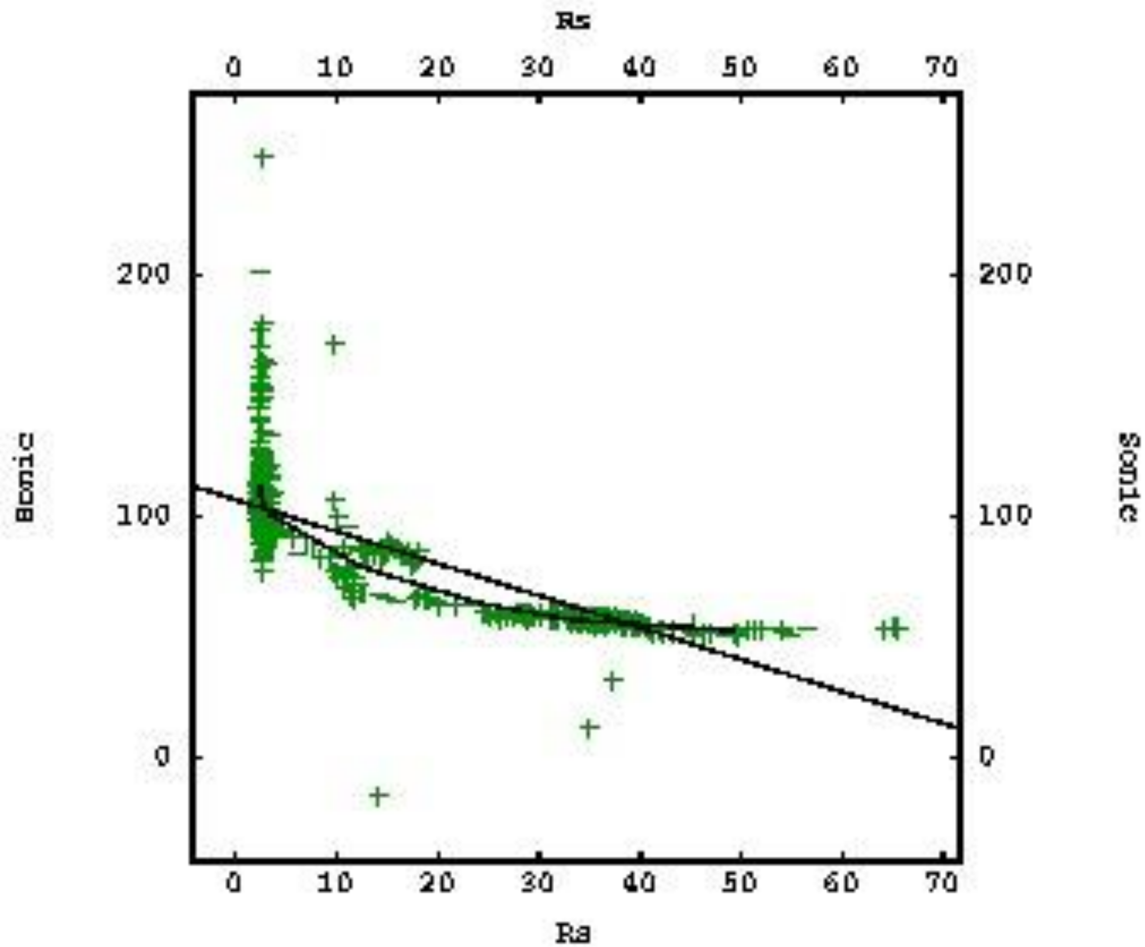

Courtesy D. Renoir

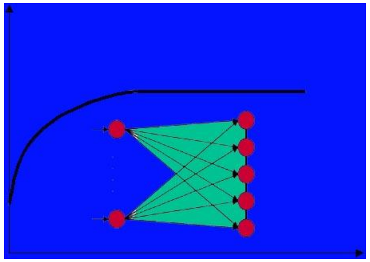

CARBONATE PETROPHYSICS
RESEARCH PROJECT

LUCIA CLASSIFICATION

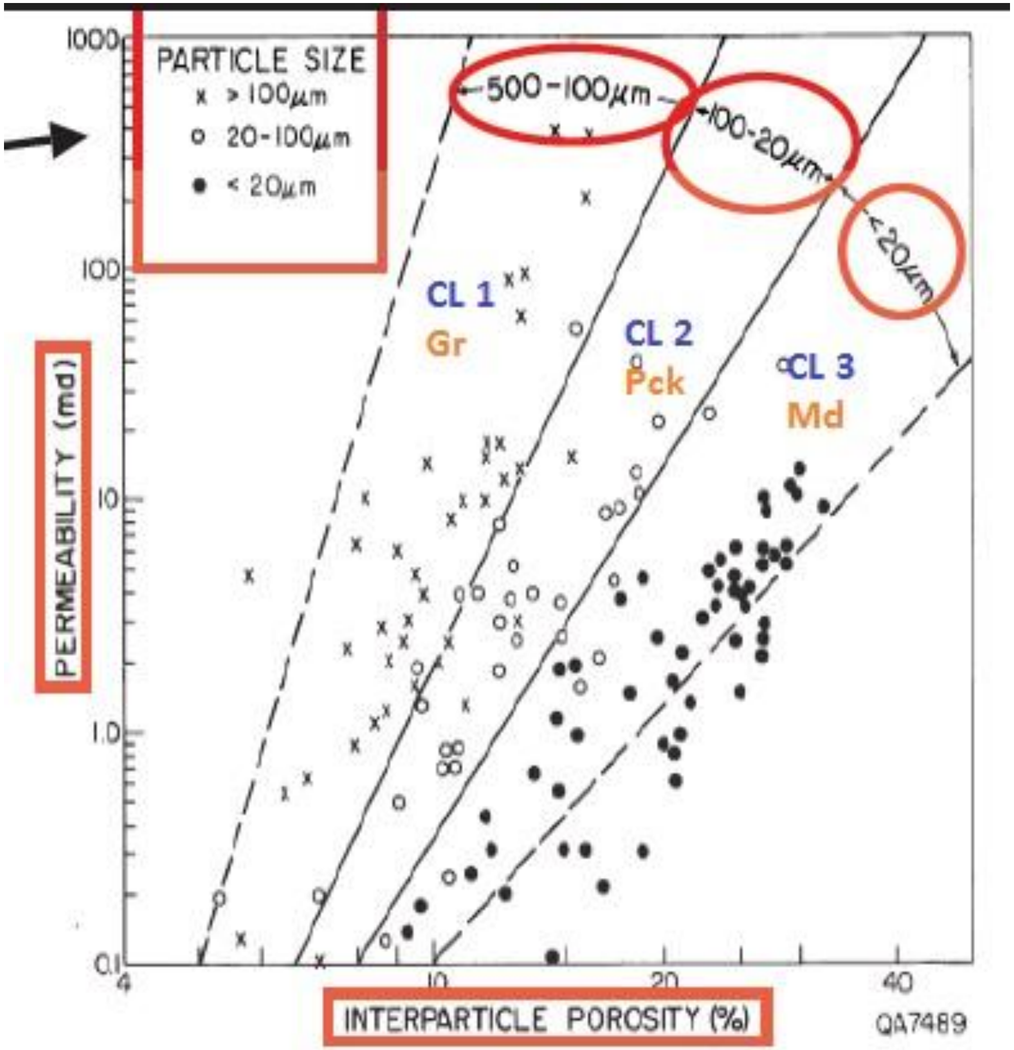

Courtesy Jerry Lucia, Gene Ballay

CAPILLARY PRESSURE CURVE - Pc

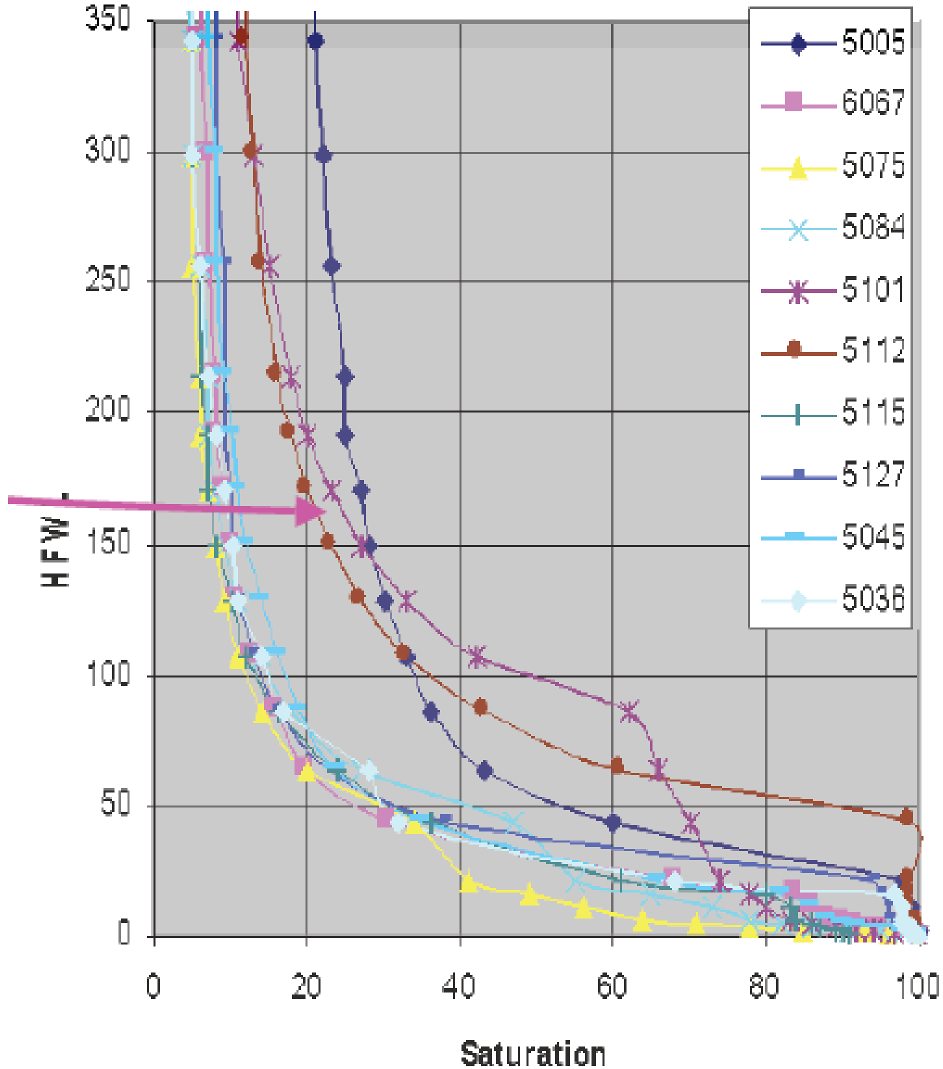

Courtesy Gene Ballay

Winland R35

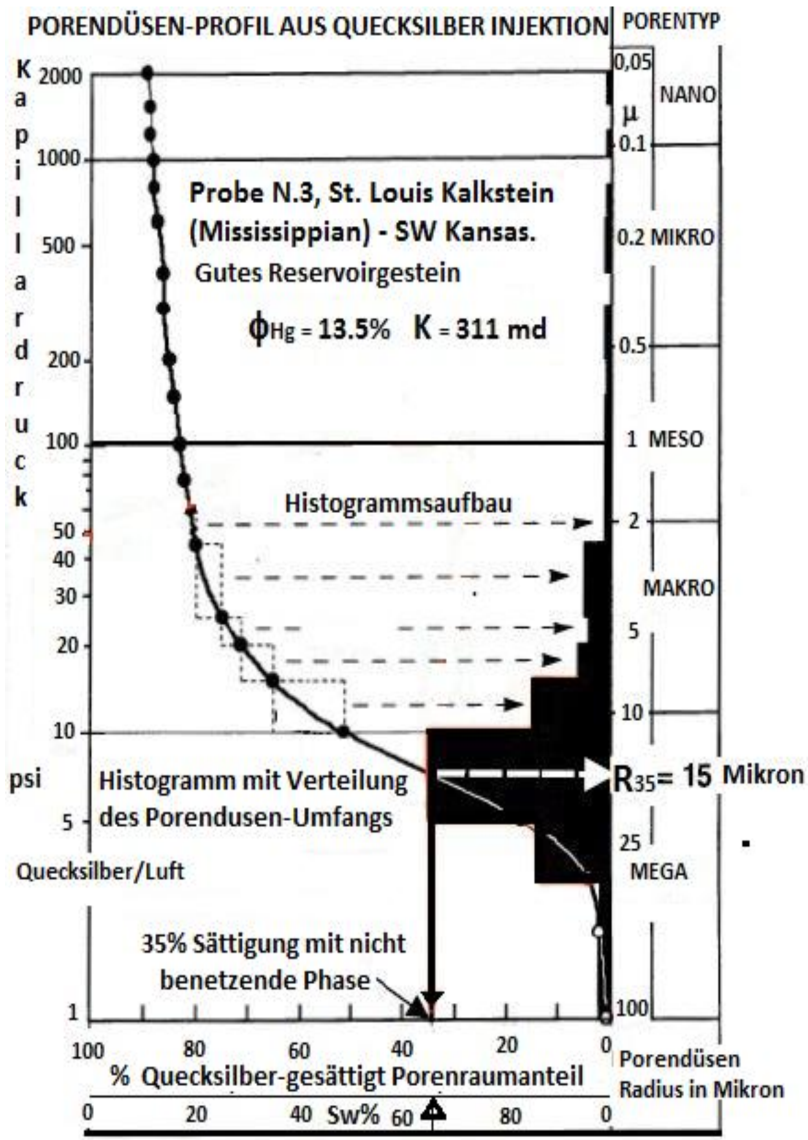

Courtesy Gene Ballay

NMR AND POROSITY

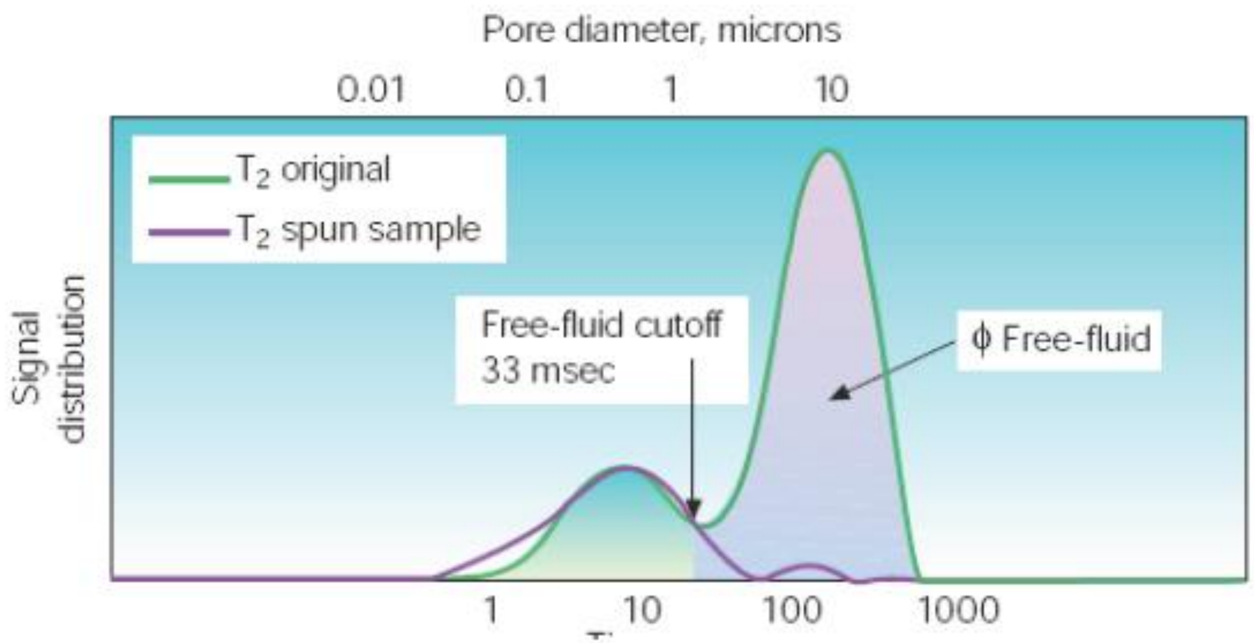

Courtesy Gene Ballay

SECONDARY POROSITY

Log and Core Examples - SWEC Mansfield No. 1 Well

•In the graphic at right, separate-vug porosity derived by the **point-count method** is compared with separate-vug porosities calculated by the **SPI**, **Nurmi**, **quadratic**, and **power-law** models.

$$\phi_2 = \phi_t - \phi_s \quad (5)$$

$$\phi_{om} = 2(\phi_t - \phi_s) \quad (6)$$

$$\phi_{sv} = (\phi_t - \phi_s) + p\,(\phi_t - \phi_s)^2 \quad (8)$$

$$\phi_{sv} = \left(\frac{\phi_t}{\phi_s}\right)^{\alpha} (\phi_t - \phi_s) \quad (9)$$

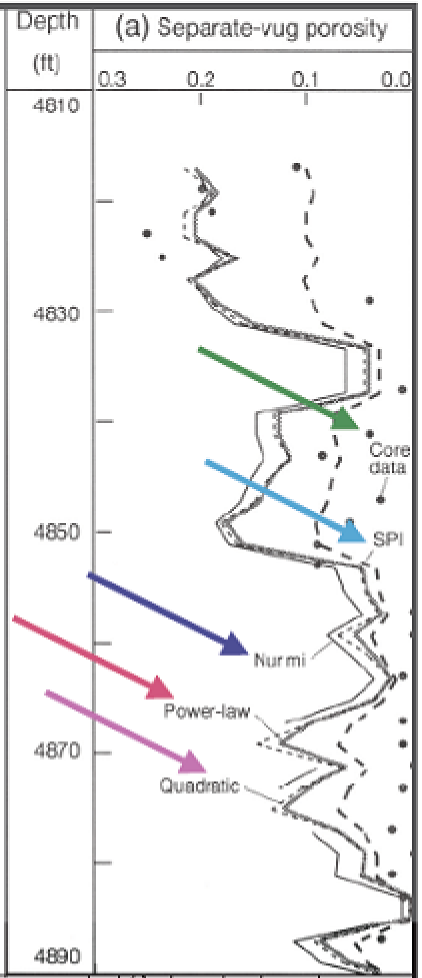

Comparison of Empirical Models for Calculating the Vuggy Porosity and Cementation Exponent of Carbonates from Log Responses. Fred P. Wang and F. Jerry Lucia

$$\phi_{sv} = 10^{4.09 - 0.1298\,(\Delta t - 141.5\phi_t)}$$

Courtesy F.J. Lucia, F.P. Wang, R.E. Ballay

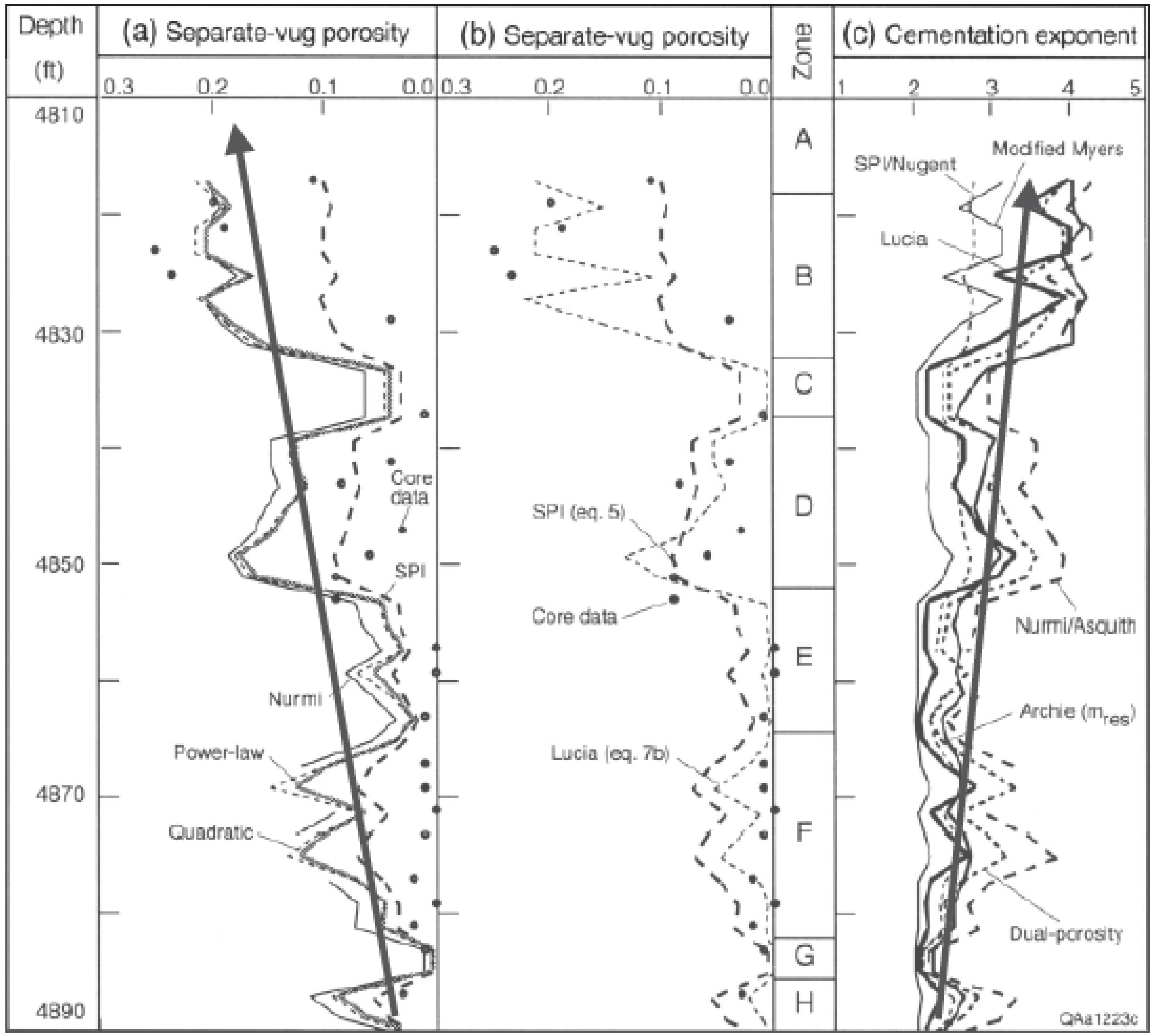

Courtesy F.J. Lucia, F.P. Wang, R.E. (Gene) Ballay

DUAL POROSITY MODEL

$$\boxed{C_0 = C_w \left(\phi_{ip}^{m_{ip}} + \frac{\phi_v^{m_v}}{a_v} \right) \qquad (28)}$$

- The constant a_v may be used to characterize the connectivity of different types of vuggy pores:
  - an a_v greater than 100 for ***separate-vug dominated carbonates***,
  - an a_v less than 20 for ***touching-vug-dominated carbonates***,
  - and an a_v of 1 for ***well-connected planar fractures***.
- ***When multiple vuggy pore types are present***, a characteristic value for a_v must be determined.

$$m = \frac{\log\left(\phi_{ip}^{m_{ip}} + \frac{\phi_v}{a_v} \right)}{\log \phi_t}$$

Courtesy F.J. Lucia, F.P. Wang, R.E. (Gene) Ballay

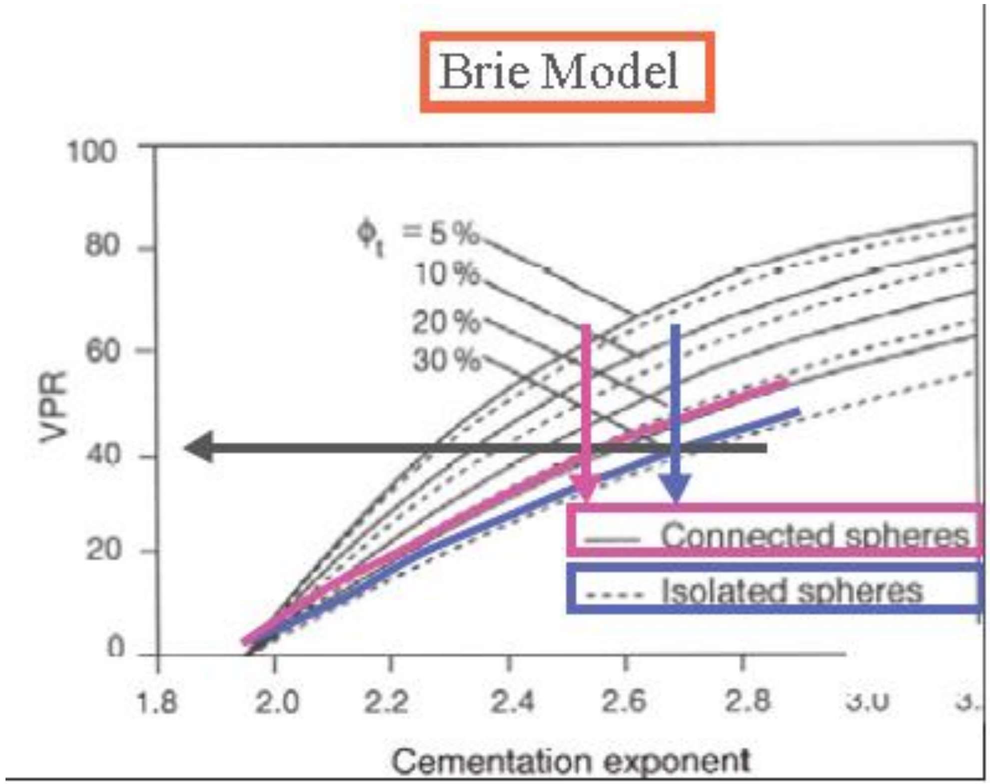

Courtesy R.E. (Gene) Ballay

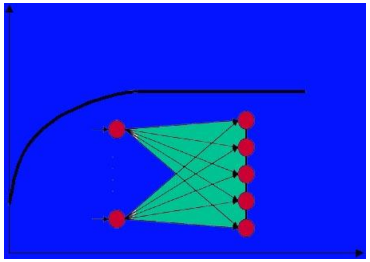

2D / 3D REFLECTION SEISMIC

STRESS COMPONENTS - EQUILIBRIUM CONDITIONS

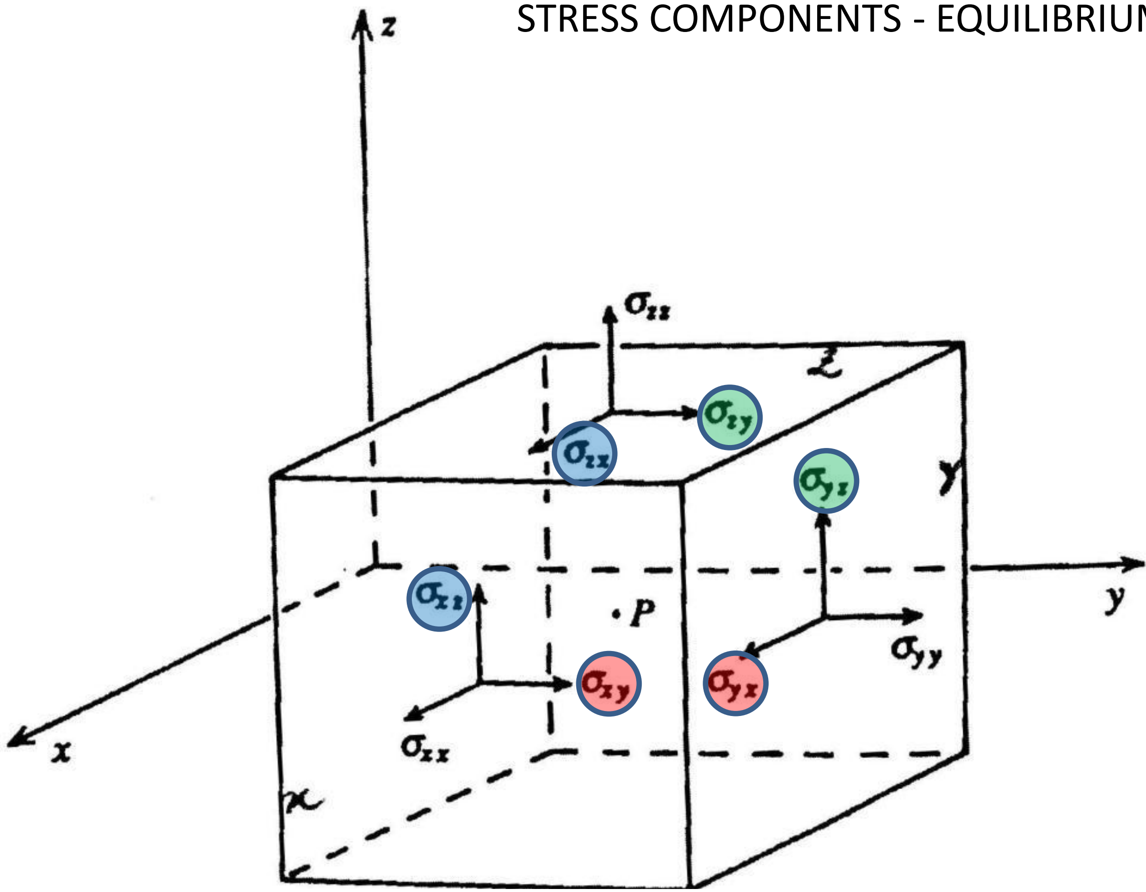

The 9 stress components are expressed in a convenient form in a 3X3 matrix array

$$\begin{bmatrix} \sigma_{xx} & \sigma_{xy} & \sigma_{xz} \\ \sigma_{yx} & \sigma_{yy} & \sigma_{yz} \\ \sigma_{zx} & \sigma_{zy} & \sigma_{zz} \end{bmatrix}$$

$$\sigma_{xy} = \sigma_{yx}, \quad \sigma_{yz} = \sigma_{zy}, \quad \sigma_{zx} = \sigma_{xz}$$

In equilibrium conditions the normal stresses which are normal to the faces (laying on the main matrix diagonal and marked with same index xx,yy,zz)have to be equal (volumetric deformation equilibrium).

For rotational equilibrium each shear stress couple (marked with the same color) have to be equal (i.e. $\sigma xy = \sigma yx$ to prevent the cube to rotare around the zz simmetry/rotation axis).

Therefore alltogether only 6 independent components are required to describe the state of stress in a point. 3 Normal and 3 Shear Stresses.

PRINCIPAL STRESSES

$$\begin{bmatrix} \sigma_x & 0 & 0 \\ 0 & \sigma_y & 0 \\ 0 & 0 & \sigma_z \end{bmatrix}$$

The stresses on the main diagonal (normal to the main faces) are called principal / normal stresses , their directions are called principal axes and the plane perpendicular are the principal planes.

On the principal stresses matrix there are no shear stresses. It can be shown that there is always an orientation of the axes relative to the body where the shear stresses are all zero.

UNIAXIAL STRESS

$$\begin{bmatrix} 0 & 0 & 0 \\ 0 & 0 & 0 \\ 0 & 0 & \sigma \end{bmatrix}$$

HYDROSTATIC STRESS

$$\begin{bmatrix} -p & 0 & 0 \\ 0 & -p & 0 \\ 0 & 0 & -p \end{bmatrix}$$

PURE SHEAR STRESS

$$\begin{bmatrix} 0 & \sigma & 0 \\ \sigma & 0 & 0 \\ 0 & 0 & 0 \end{bmatrix}$$

Review note: For triangular Matrices the Determinant is equal to the product of the main diagonal elements

GENERALIZED HOOKE´S LAW

We can finally express the Hooke´s law as a general form : $\sigma_i = \sum_j c_{ij}\varepsilon_j$

Where the Stiffness matrix C_{ij} is represented by a 6X6 matrix of the 6X6 independent tensor components acting on the 6 independent strain components .

To simplify the description we denote the subscripts as follows:

full	xx	yy	zz	yz	zx	xy
abbreviated	1	2	3	4	5	6

Therefore: $\sigma_1=\sigma_{xx}$; $\sigma_2=\sigma_{yy}$; $\sigma_3=\sigma_{zz}$; $\sigma_4=\sigma_{yz}$; $\sigma_5=\sigma_{zx}$; $\sigma_6=\sigma_{xy}$;

The calculation of each stress component is described by the following polinomial (example for the σ_1 component):

$$\sigma_1 = c_{11}\varepsilon_1 + c_{12}\varepsilon_2 + c_{13}\varepsilon_3 + c_{14}\varepsilon_4 + c_{15}\varepsilon_5 + c_{16}\varepsilon_6$$

$$\begin{bmatrix} \sigma_1 \\ \sigma_2 \\ \sigma_3 \\ \sigma_4 \\ \sigma_5 \\ \sigma_6 \end{bmatrix} = \begin{bmatrix} c_{11} & c_{12} & c_{13} & c_{14} & c_{15} & c_{16} \\ c_{12} & c_{22} & c_{23} & c_{24} & c_{25} & c_{26} \\ c_{13} & c_{23} & c_{33} & c_{34} & c_{35} & c_{36} \\ c_{14} & c_{24} & c_{34} & c_{44} & c_{45} & c_{46} \\ c_{15} & c_{25} & c_{35} & c_{45} & c_{55} & c_{56} \\ c_{16} & c_{26} & c_{36} & c_{46} & c_{56} & c_{66} \end{bmatrix} \begin{bmatrix} \varepsilon_1 \\ \varepsilon_2 \\ \varepsilon_3 \\ \varepsilon_4 \\ \varepsilon_5 \\ \varepsilon_6 \end{bmatrix}$$

ISOTROPIC MATERIAL

In the isotropic case the Stiffness tensor will have the form:

$$\begin{bmatrix} c_{11} & c_{12} & c_{12} & 0 & 0 & 0 \\ c_{12} & c_{11} & c_{12} & 0 & 0 & 0 \\ c_{12} & c_{12} & c_{11} & 0 & 0 & 0 \\ 0 & 0 & 0 & \frac{1}{2}(c_{11} - c_{12}) & 0 & 0 \\ 0 & 0 & 0 & 0 & \frac{1}{2}(c_{11} - c_{12}) & 0 \\ 0 & 0 & 0 & 0 & 0 & \frac{1}{2}(c_{11} - c_{12}) \end{bmatrix}$$

In terms of Lamé elastic parameters the matrix assume sthe form:

$$\begin{bmatrix} \lambda + 2\mu & \lambda & \lambda & 0 & 0 & 0 \\ \lambda & \lambda + 2\mu & \lambda & 0 & 0 & 0 \\ \lambda & \lambda & \lambda + 2\mu & 0 & 0 & 0 \\ 0 & 0 & 0 & \mu & 0 & 0 \\ 0 & 0 & 0 & 0 & \mu & 0 \\ 0 & 0 & 0 & 0 & 0 & \mu \end{bmatrix}$$

ISOTROPY: The upper left 3x3 submatrix is responsible for the normal stresses

$$\begin{bmatrix} \lambda + 2\mu & \lambda & \lambda & 0 & 0 & 0 \\ \lambda & \lambda + 2\mu & \lambda & 0 & 0 & 0 \\ \lambda & \lambda & \lambda + 2\mu & 0 & 0 & 0 \\ 0 & 0 & 0 & \mu & 0 & 0 \\ 0 & 0 & 0 & 0 & \mu & 0 \\ 0 & 0 & 0 & 0 & 0 & \mu \end{bmatrix}$$

VTI ANISOTROPY

For a simple case of anisotropic material, we can notice how the stiffnesss tensor is described by 5 parameters , additionally the $V_P = \mathbf{V}$ which depend on the direction of propagation must be considered at the proper position C13, C23 ,etc.

$$\begin{bmatrix} \lambda_\perp + 2\mu_\perp & \lambda_\perp & \upsilon & 0 & 0 & 0 \\ \lambda_\perp & \lambda_\perp + 2\mu_\perp & \upsilon & 0 & 0 & 0 \\ \upsilon & \upsilon & \lambda_\parallel + 2\mu_\parallel & 0 & 0 & 0 \\ 0 & 0 & 0 & \mu_\parallel & 0 & 0 \\ 0 & 0 & 0 & 0 & \mu_\parallel & 0 \\ 0 & 0 & 0 & 0 & 0 & \mu_\perp \end{bmatrix}$$

ZOEPPRITZ EQUATIONS

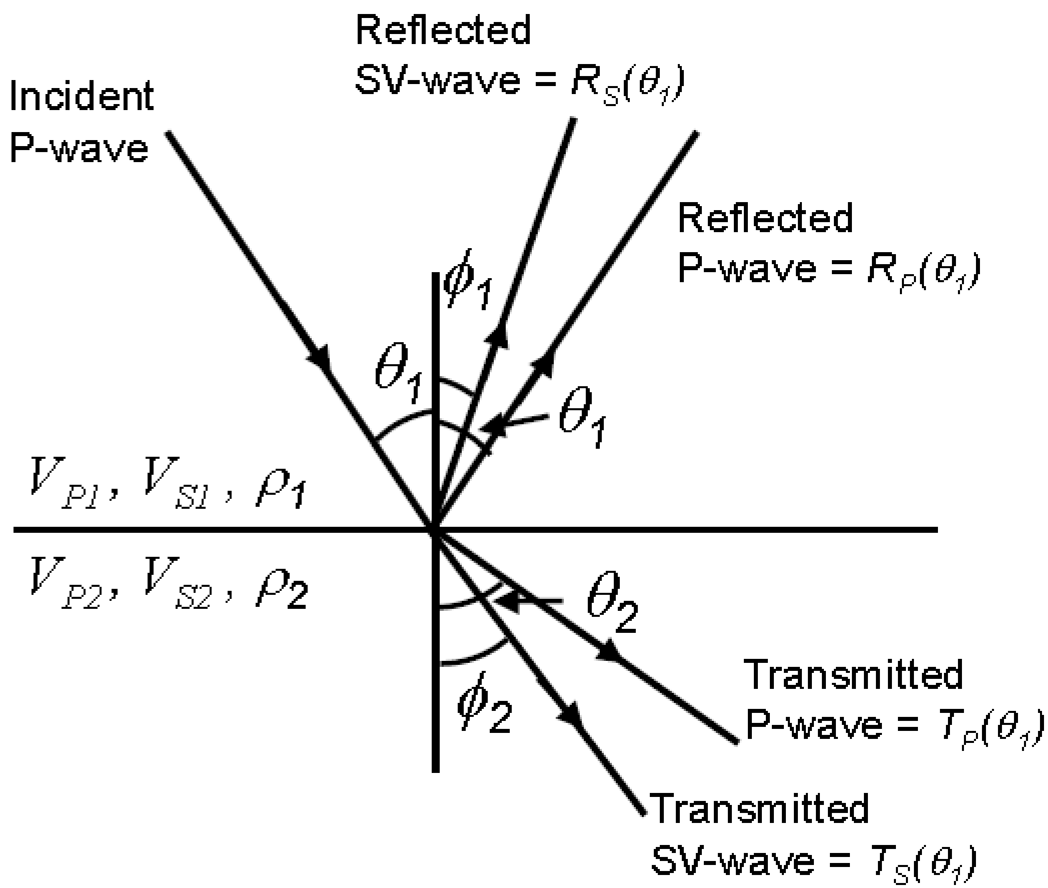

E conservation – Seismic Impedance – Elastic Impedance – Reflection Coefficients

ZOEPPRITZ

P incident wave with amplitude Ap=1

$$\begin{bmatrix} R_P(\theta_1) \\ R_S(\theta_1) \\ T_P(\theta_1) \\ T_S(\theta_1) \end{bmatrix} = \begin{bmatrix} -\sin\ \theta_1 & -\cos\ \phi_1 & \sin\ \theta_2 & \cos\ \phi_2 \\ \cos\ \theta_1 & -\sin\ \phi_1 & \cos\ \theta_2 & -\sin\ \phi_2 \\ \sin\ 2\theta_1 & \dfrac{V_{P1}}{V_{S1}}\cos\ 2\phi_1 & \dfrac{\rho_2 V_{S2}^{\,2} V_{P1}}{\rho_1 V_{S1}^{\,2} V_{P2}}\cos\ 2\phi_1 & \dfrac{\rho_2 V_{S2} V_{P1}}{\rho_1 V_{S1}^{\,2}}\cos\ 2\phi_2 \\ -\cos\ 2\phi_1 & \dfrac{V_{S1}}{V_{P1}}\sin\ 2\phi_1 & \dfrac{\rho_2 V_{P2}}{\rho_1 V_{P1}}\cos\ 2\phi_2 & -\dfrac{\rho_2 V_{S2}}{\rho_1 V_{P1}}\sin\ 2\phi_2 \end{bmatrix}^{-1} \begin{bmatrix} \sin\ \theta_1 \\ \cos\ \theta_1 \\ \sin\ 2\theta_1 \\ \cos\ 2\phi_1 \end{bmatrix}$$

$$\begin{bmatrix} R_P(0^\circ) \\ R_S(0^\circ) \\ T_P(0^\circ) \\ T_S(0^\circ) \end{bmatrix} = \begin{bmatrix} R_{P0} \\ R_{S0} \\ T_{P0} \\ T_{S0} \end{bmatrix} = \begin{bmatrix} 0 & -1 & 0 & 1 \\ 1 & 0 & 1 & 0 \\ 0 & \dfrac{V_{P1}}{V_{S1}} & 0 & \dfrac{\rho_2 V_{S2} V_{P1}}{\rho_1 V_{S1}^{\,2}} \\ -1 & 0 & \dfrac{\rho_2 V_{P2}}{\rho_1 V_{P1}} & 0 \end{bmatrix}^{-1} \begin{bmatrix} 0 \\ 1 \\ 0 \\ 1 \end{bmatrix}$$

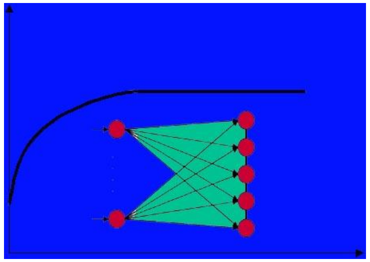

STD PROCESSING SEQUENCE

Field Tapes and Observer's Log

(1) Preprocessing:
- **Demultiplexing**
- **Reformatting**
- **Editing**
- **Geometric Spreading Correction**
- **Setup of Field Geometry**
- **Application of Field Statics**

(2) Deconvolution and Trace Balancing

(3) CMP Sorting

(4) Velocity Analysis

(5) Residual Statics Corrections

(6) Velocity Analysis

(7) NMO Correction

(8) DMO Correction

(9) Inverse NMO Correction

(10) Velocity Analysis

(11) NMO Correction, Muting and Stacking

(12) Deconvolution

(13) Time-Variant Spectral Whitening

(14) Time-Variant Filtering

(15) Migration

(16) Gain Application

BASIC CONCEPTS

- Geometry
- Spread ~ 1/r2
- Bin
- Fold
- Source Domain / Gather - CMP Gather
- NMO Correction
- Stack
- Kirchhoff Migration

CMP

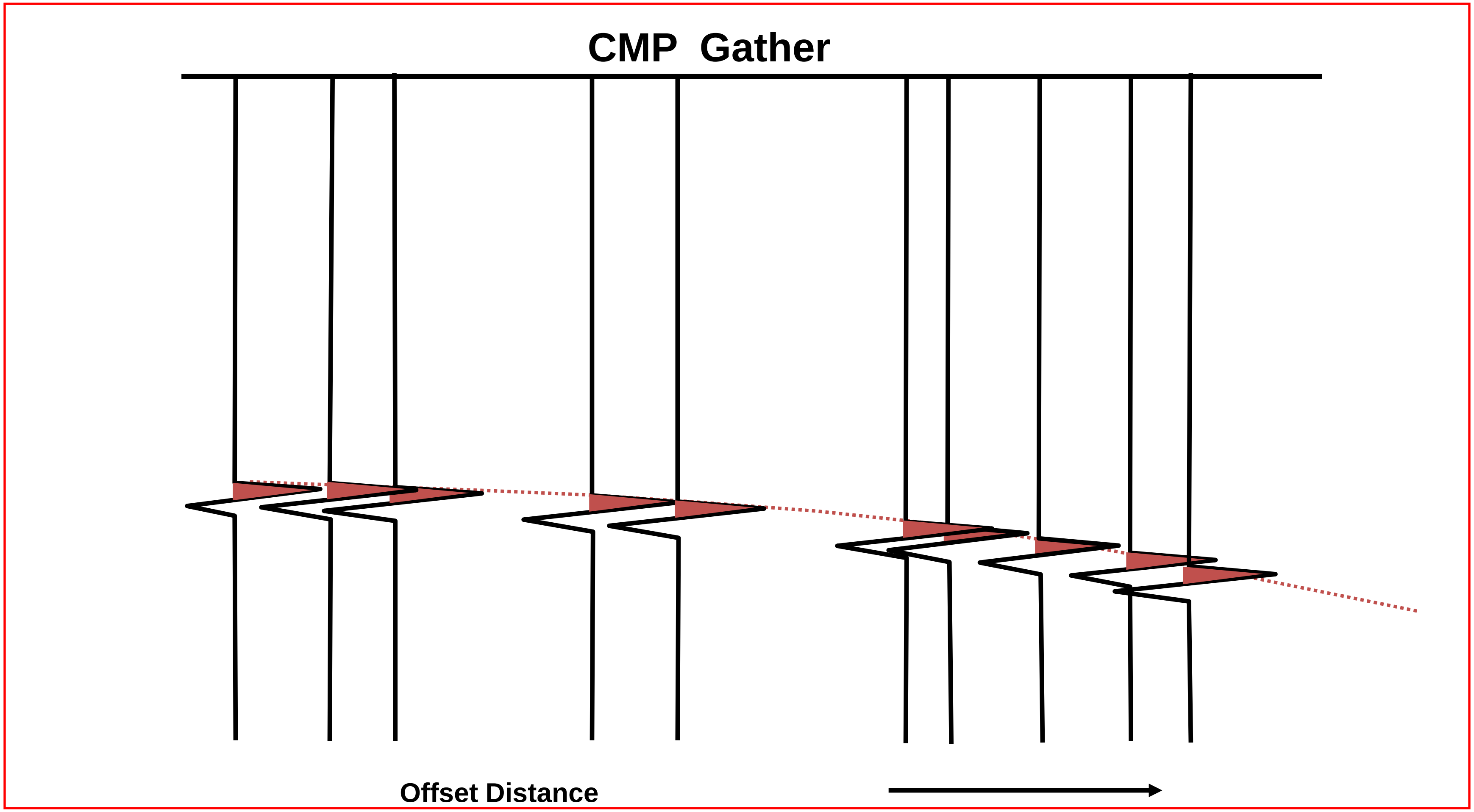

AFTER NMO CORRECTION

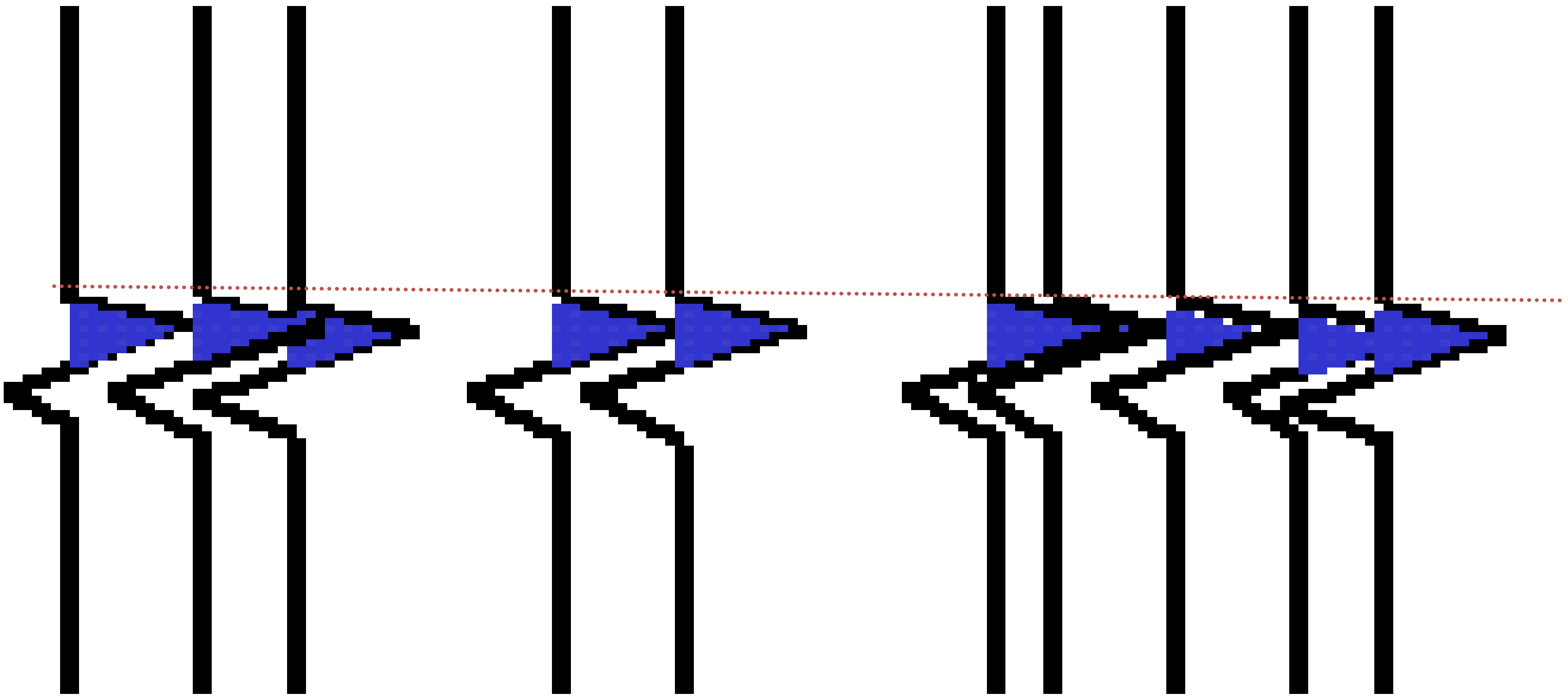

VELOCITY ANALYSIS

Coherency Measure

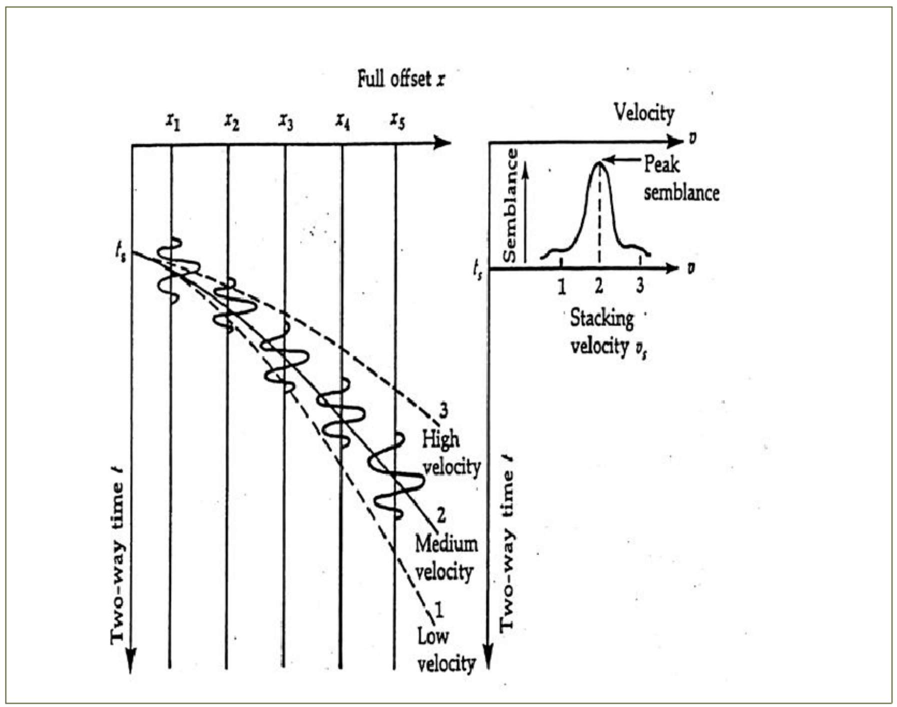

VELOCITY ANALYSIS

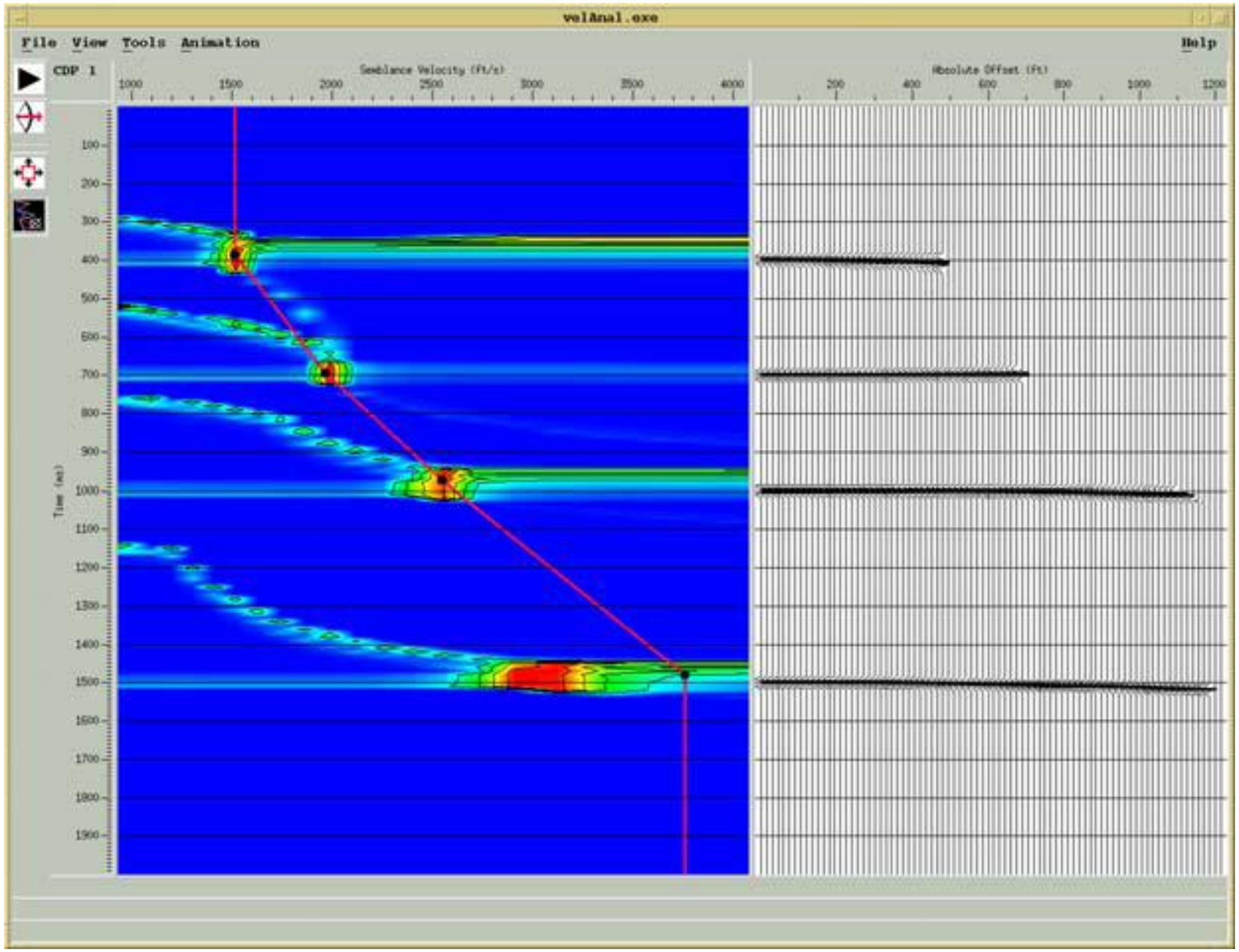

NMO-STACKING SEQUENCE

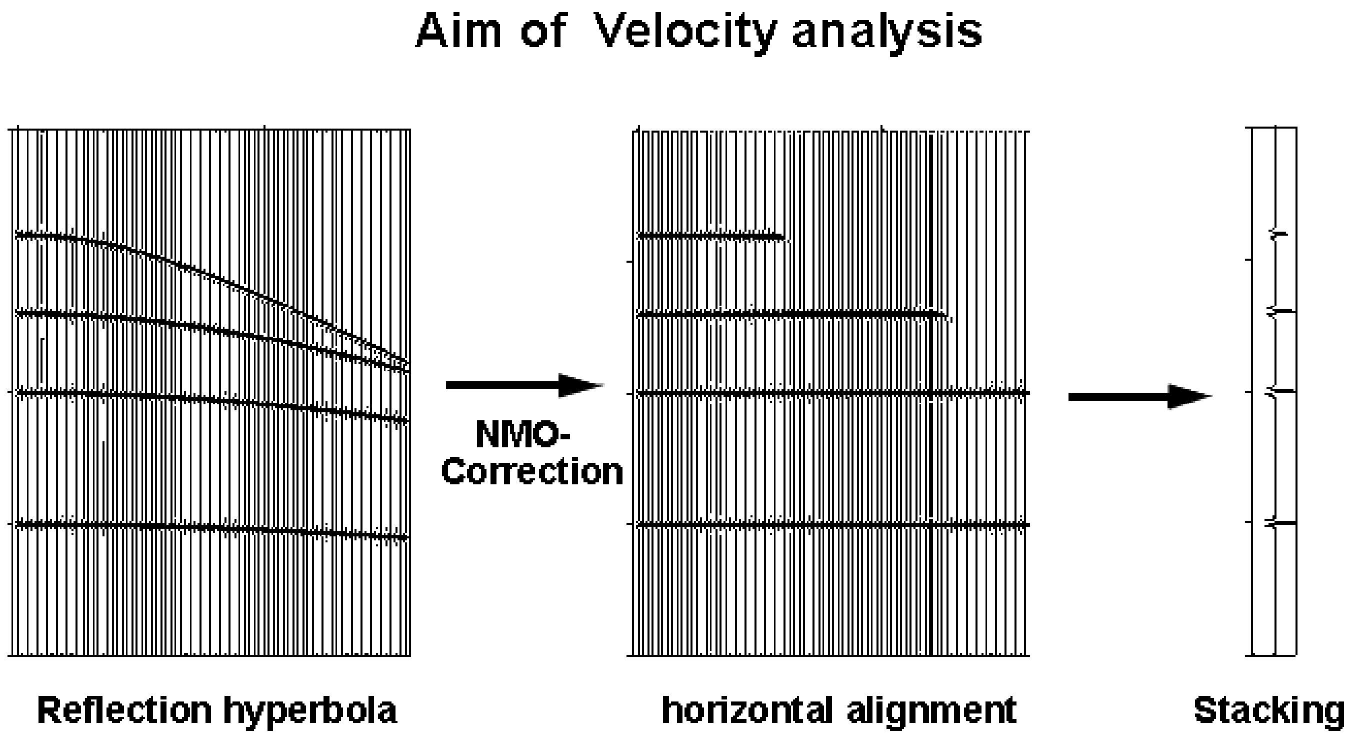

(NMO = Normal Moveout)

SIGNAL / NOISE RATIO AND STACKING

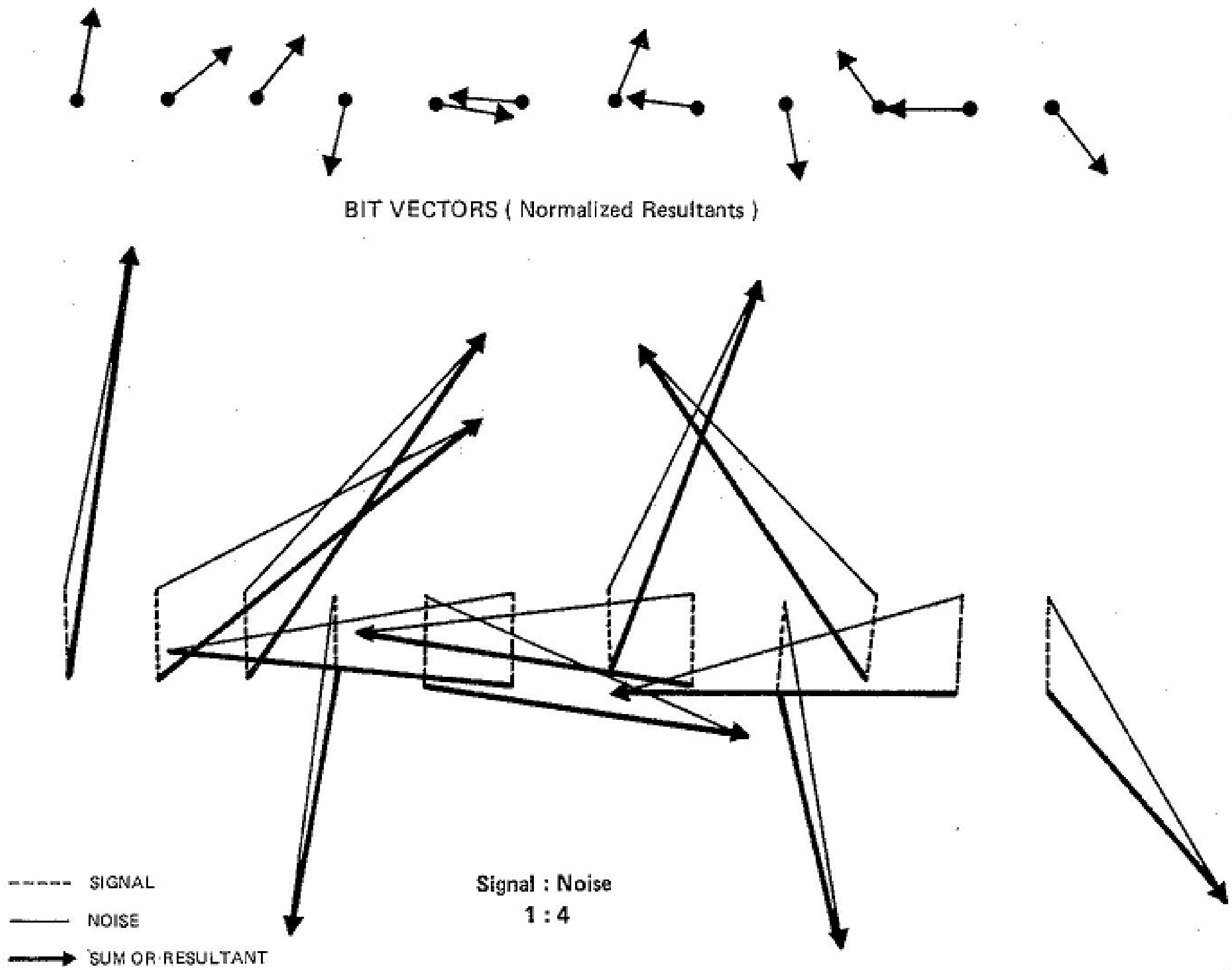

MIGRATION CONCEPTS

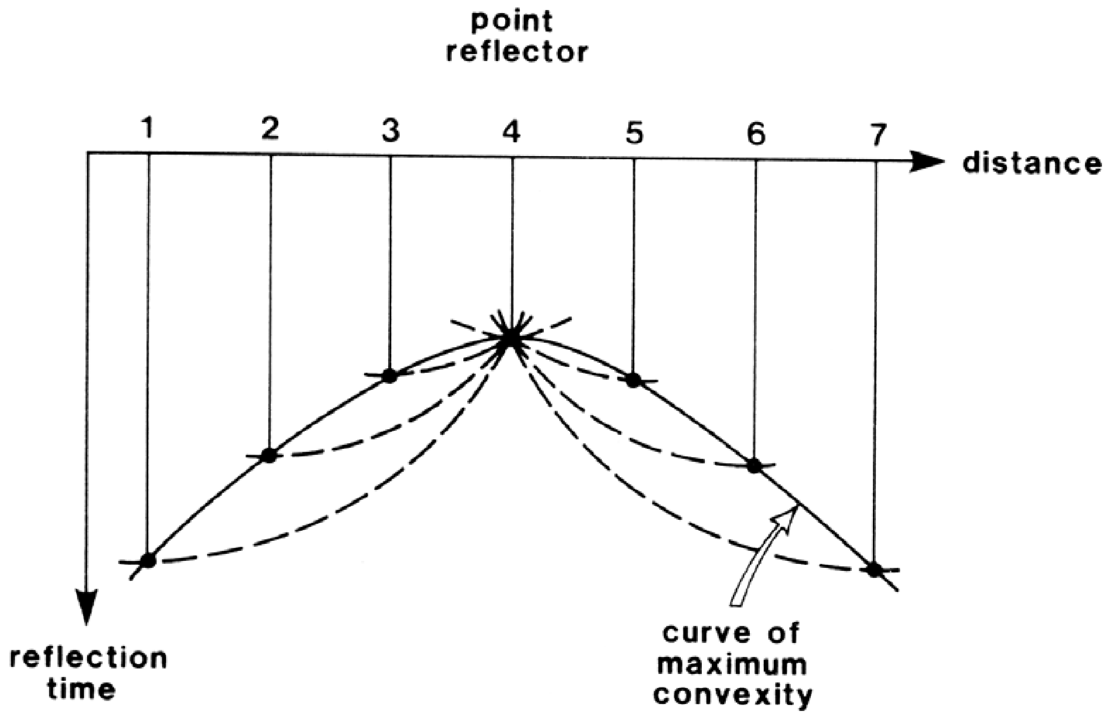

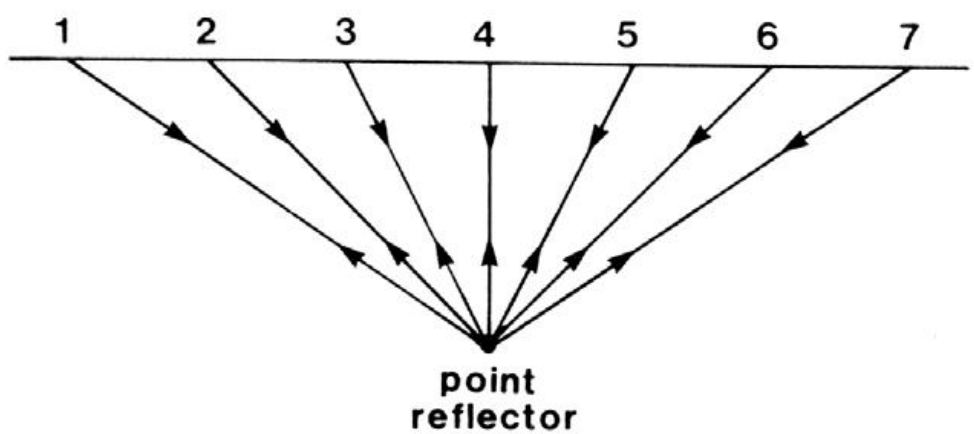

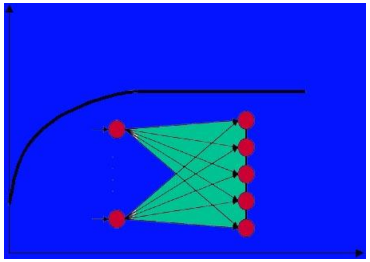

QUANTITATIVE SEISMIC INVERSION

- Prestack
- Poststack
- Stochastic
- Attributes
- FWI

The Aki-Richards linearized Zoeppritz equation has the form (Fatti):

$$R_p(\theta) = p \frac{\Delta V_p}{2V_p} + q \frac{\Delta V_s}{2V_s} + r \frac{\Delta \rho}{2\rho}$$

Where: **p,q,r** are the weights function of the incidence angle **q** which multiply the elastic Parameters.

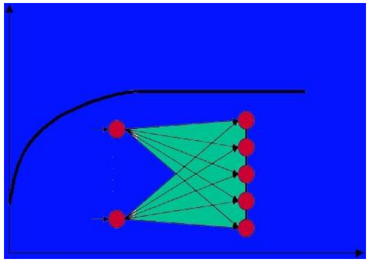

Reflectivity Aki-Richards (Wiggins)

$$R_P(\theta) = A + B\sin^2\theta + C\tan^2\theta\sin^2\theta, \text{ where:}$$

$$A = \frac{1}{2}\left[\frac{\Delta V_P}{V_p} + \frac{\Delta\rho}{\rho}\right], B = \frac{1}{2}\frac{\Delta V_P}{V_p} - 4\left[\frac{V_S}{V_P}\right]^2\frac{\Delta V_S}{V_S} - 2\left[\frac{V_S}{V_P}\right]^2\frac{\Delta\rho}{\rho}, C = \frac{1}{2}\frac{\Delta V_P}{V_p}.$$

Reflectivity Aki-Richards (Fatti)

$$R_P(\theta) = c_1 R_P(0^\circ) + c_2 R_S(0^\circ) + c_3 R_D, \text{ where:}$$

$$c_1 = 1 + \tan^2\theta, c_2 = -8(V_S/V_P)^2\sin^2\theta, c_3 = 4(V_S/V_P)^2\sin^2\theta - \tan^2\theta,$$

$$R_P(0^\circ) = \frac{1}{2}\left[\frac{\Delta V_P}{V_P} + \frac{\Delta\rho}{\rho}\right], R_S(0^\circ) = \frac{1}{2}\left[\frac{\Delta V_S}{V_S} + \frac{\Delta\rho}{\rho}\right], \text{and } R_D = \frac{\Delta\rho}{\rho}.$$

AVO applied on CDP GATHERS

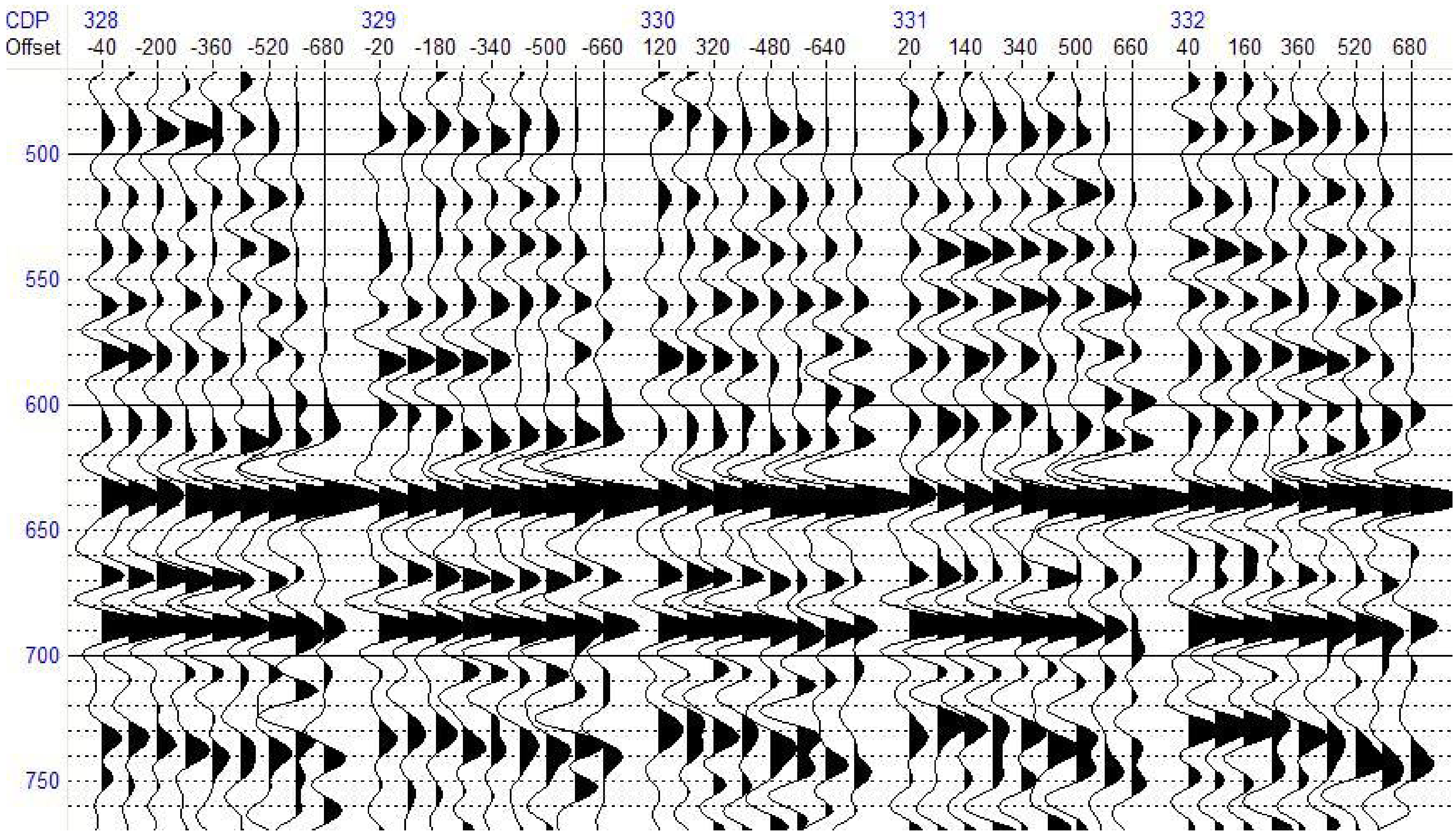

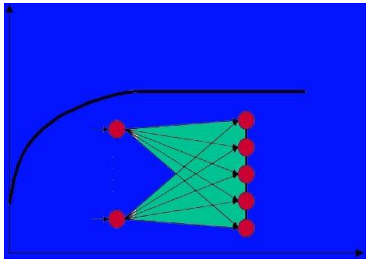

Wiggins extracted in the Aki-Richards equation the 3 components **A,B,C** thus also deriving from Zoeppritz (not zero-offset incidence equations). Where: **A** = linearized zero-offset reflection coefficient (Intercept), **B**= Gradient **C**= Curvature.

$Rp(\theta) = A + B \sin^2\theta + C \tan^2\theta \sin^2\theta$ Aki-Richards (Wiggins et al. modified version)

Further, Fatti derived a linearization where the elastic parameters are expressed as Zero-Offset Reflections coefficients: **Rp(0), Rs(0), Rd**.

Following this both Wiggins variant and Fatti variant contain the weighting Coefficient $\frac{\Delta\rho}{\rho}$.

Shuey Linearization of Zoeppritz Equations (be aware of different notations from Fatti and Wiggins)

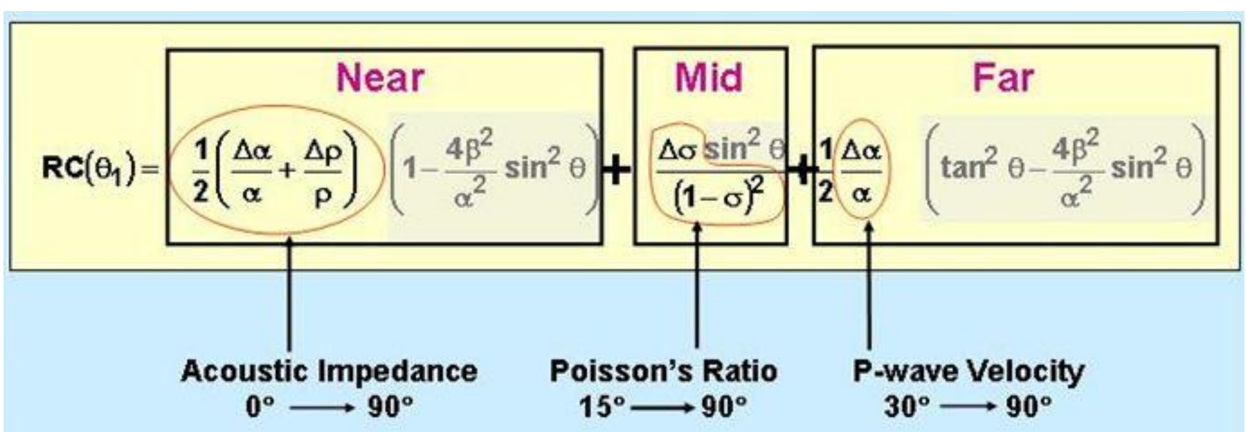

Courtesy Fred Hilterman Geokinetics

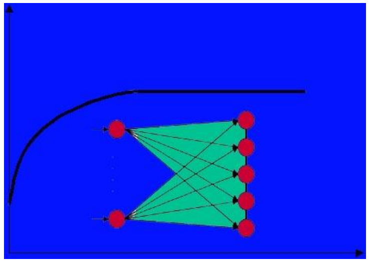

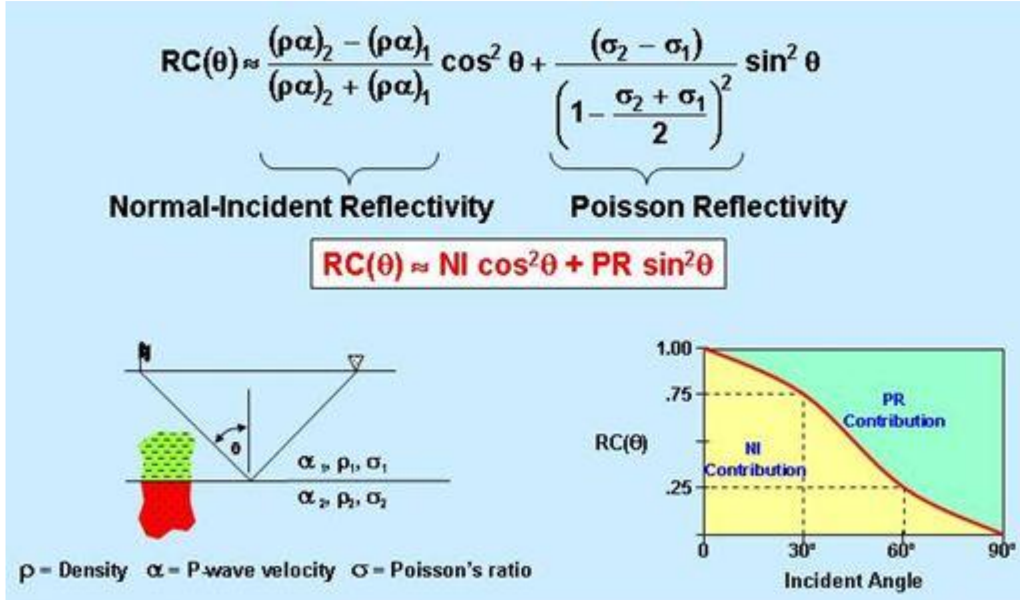

Angle stack reflectivities

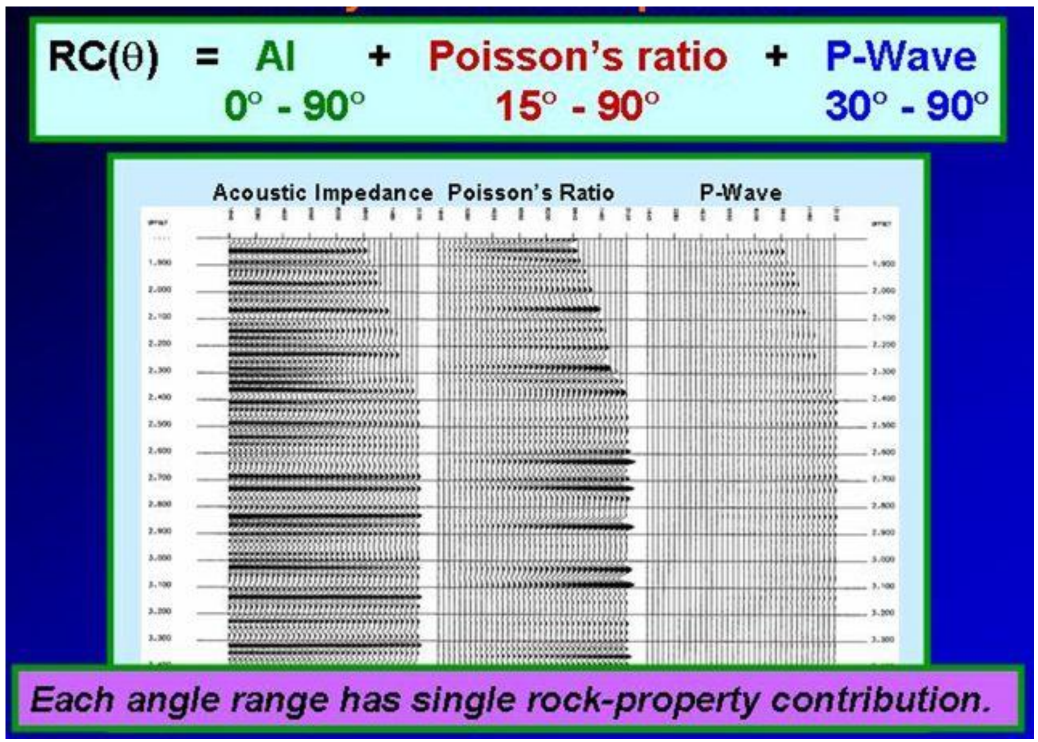

Courtesy Fred Hilterman Geokinetics

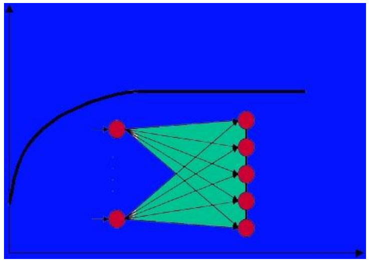

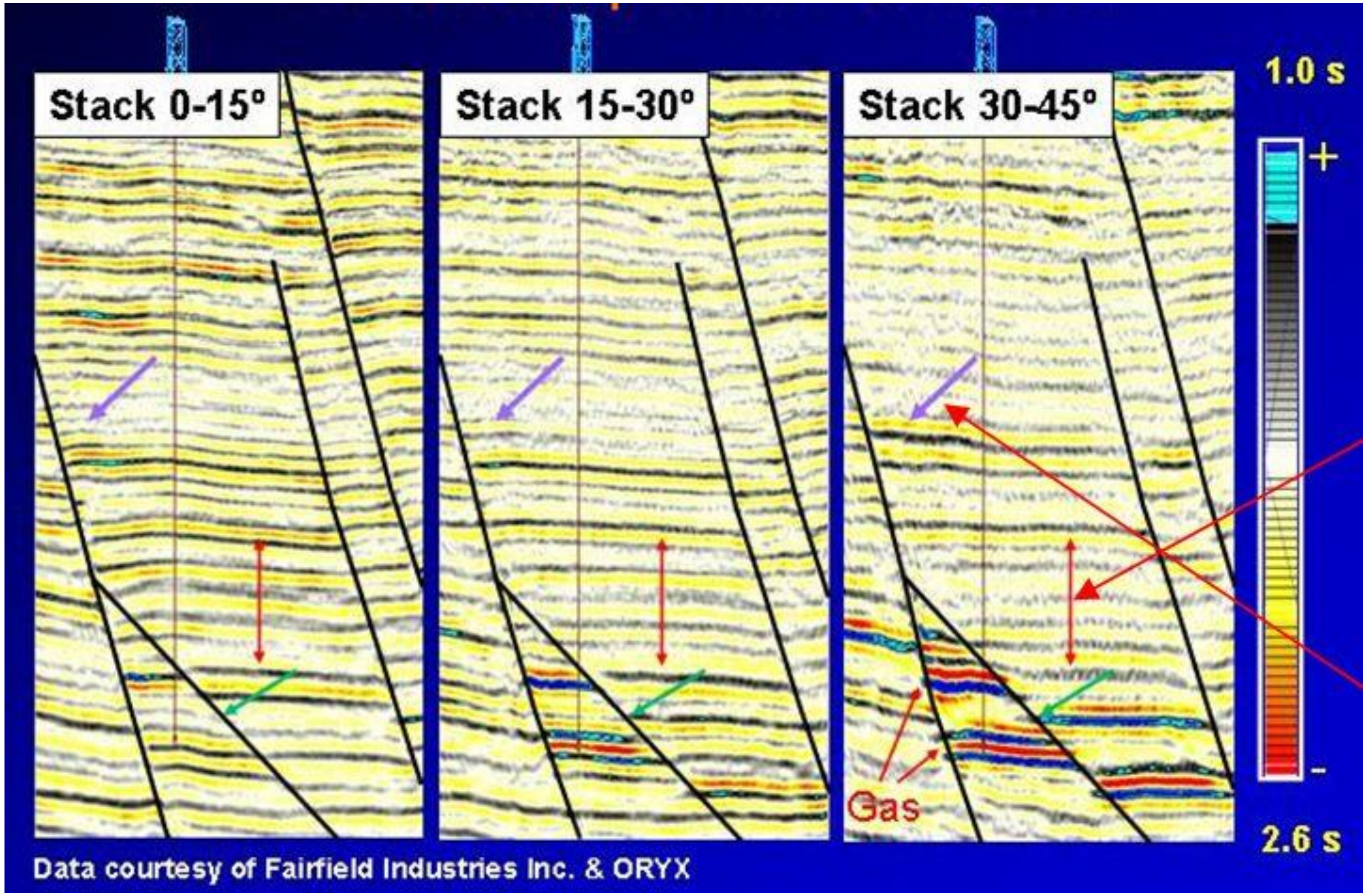

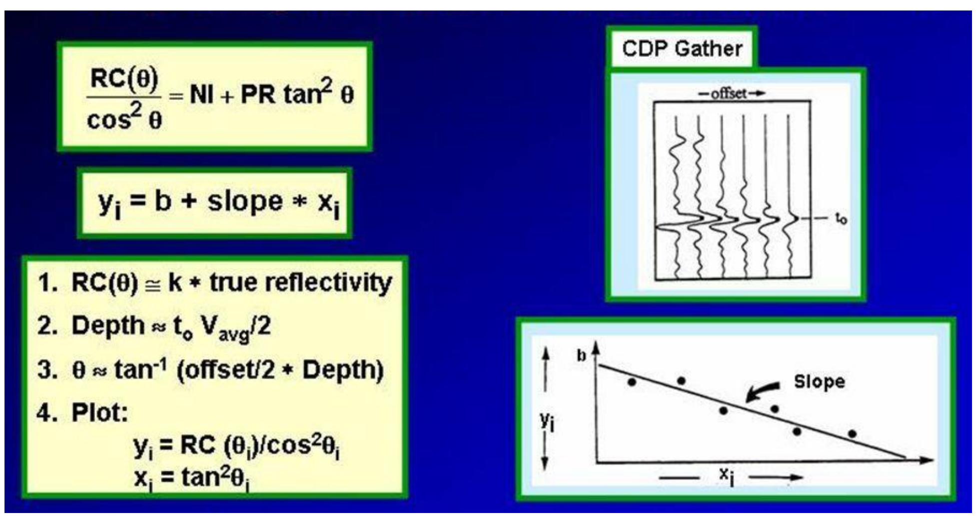

Courtesy Fred Hilterman Geokinetics

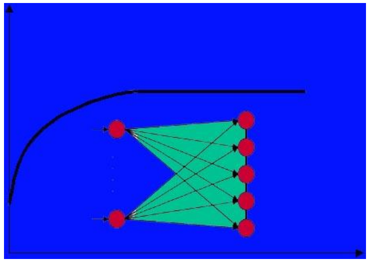

AVO CLASSIFICATION

CLASS 3: < 9000 Ft/Sec

CLASS 2: 9000 - 14000 Ft/Sec

CLASS 1: ANY TIME WE HAVE A SAND W/ V>14000Ft/Sec

Courtesy Fred Hilterman Geokinetics

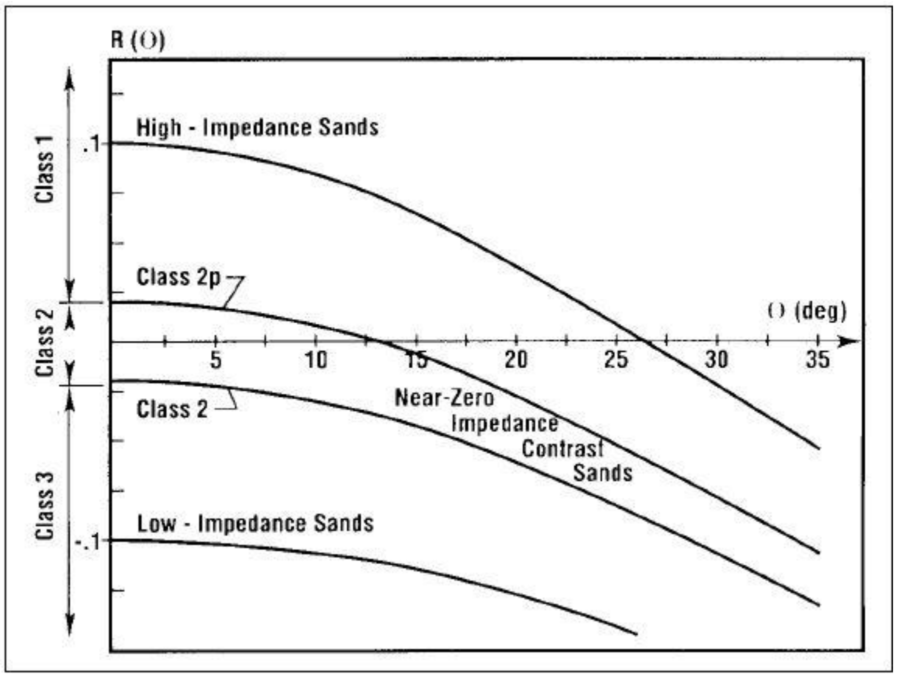

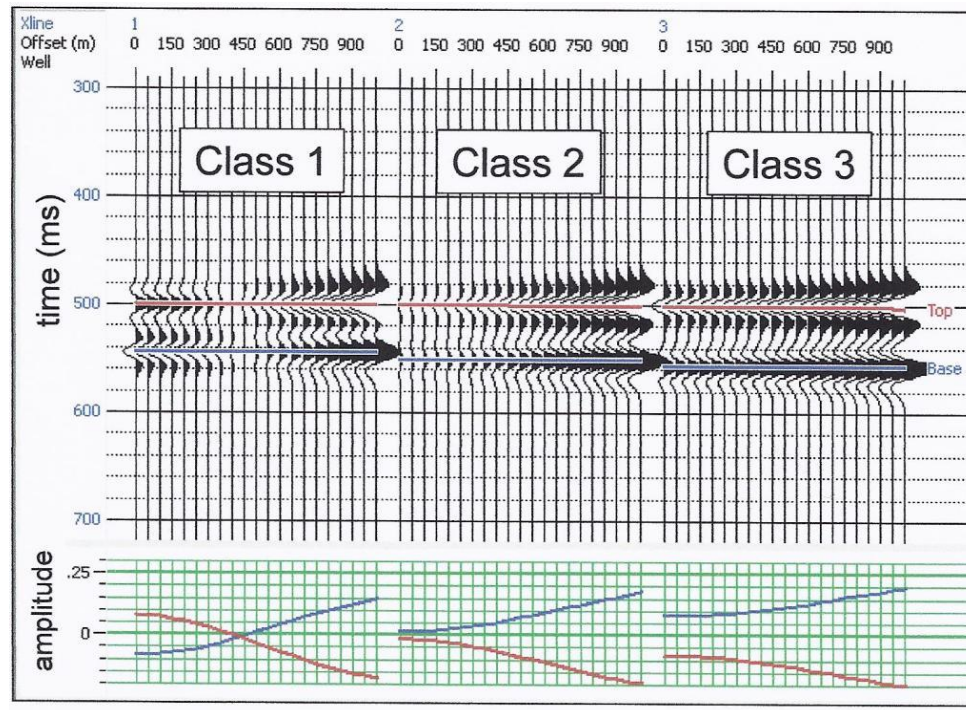

Courtesy Dan Hampson, Brian Russell Hampson-Russell / CGG

BASIC AVO ATTRIBUTES

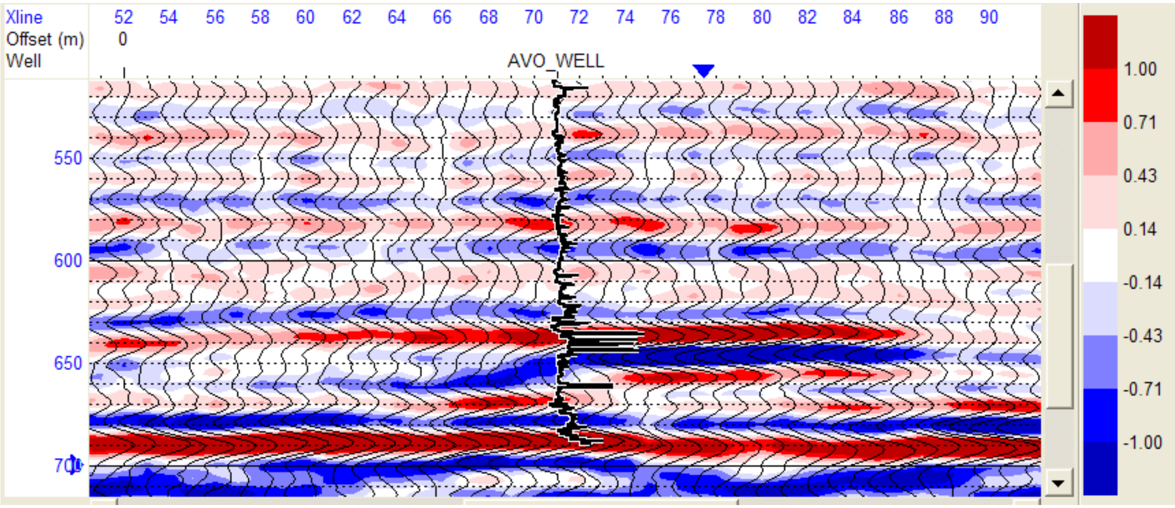

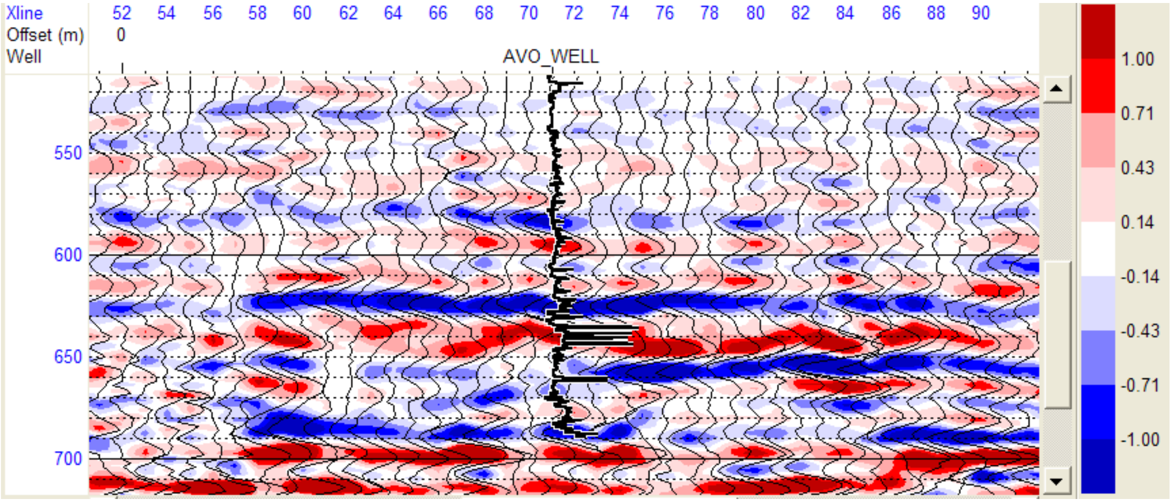

Courtesy Dan Hampson, Brian Russell Hampson-Russell / CGG

POSTSTACK INVERSION - CONVOLUTION

Convolution with the seismic wavelet, which can be written mathematically as $S = W*R$, is illustrated pictorially below:

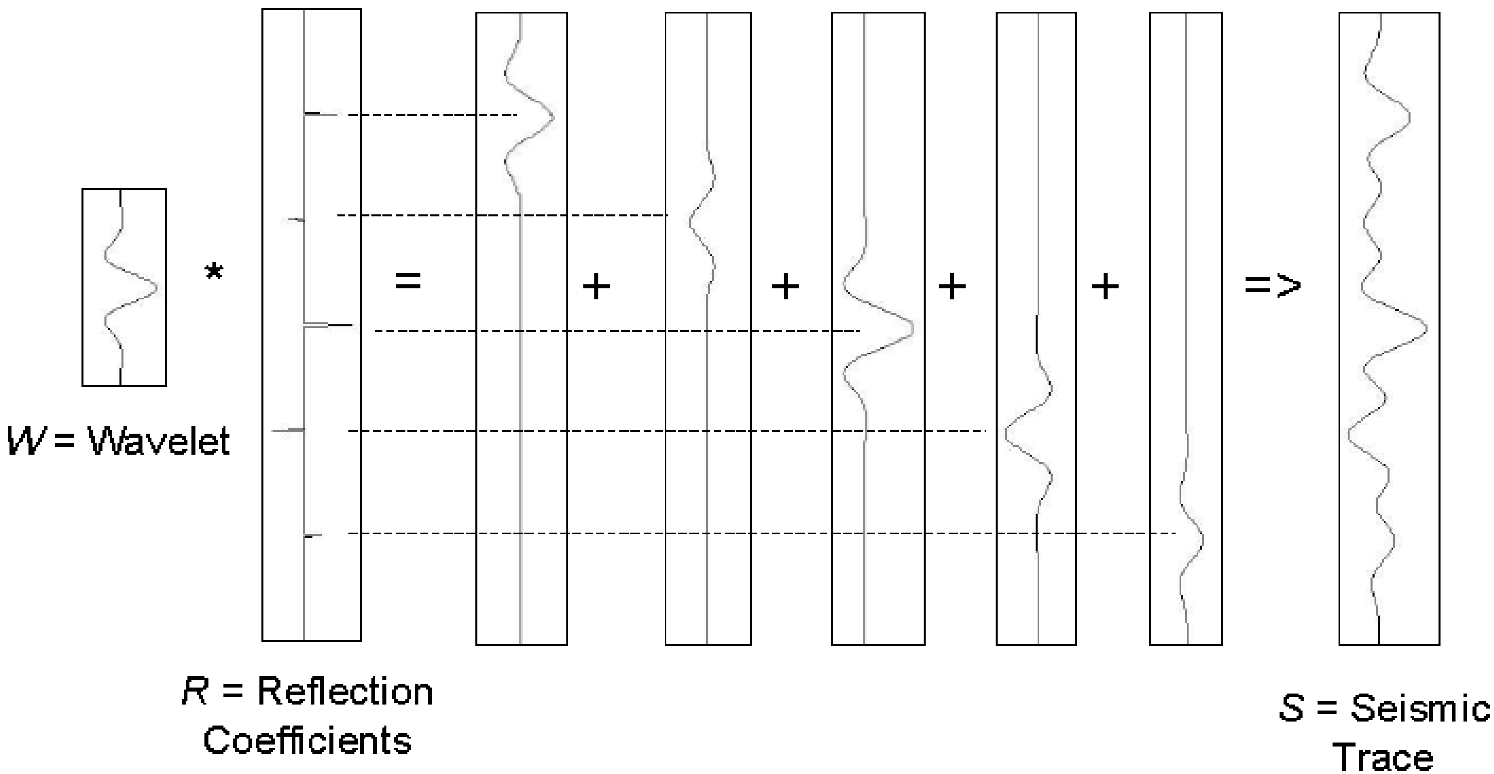

Courtesy Dan Hampson, Brian Russell Hampson-Russell / CGG

Banisotropy

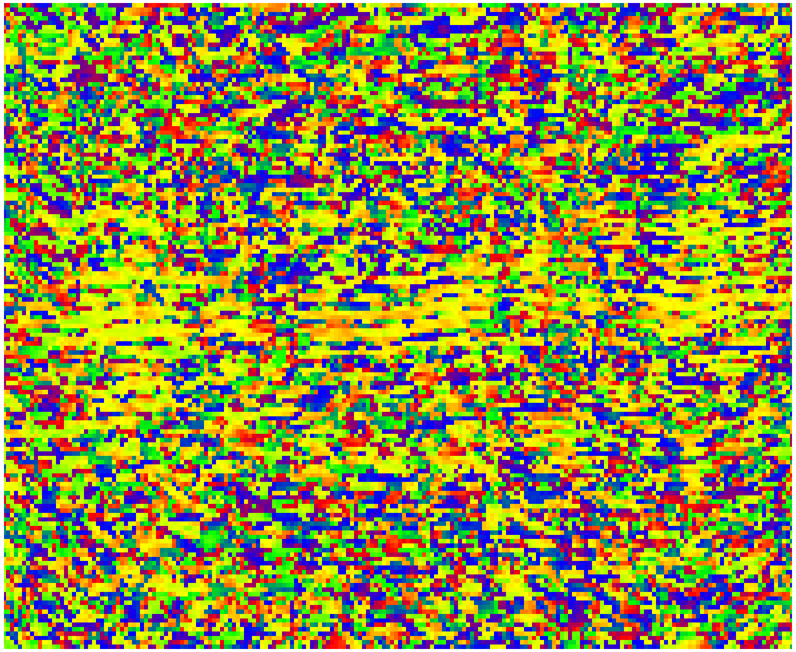

Courtesy Dan Hampson, Brian Russell   Hampson-Russell / CGG

SEISMIC INVERSION – ACUSTIC IMPEDANCE MODEL

The acoustic impedance model

To physically understand elastic impedance, let us start with the model that forms the basis for acoustic impedance inversion:

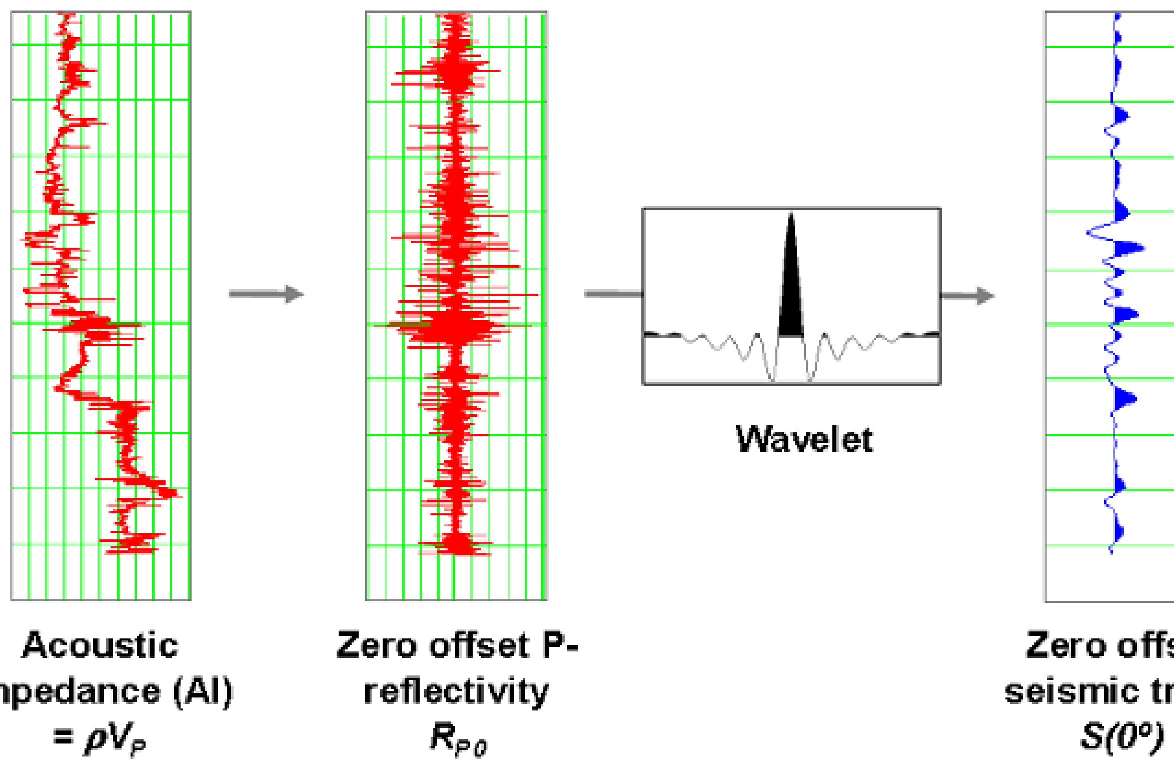

Courtesy Dan Hampson, Brian Russell Hampson-Russell / CGG

SEISMIC INVERSION – ELASTIC IMPEDANCE MODEL

The elastic impedance model

The model that forms the basis for elastic impedance inversion is therefore simply an extension of the acoustic impedance model:

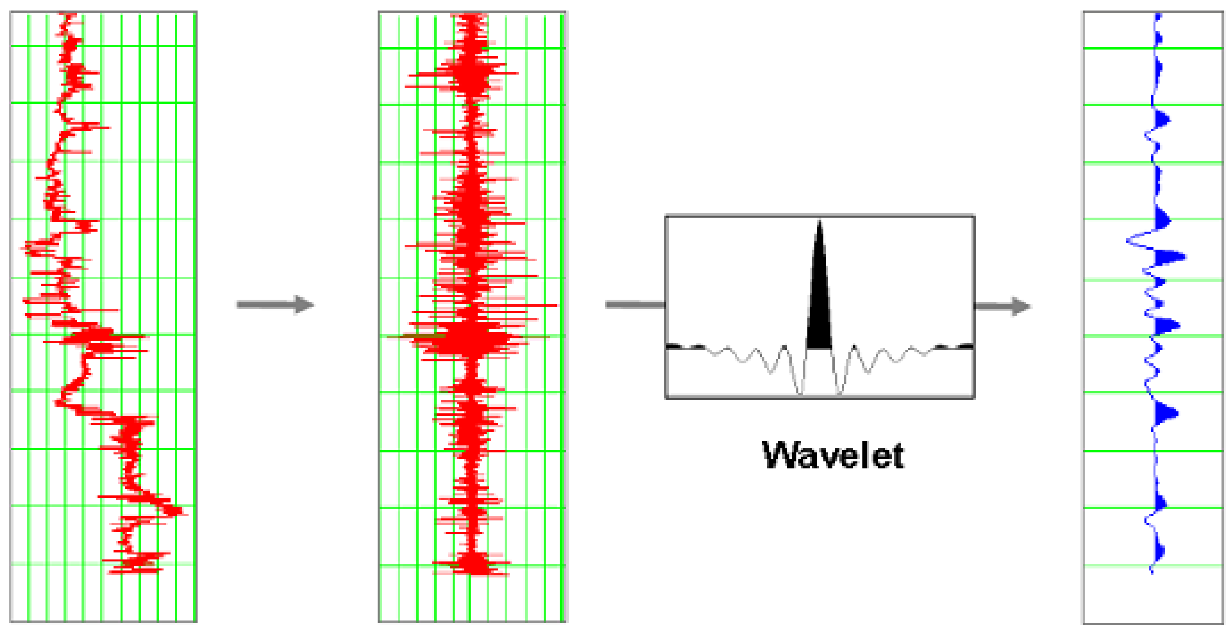

Elastic Impedance (*EI*) = $V_P{}^a V_S{}^b \rho^c$

Aki-Richards reflectivity at θ $R_P(\theta)$

Seismic trace at angle θ $S(\theta)$

Courtesy Dan Hampson, Brian Russell Hampson-Russell / CGG

ELASTIC INVERSION RESULTS

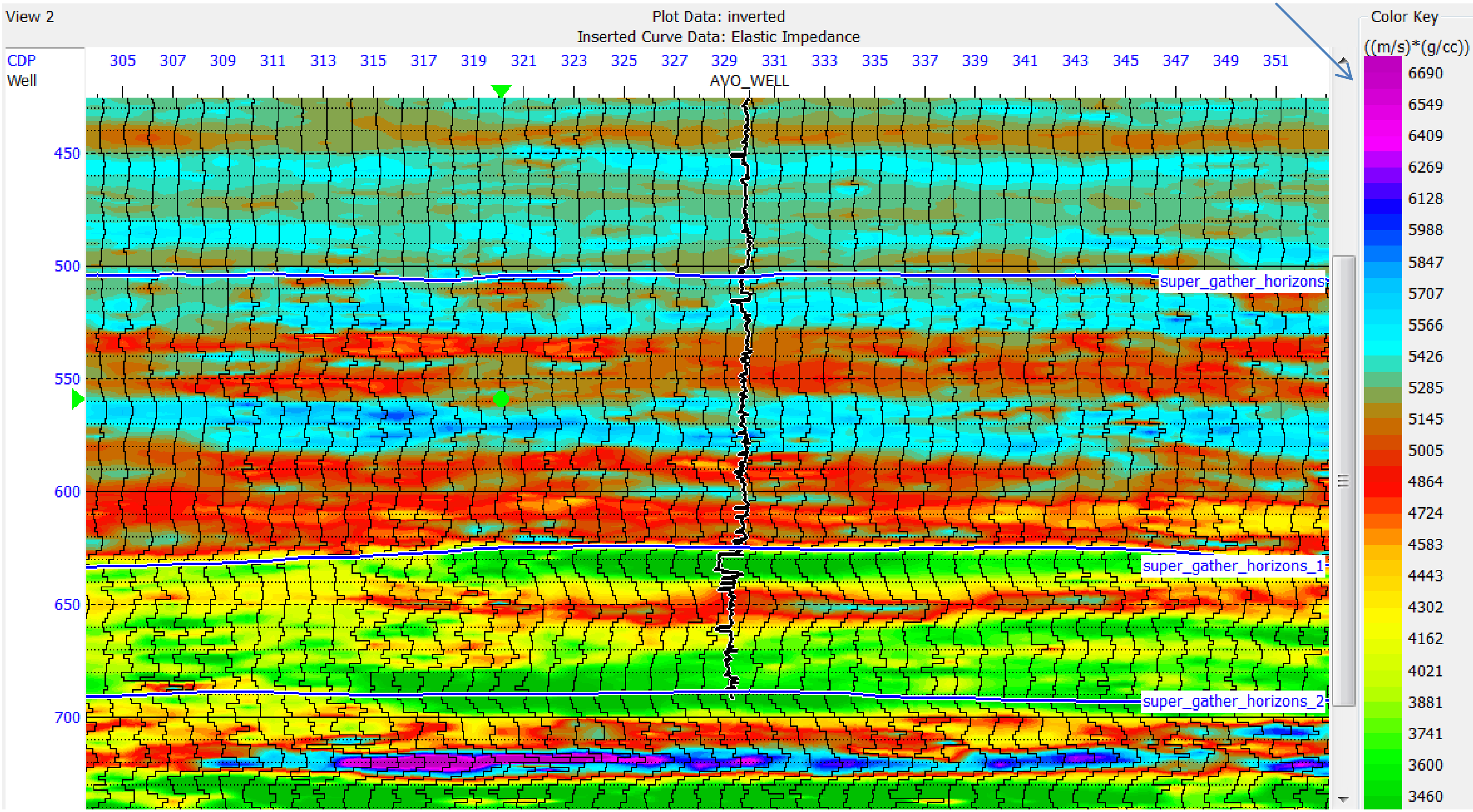

Courtesy Dan Hampson, Brian Russell Hampson-Russell / CGG

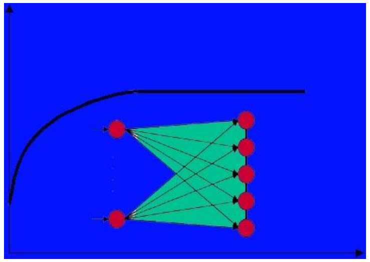

PRESTACK INVERSIONS

- INDEPENDENT INVERSION
- SIMULTANEOUS INVERSIO
- LAMBDA – MU RHO

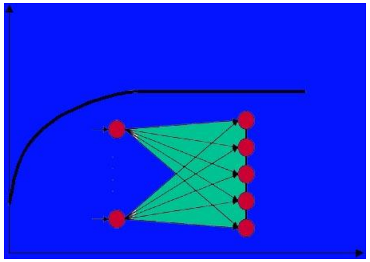

POST STACK SEISMIC INVERSION

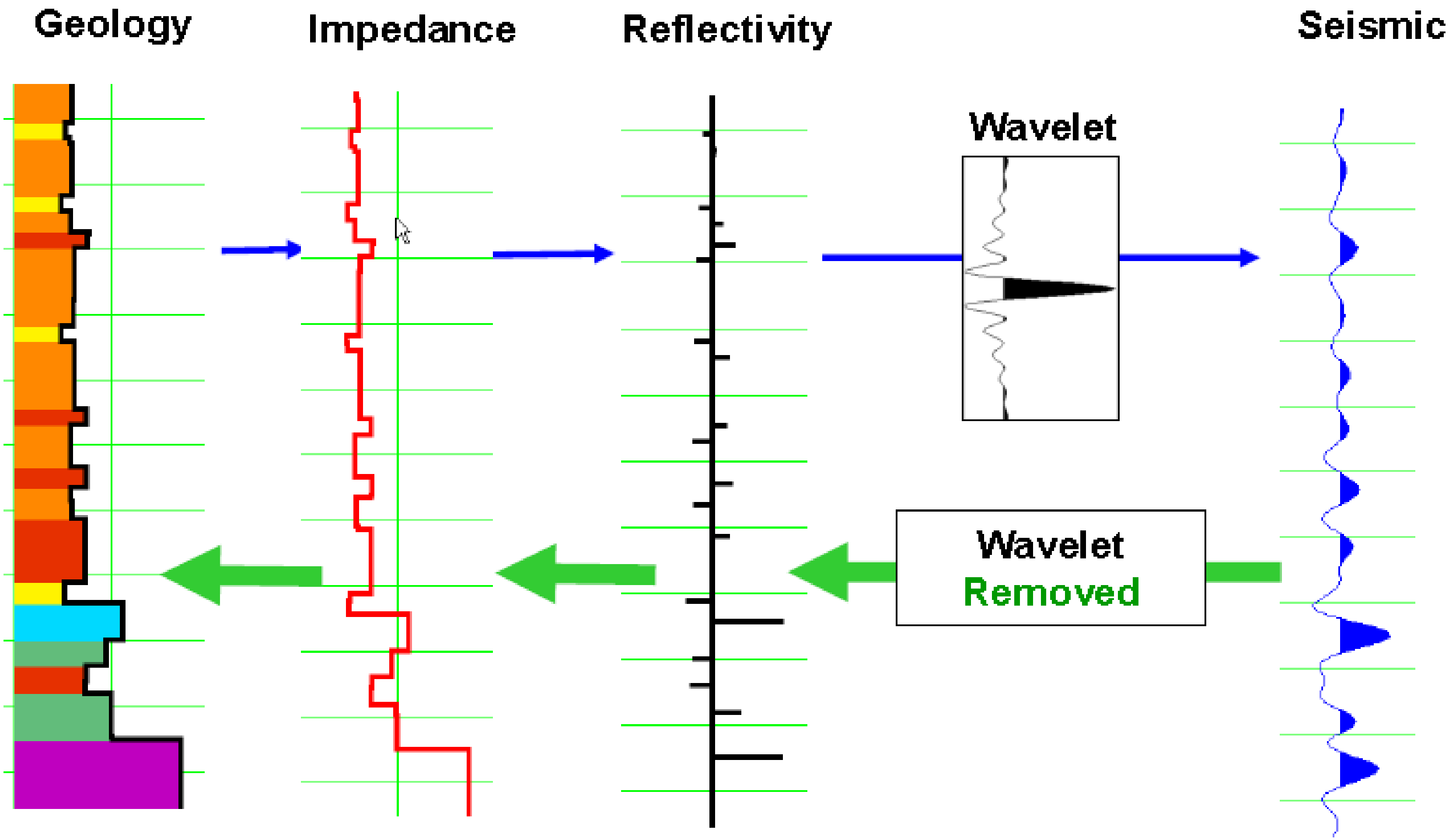

Courtesy Dan Hampson, Brian Russell Hampson-Russell / CGG

WAVELETS SAME AMPLITUDE AND DIFFERENT PHASE

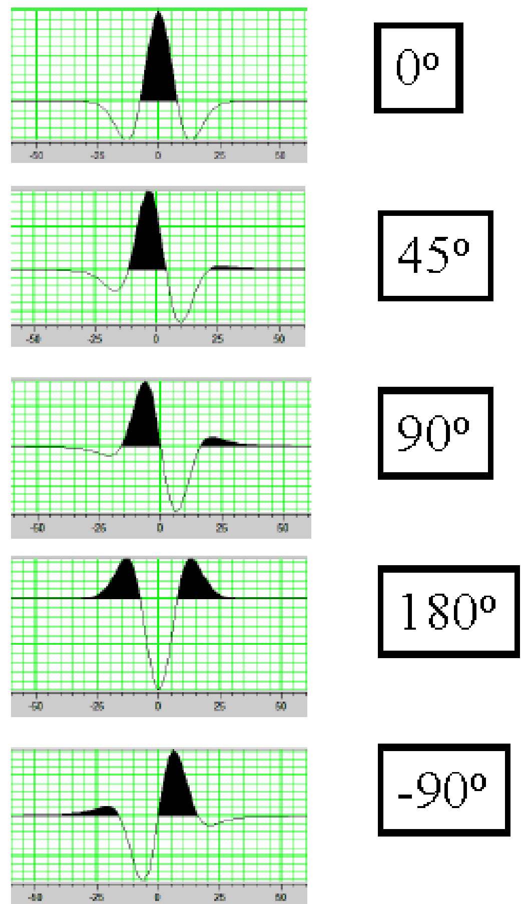

Courtesy Dan Hampson, Brian Russell Hampson-Russell / CGG

ACOUSTIC IMPEDANCE CALCULATION - LOGS DO NOT CONTAIN LOW FREQUENCIES

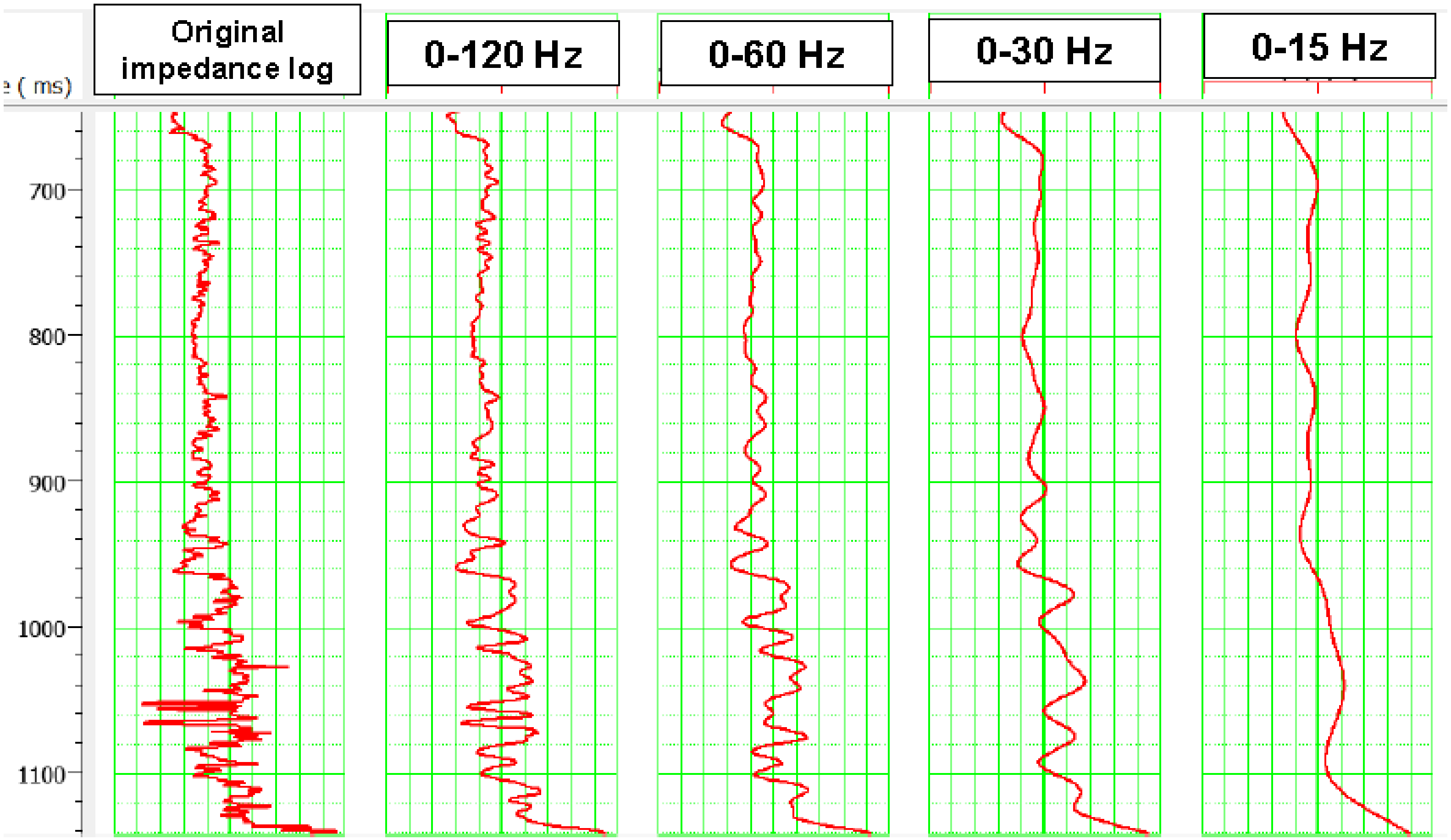

Courtesy Dan Hampson, Brian Russell Hampson-Russell / CGG

POSTSTACK INVERSION RESULTS

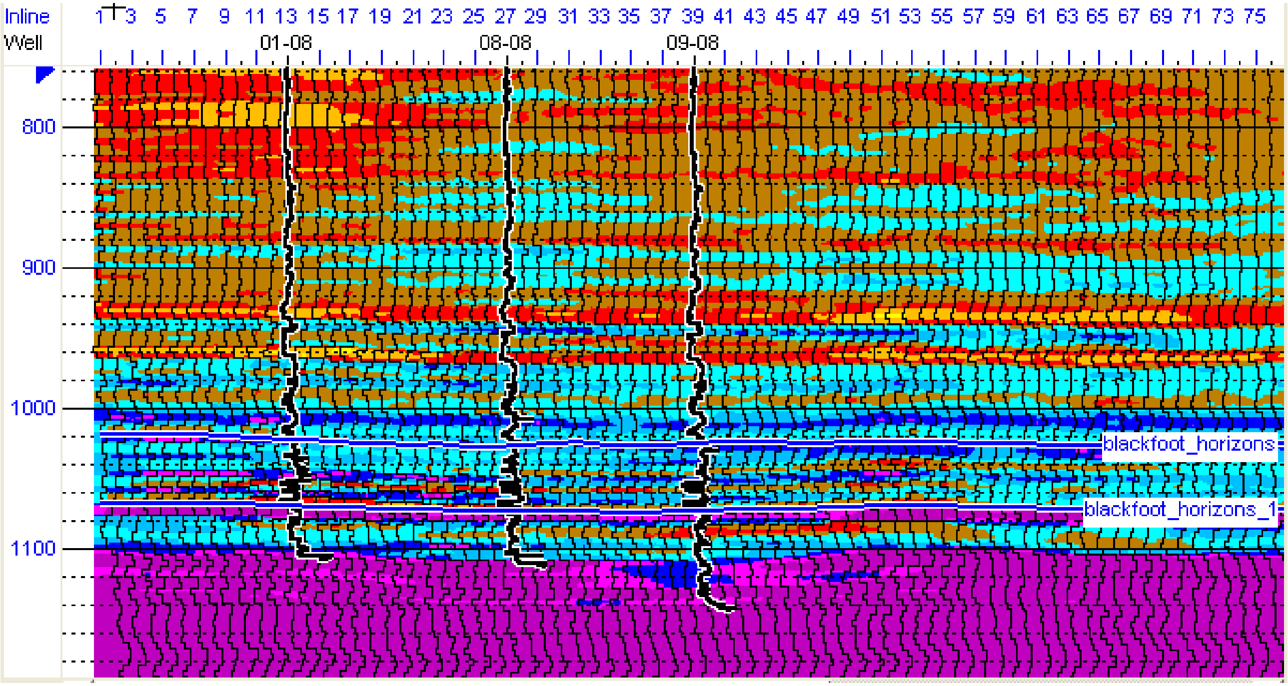

Courtesy Dan Hampson, Brian Russell Hampson-Russell / CGG

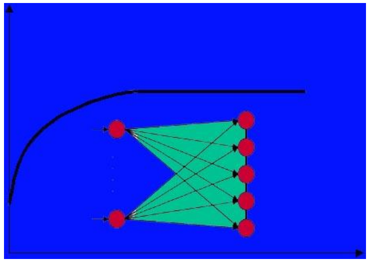

STOCHASTIC INVERSION

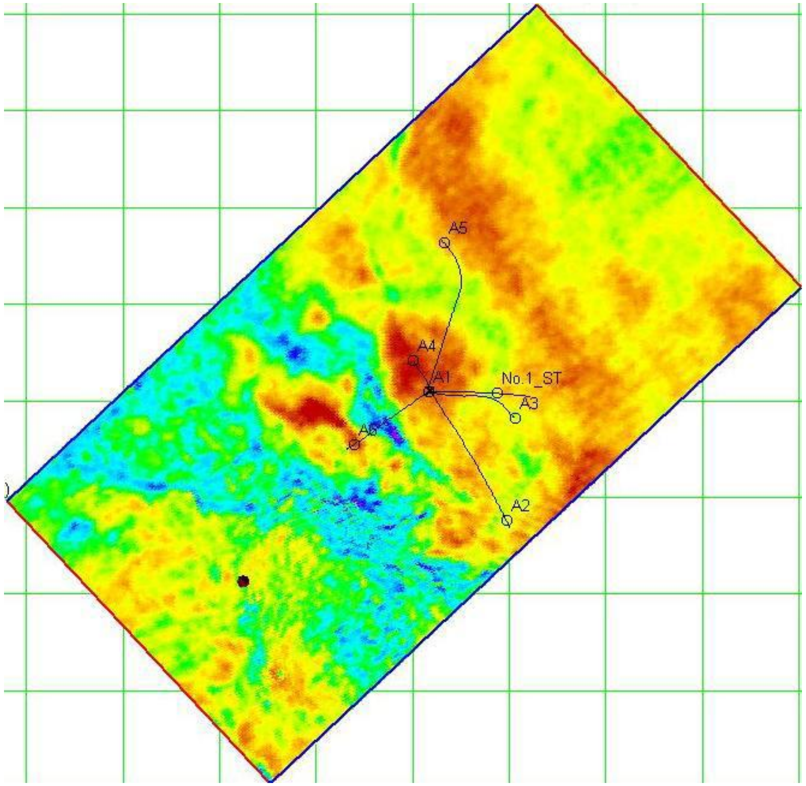

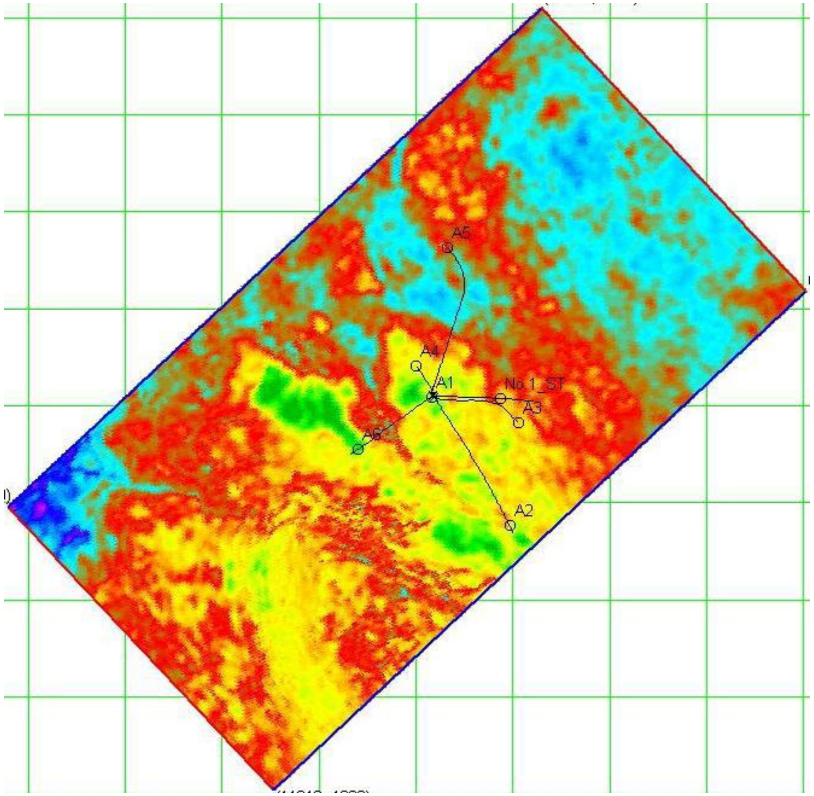

SEISMIC AMPLITUDE

Sw

Courtesy Dan Hampson, Brian Russell Hampson-Russell / CGG

VARIOGRAPHIC ANALYSIS

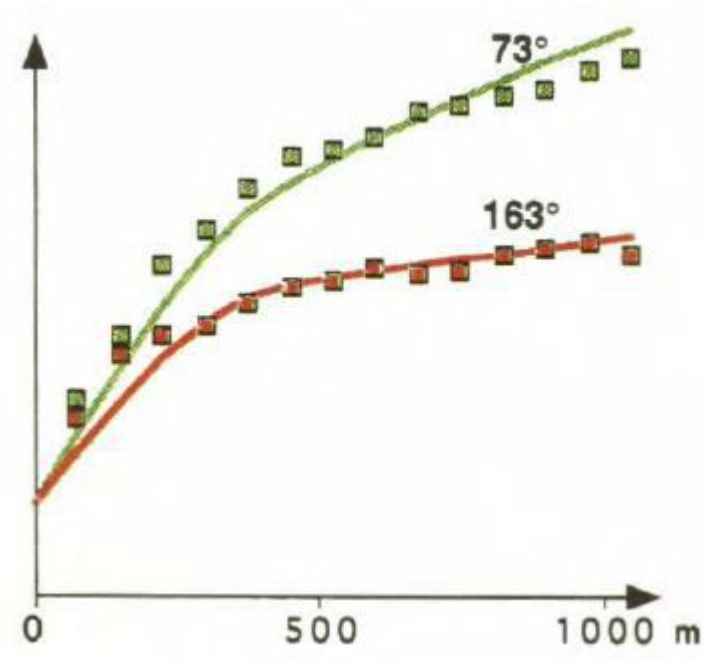

Courtesy Dan Hampson, Brian Russell Hampson-Russell / CGG

STOCHASTIC INVERSION

- SEQUENTIAL GAUSSIAN SIMULATION
- MONTECARLO SIMULATION
- MULTIPLE REALIZATIONS

- MOST STATIC PROPERTIES ARE NORMAL DISTRIBUTED
- MOST DYNAMIC PROPERTIES ARE LOG-NORMAL DISTRIBUTED

- KRIGING USES ONLY MEASURED POINTS, SGM USES ALSO SIMULATED POINTS

- ERROR VARIANCE IS CALCULATED BY CROSS-VALIDATION
- UNCERTAINTY / RISK IS A DIRECT FUNCTION OF ERROR VARIANCE

- MULTIPLE REALIZATIONS GIVE A MEASURE OF UNCERTAINTY

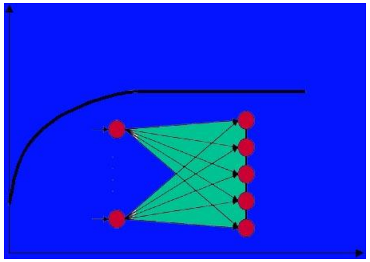

RESULTS OF SEISMIC INVERSION IN KÖNIGSDORF

NEAR STACK

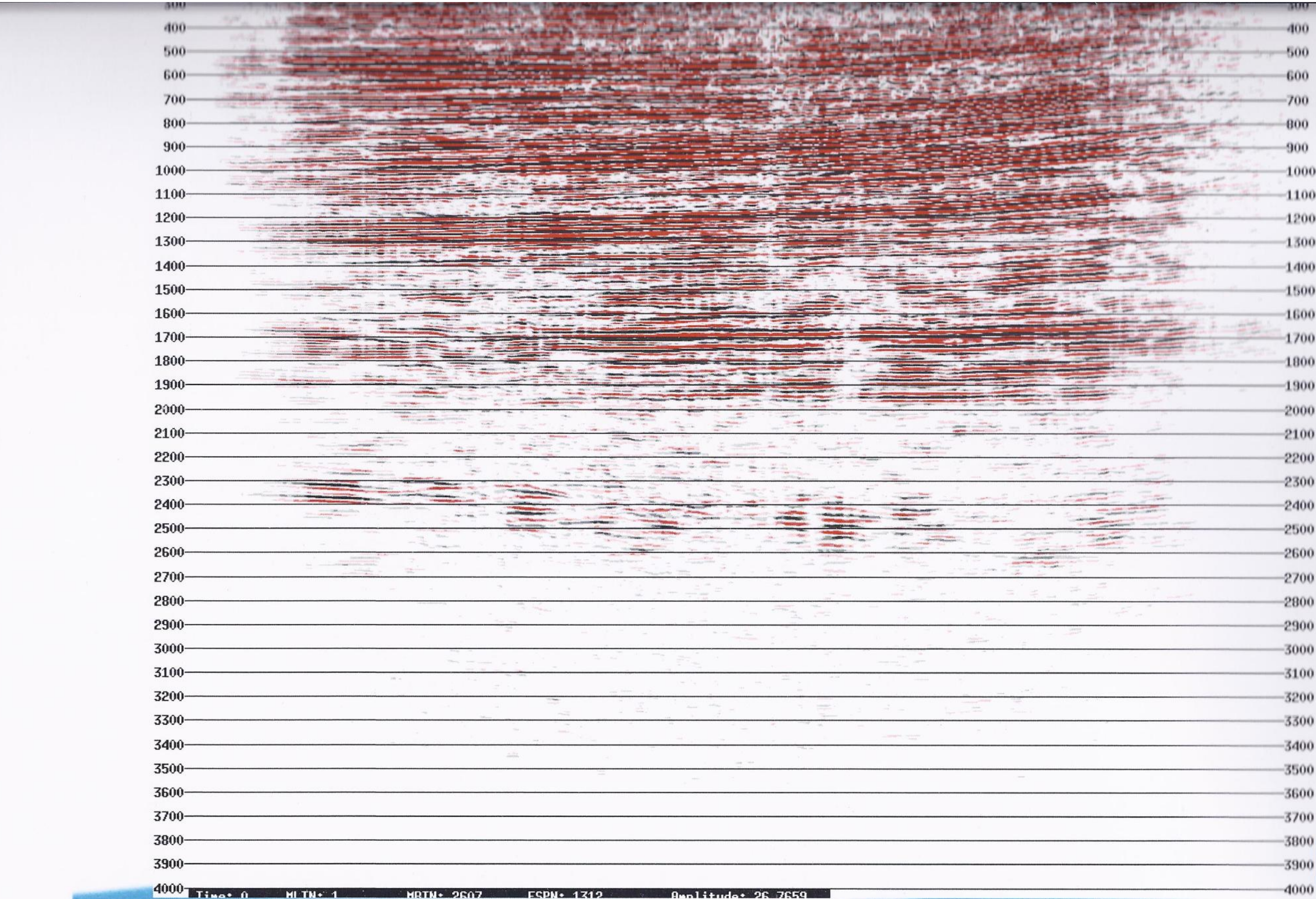
400
500
600
700
800
900
1000
1100
1200
1300
1400
1500
1600
1700
1800
1900
2000
2100
2200
2300
2400
2500
2600
2700
2800
2900
3000
3100
3200
3300
3400
3500
3600
3700
3800
3900
4000

FAR STACK

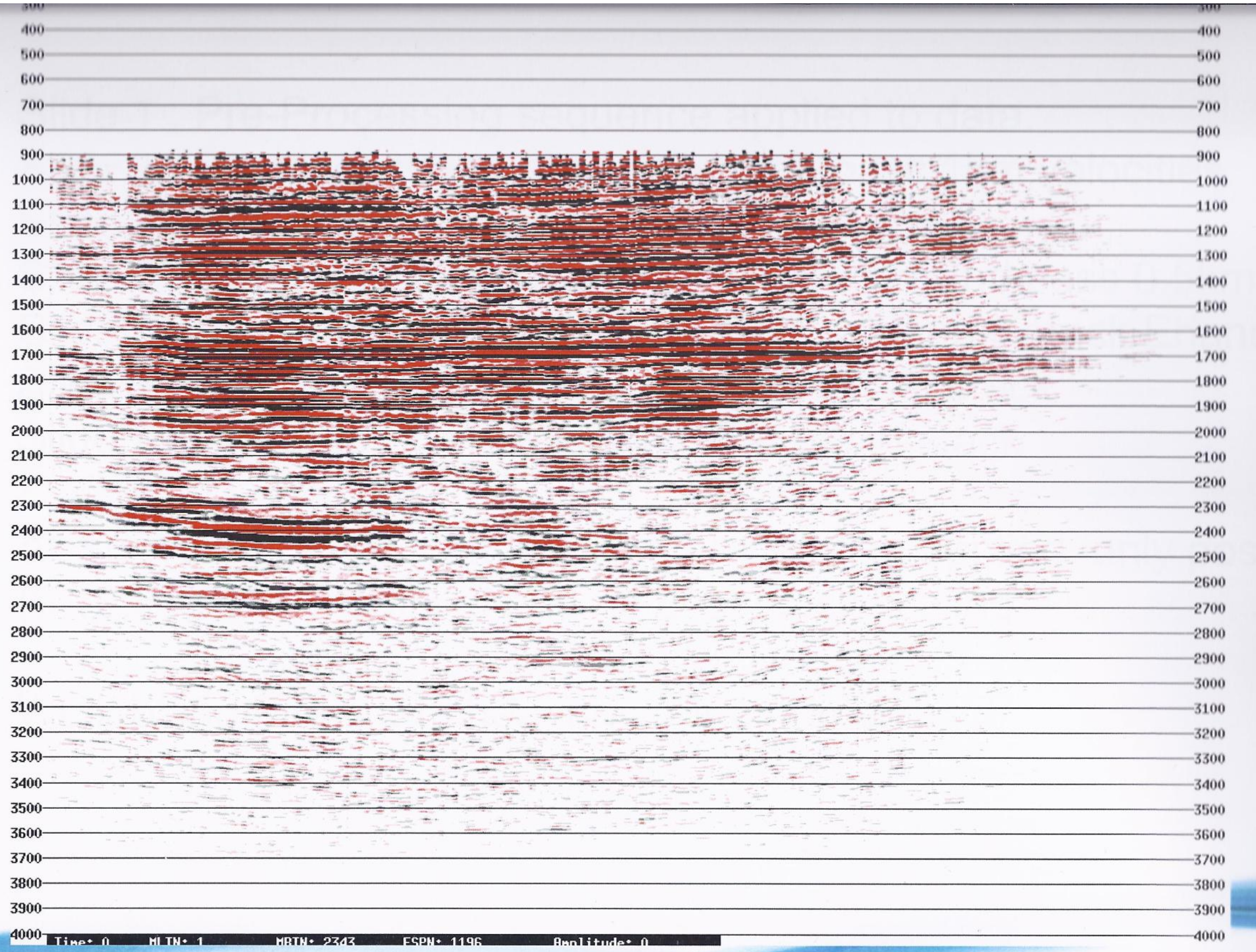

400
500
600
700
800
900
1000
1100
1200
1300
1400
1500
1600
1700
1800
1900
2000
2100
2200
2300
2400
2500
2600
2700
2800
2900
3000
3100
3200
3300
3400
3500
3600
3700
3800
3900
4000
Time: 0
MLIN: 1
MBIN: 2343
FSPN: 1196
Amplitude: 0

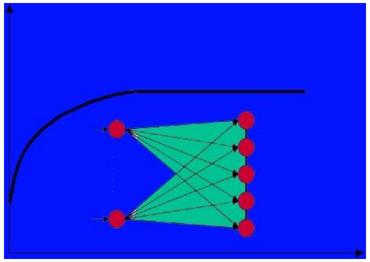

SEISMIC ATTRIBUTES ANALYSIS

SEISMIC ATTRIBUTES

- GEOMETRIC ATTRIBUTES
- COMPLEX ATTRIBUTES
- TRACKING ATTRIBUTES
- PATTERN RECOGNITION
- SPECTRAL ATTRIBUTES
- PROPERTY DISTRIBUTION ON SEISMIC VOLUME

HILBERT TRANSFORM

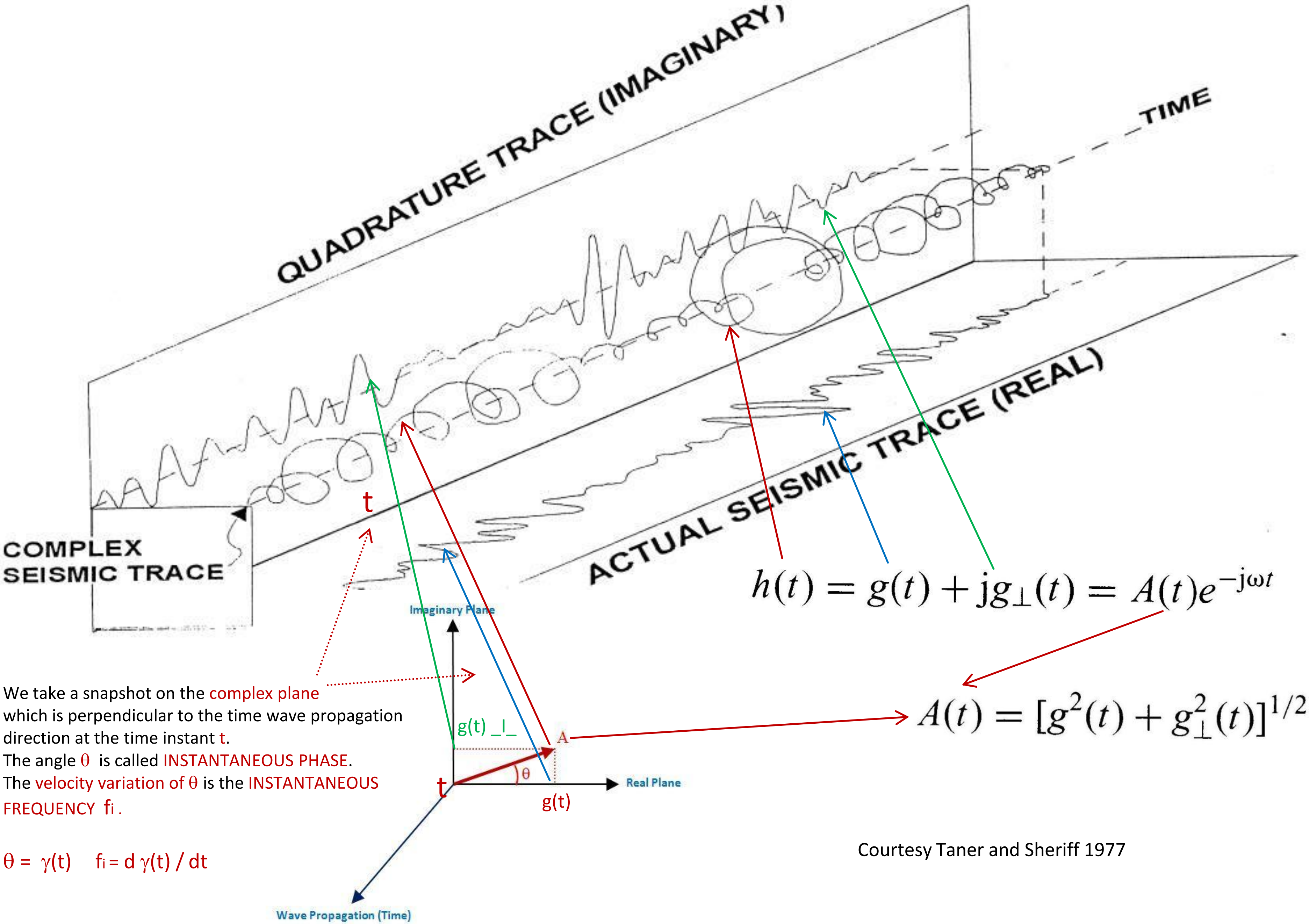

$$h(t) = g(t) + jg_{\perp}(t) = A(t)e^{-j\omega t}$$

$$A(t) = [g^2(t) + g_{\perp}^2(t)]^{1/2}$$

We take a snapshot on the complex plane which is perpendicular to the time wave propagation direction at the time instant t.
The angle θ is called INSTANTANEOUS PHASE.
The velocity variation of θ is the INSTANTANEOUS FREQUENCY f_i.

$\theta = \gamma(t) \quad f_i = d\,\gamma(t) / dt$

Courtesy Taner and Sheriff 1977

$$h(t) = g(t) + jg_\perp(t) = A(t)e^{-j\omega t}$$

$\theta = \gamma(t)$ fi = $f(t) = d\,\gamma(t) / dt$

$$A(t) = [g^2(t) + g_\perp^2(t)]^{1/2} \qquad \gamma(t) = \tan^{-1}\left(\frac{g_\perp(t)}{g(t)}\right).$$

$$f(t) = \mathrm{d}\gamma(t)/\mathrm{d}t = \frac{g(t)\frac{\mathrm{d}g_\perp(t)}{\mathrm{d}t)} - g_\perp(t)\frac{\mathrm{d}g(t)}{\mathrm{d}t)}}{g^2(t) + g_\perp^2(t)} \approx \frac{\Delta\gamma}{\Delta t} = \frac{\gamma_{i+1} - \gamma_{i-1}}{2\Delta}$$

To get the projection of g(t) → g_I_(t) into the imaginary plane we calculate the Hilbert Transform of g(t).

$$g_\perp(t) = g(t) * \frac{-1}{\pi t}$$

Hence the Hilbert Transform of the continuous function g(t) is the convolution of g(t) with -1/π t

For digital function we multiply g(t) for the quadrature filter g_t.

$$g_{\perp t} = g_t * q_t = \sum_{n=-\infty}^{+\infty} g_{t-n}(e^{jn\pi} - 1)/\pi n$$

$$g_{\perp t} = \left(\frac{-2}{\pi}\right) = \sum_{n=-\infty}^{+\infty} g_{t-n}/n, \quad n \text{ odd.}$$

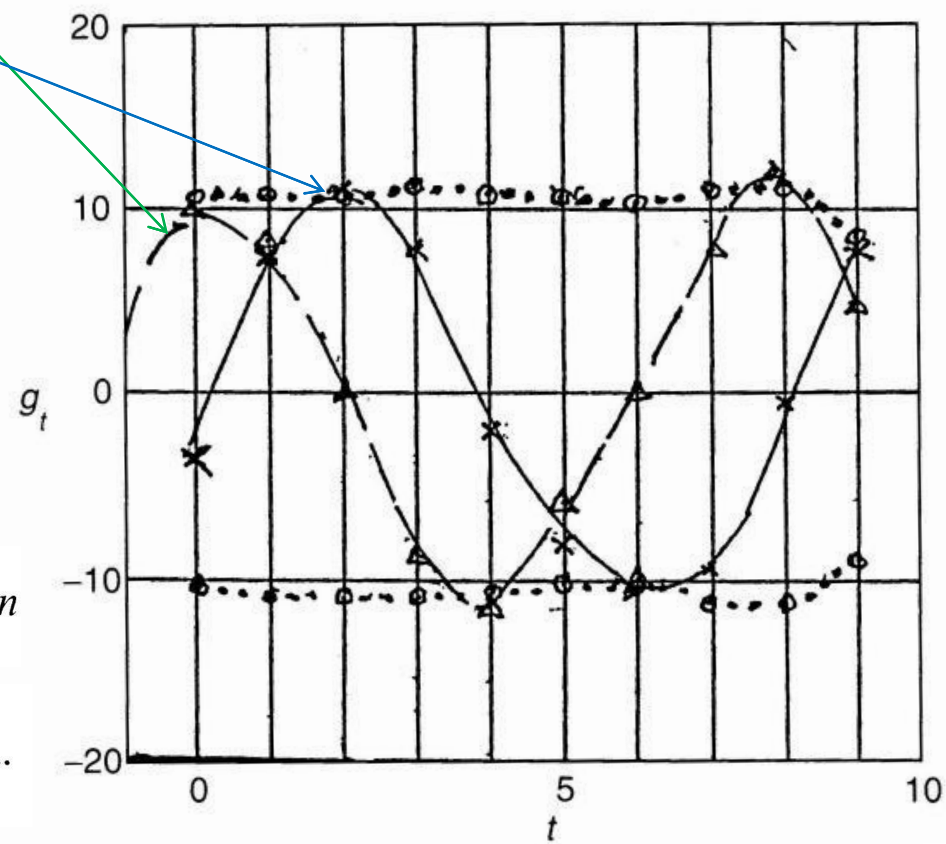

We come back to this figure already considered.   Do we notice common meanings between the 2 figures ?

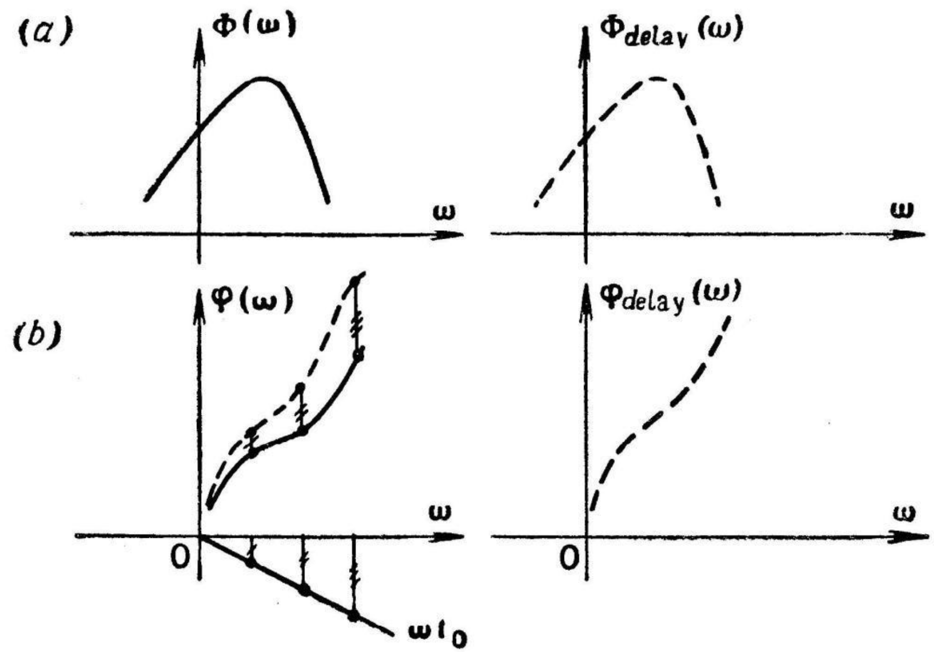

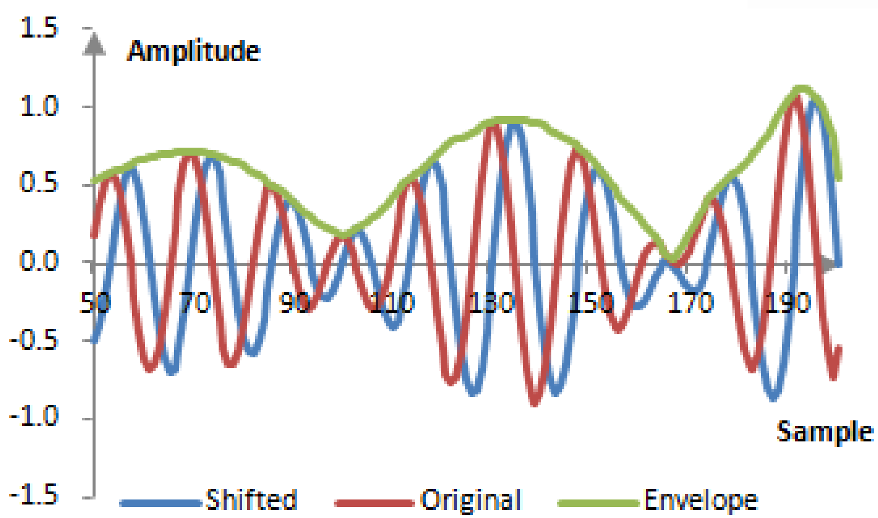

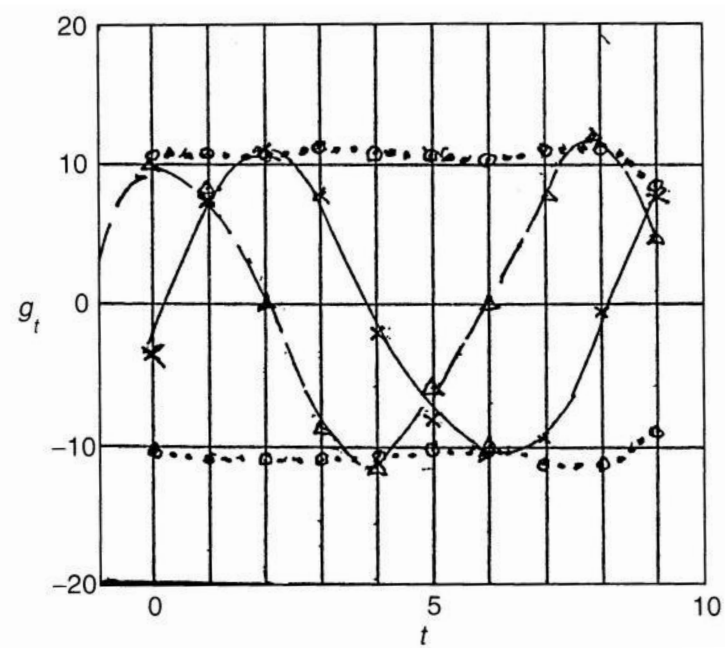

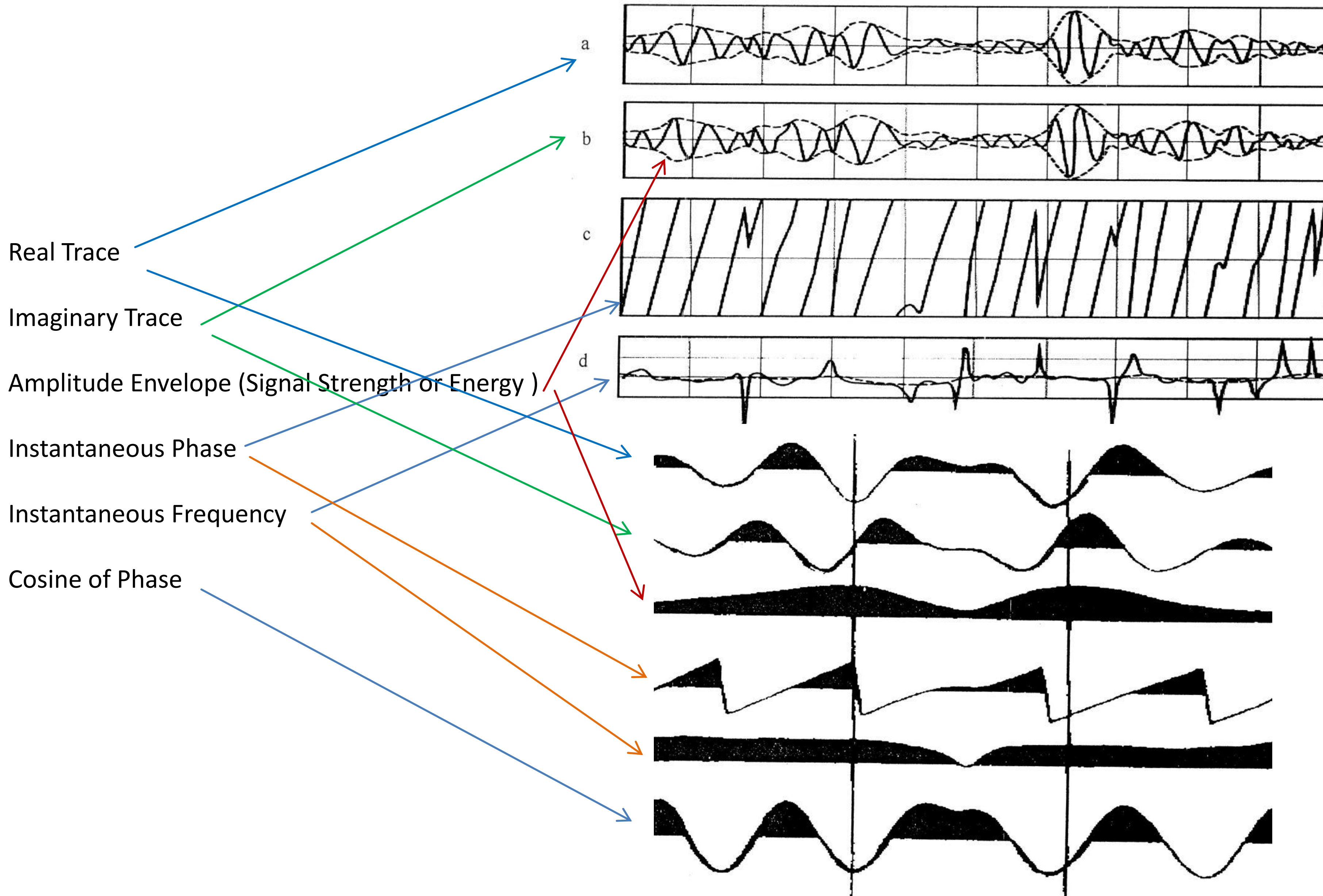

The noise is maximum at the zero-crossing point in the Real and Imaginary trace. The Envelope never reaches the zero-crossing point, therefore the S/N ratio is improved on the Signal Strength trace.

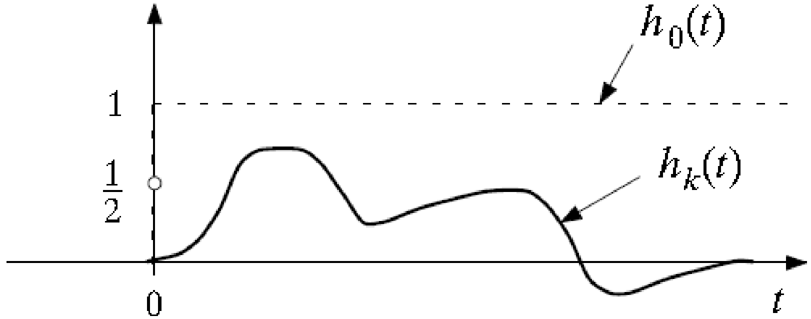

Hilbert and Causality
(unknown german mathematician

Bis hierher wurde gezeigt, dass die Forderung "keine Spektralanteile bei negativen Frequenzen" dazu führt, dass Realteil und Imaginärteil der komplexen Zeitfunktion über die Hilbert−Transformation miteinander verknüpft sein müssen. Mit einer gleichartigen Herleitung, wie sie in Abschnitt 12.3 durchgeführt wurde, lässt sich umgekehrt zeigen, dass ein komplexes Signal, bei dem Real− und Imaginärteil über die Hilbert−Transformation verknüpft sind, keine Spektralanteile bei negativen Frequenzen besitzt. Es gilt also der Satz

> Beim analytischen Signal ist der Imaginärteil die Hilbert−Transformierte des Realteils und der Realteil die inverse Hilbert−Transformierte des Imaginärteils.
> Ist umgekehrt der Imaginärteil eines komplexen Signals die Hilbert−Transformierte des Realteils und der Realteil die inverse Hilbert−Transformierte des Imaginärteils, dann ist das komplexe Signal ein analytisches Signal. Das heißt: es besitzt keine Spektralanteile bei negativen Frequenzen.

In modern programs routines Fourier Transform, Laplace, Filtering etc. will be implemented through
Z Transforms algorithms. Fourier Transform often as SFT.

GEOMETRIC – COMPLEX ATTRIBUTES

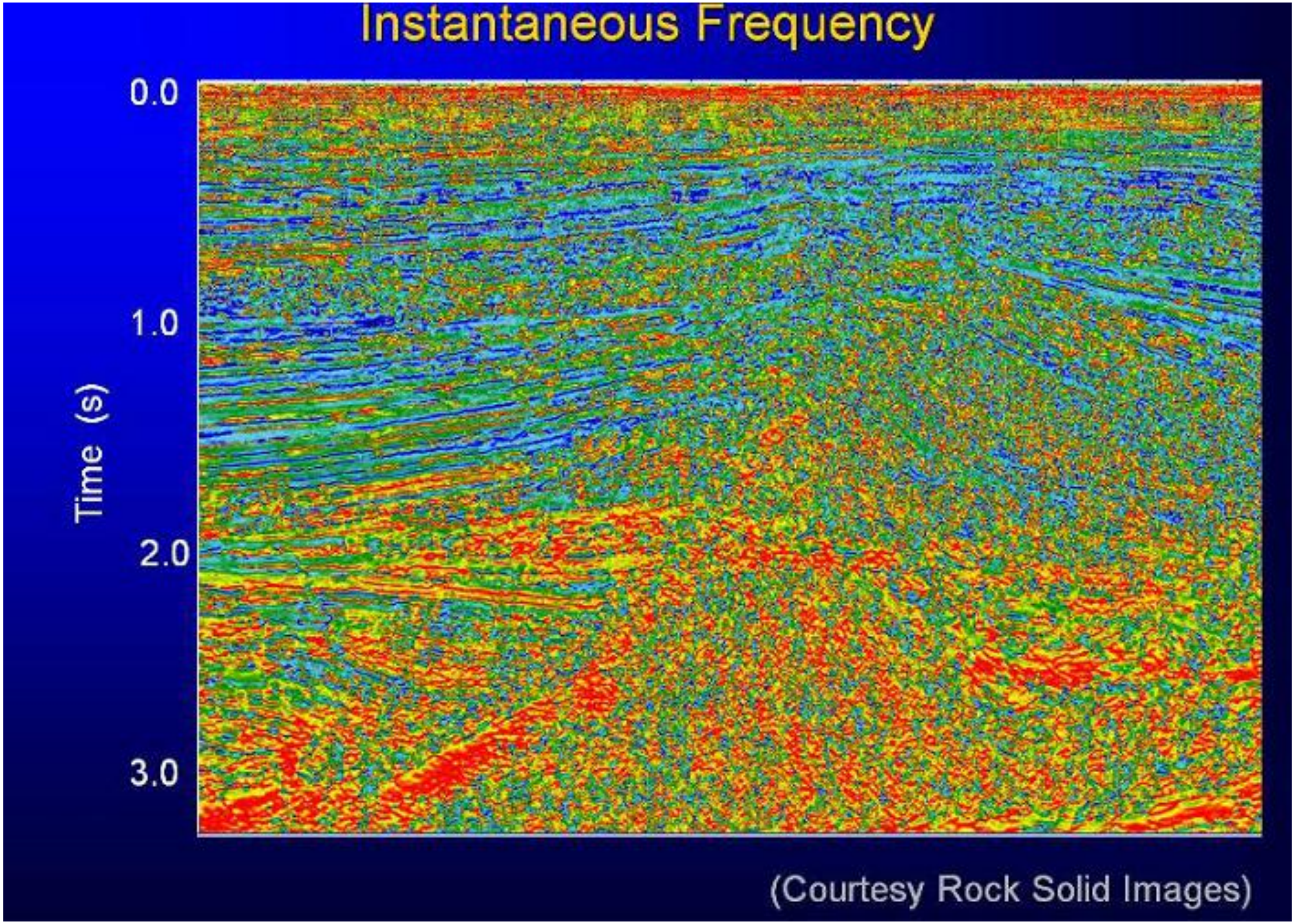

Courtesy Kurt Marfurt

SCANNING INSTANTANEOUS FREQUENCY SINGULARITIES

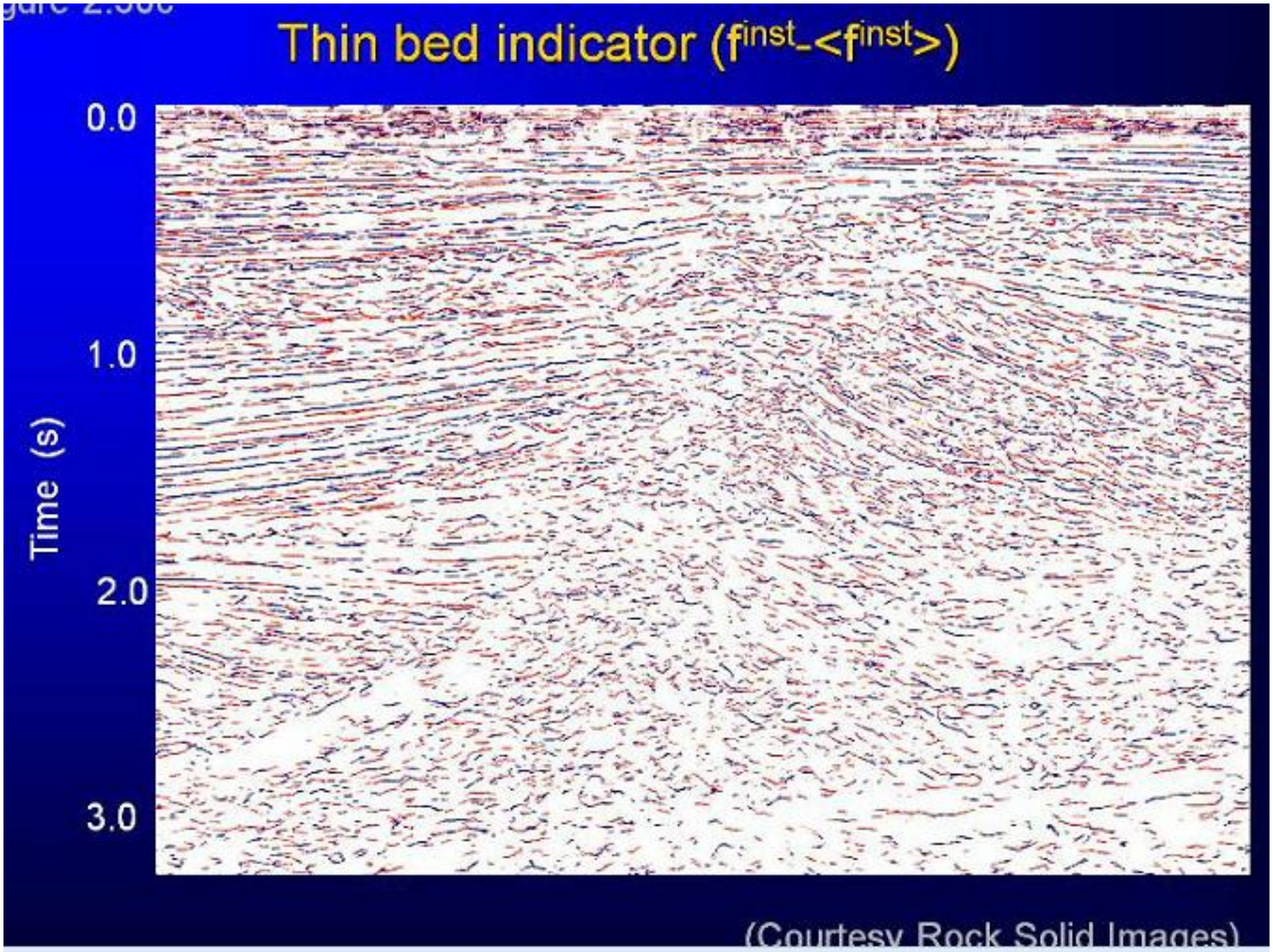

Courtesy Kurt Marfurt

GEOMETRIC ATTRIBUTES

WEIGHTED AVERAGE DIP AZIMUTH

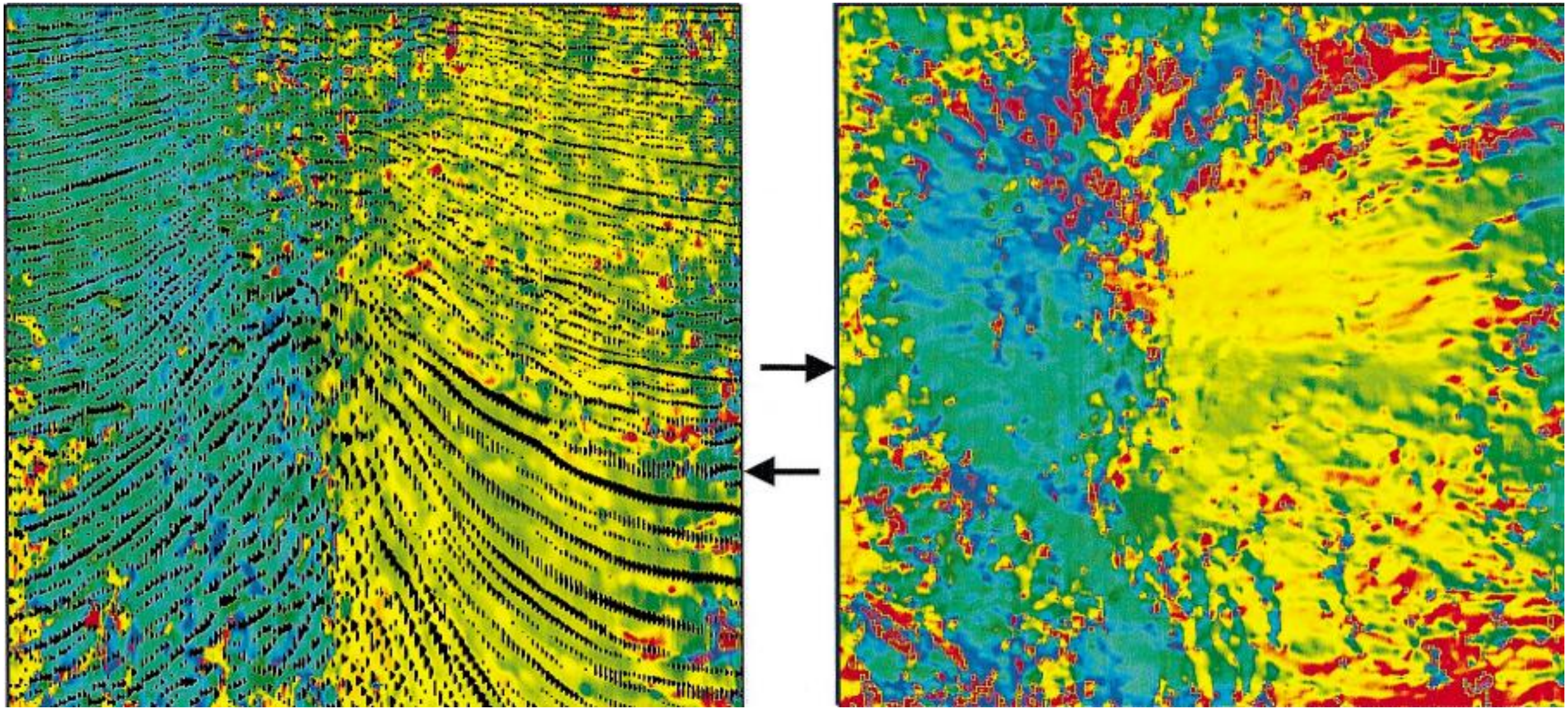

Courtesy Kurt Marfurt

GEOMETRIC COHERENCE ATTRIBUTES

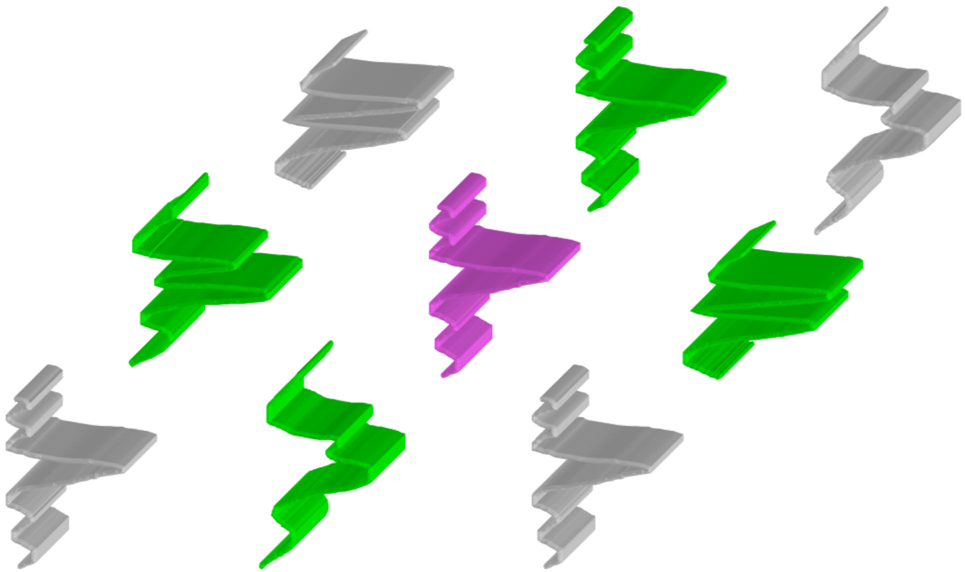

CROSSCORRELATION, VARIANCE, EIGENSTRUCTURE, GRADIENT STRUCTURAL TENSOR, SEMBLANCE, SINGULARITY

Courtesy Kurt Marfurt

ENERGY WEIGHTED COHERENCE AMPLITUDE GRADIENT

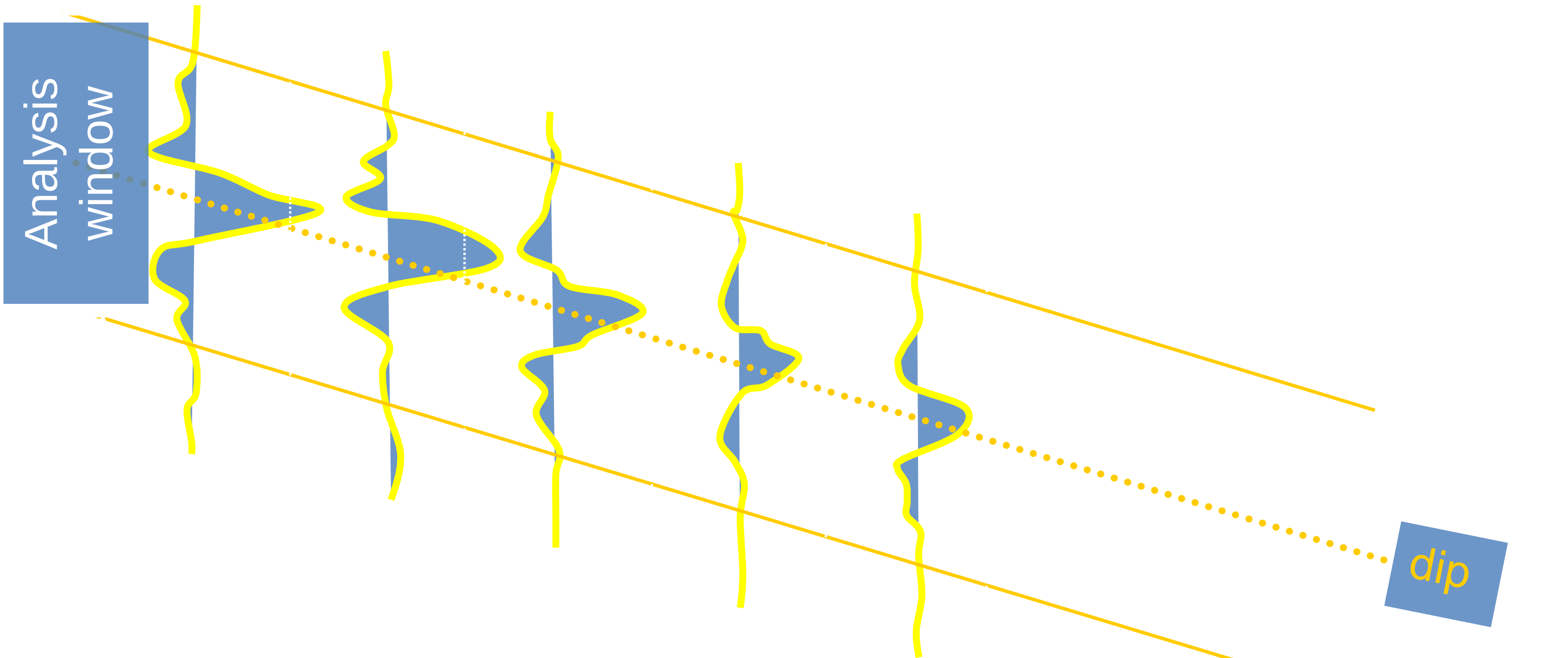

Courtesy Kurt Marfurt

CURVATURE

Courtesy Kurt Marfurt

CURV PARAMETRIZATION

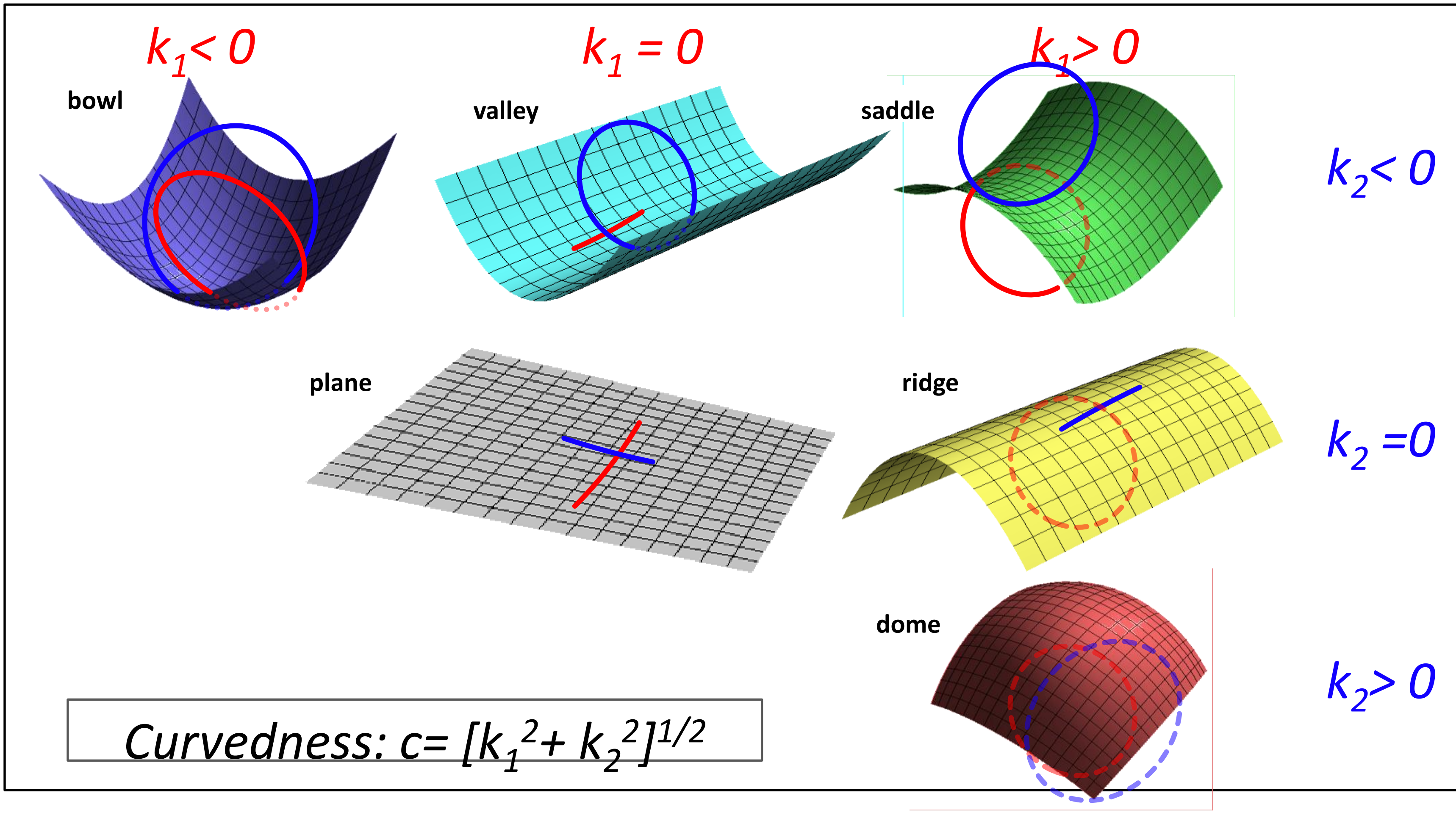

$$Curvedness: c = [k_1^2 + k_2^2]^{1/2}$$

Courtesy Kurt Marfurt

OUR SUSPECTED INSTRUCTOR KURT MARFURT

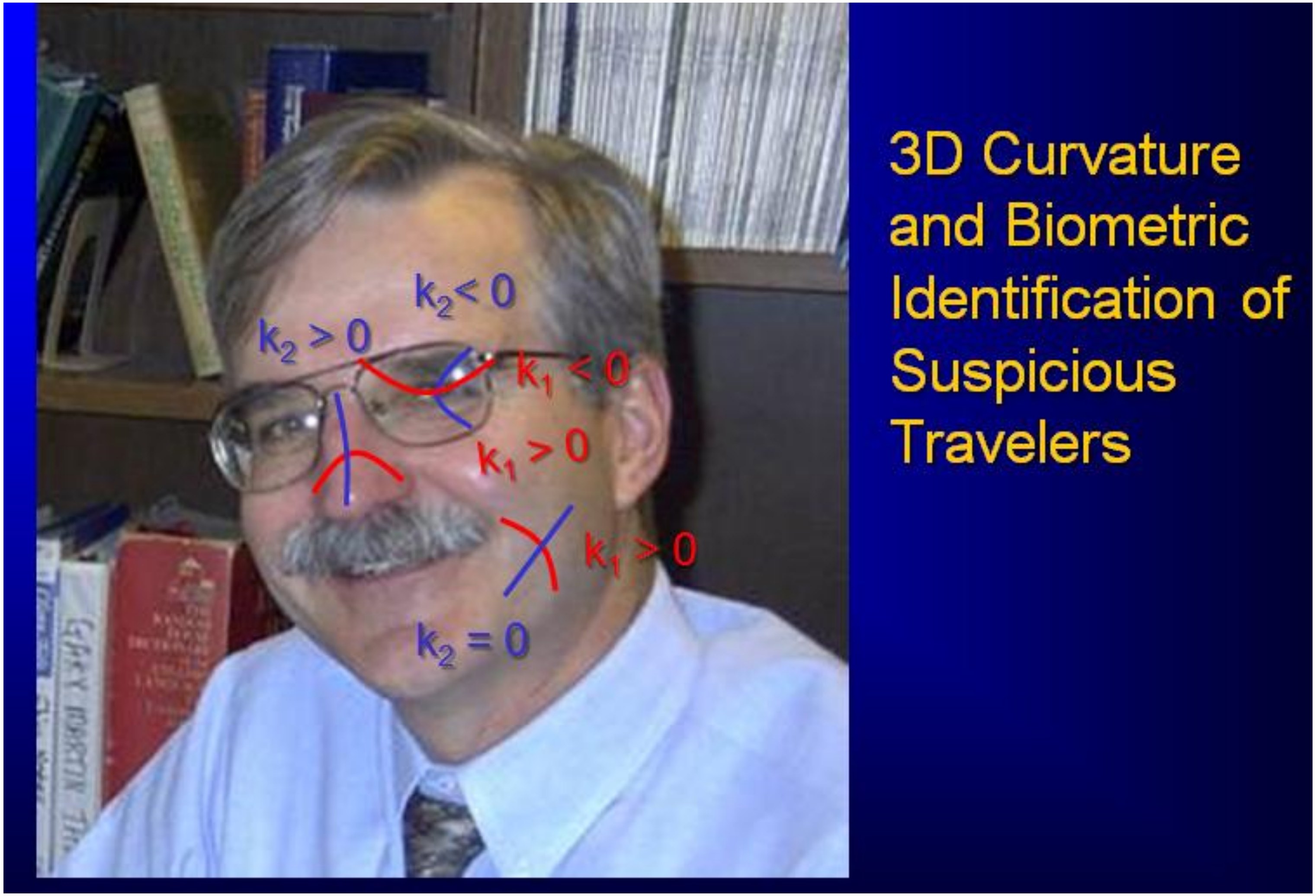

CURV + ILLUMINATION

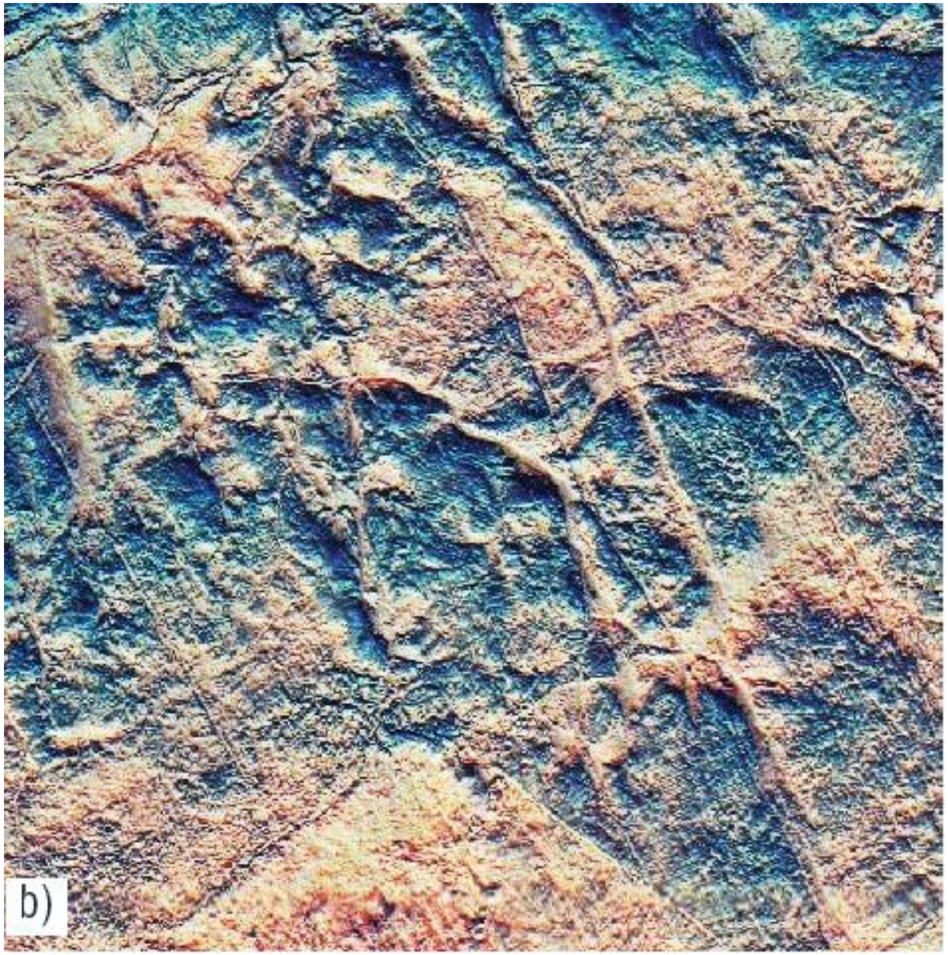

Courtesy Kurt Marfurt

FAULT / ANISOTROPY

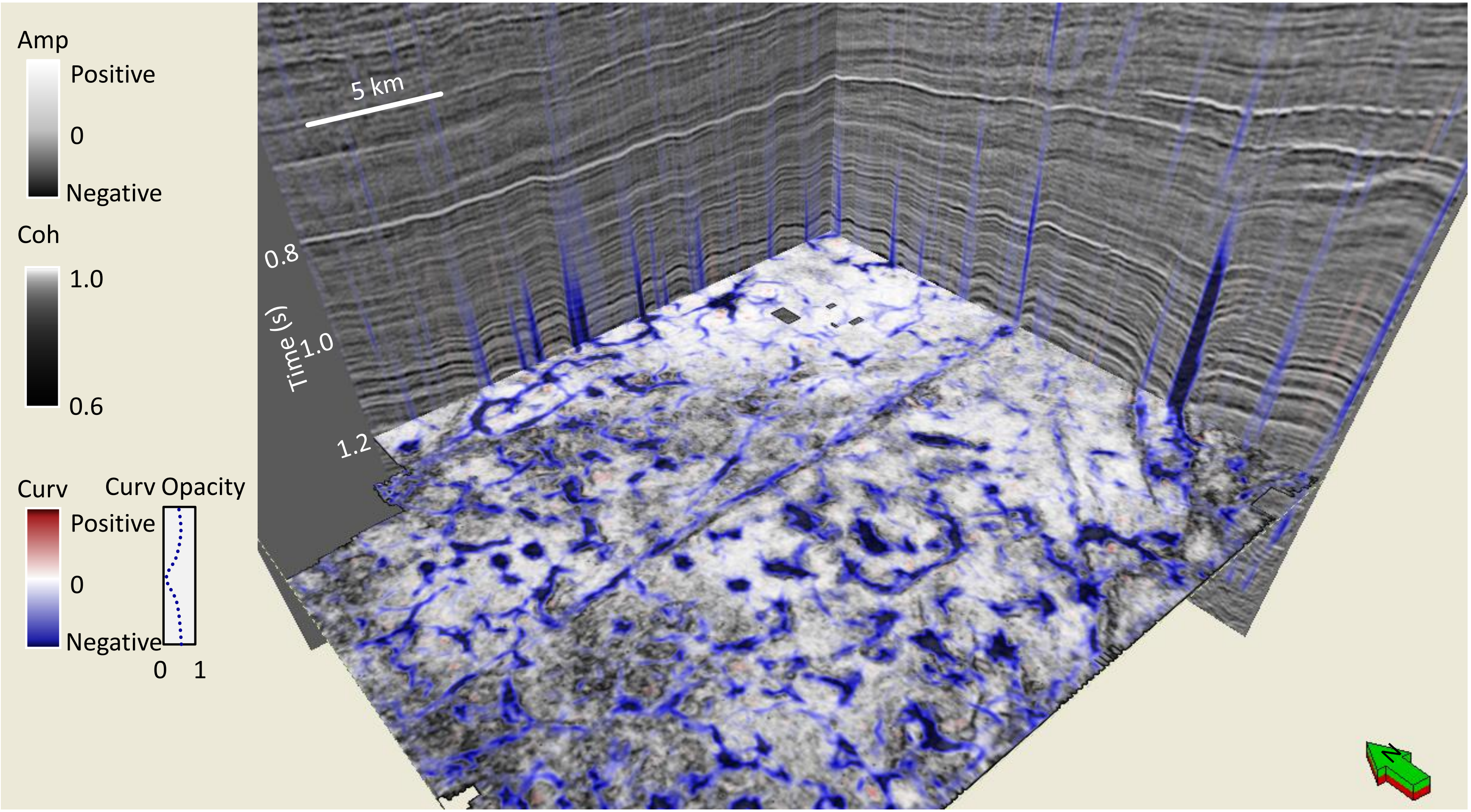

Courtesy Kurt Marfurt

SPECTRAL ATTRIBUTES

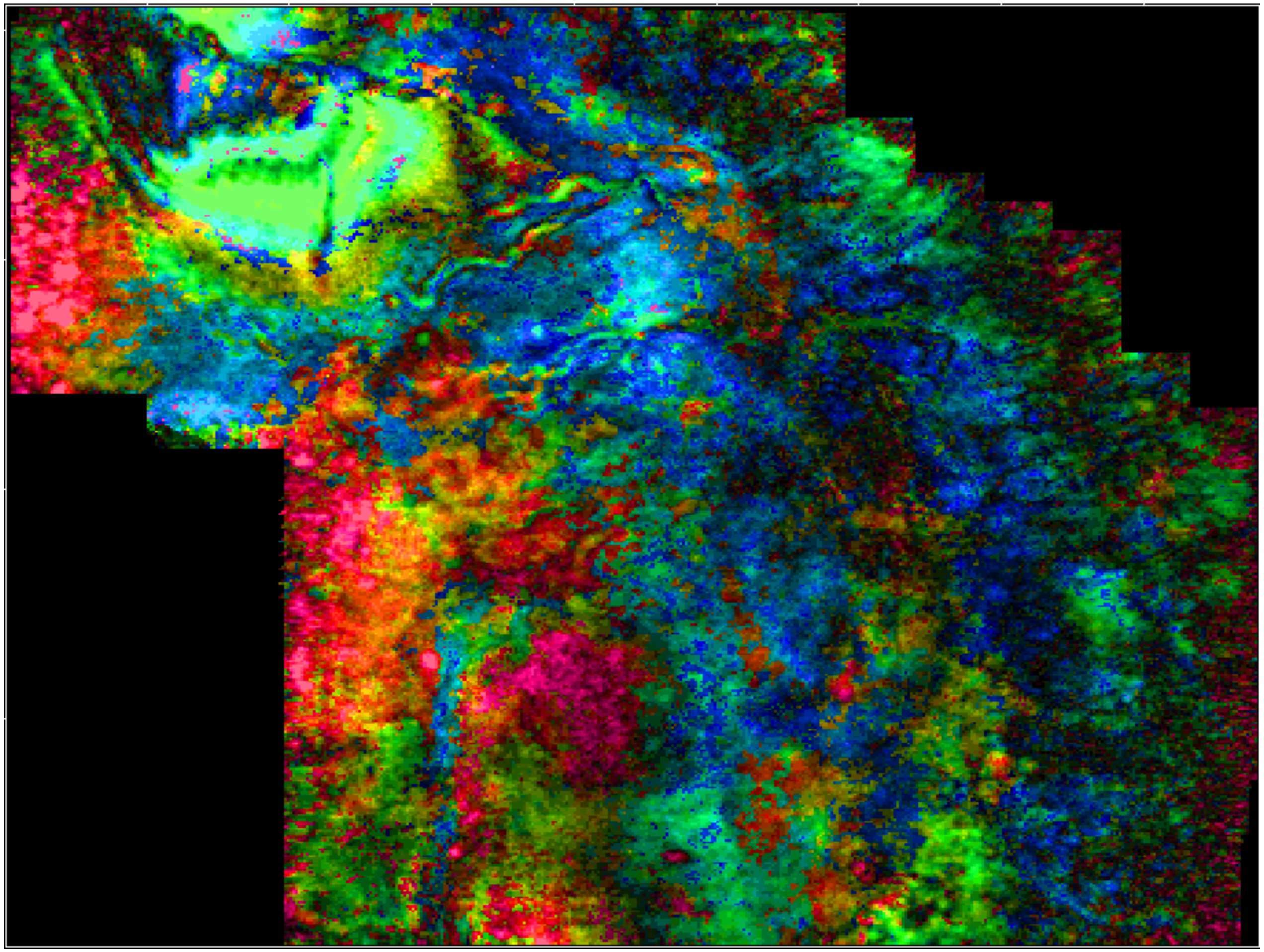

Courtesy Kurt Marfurt

SPECTRAL FILTERED SLICE

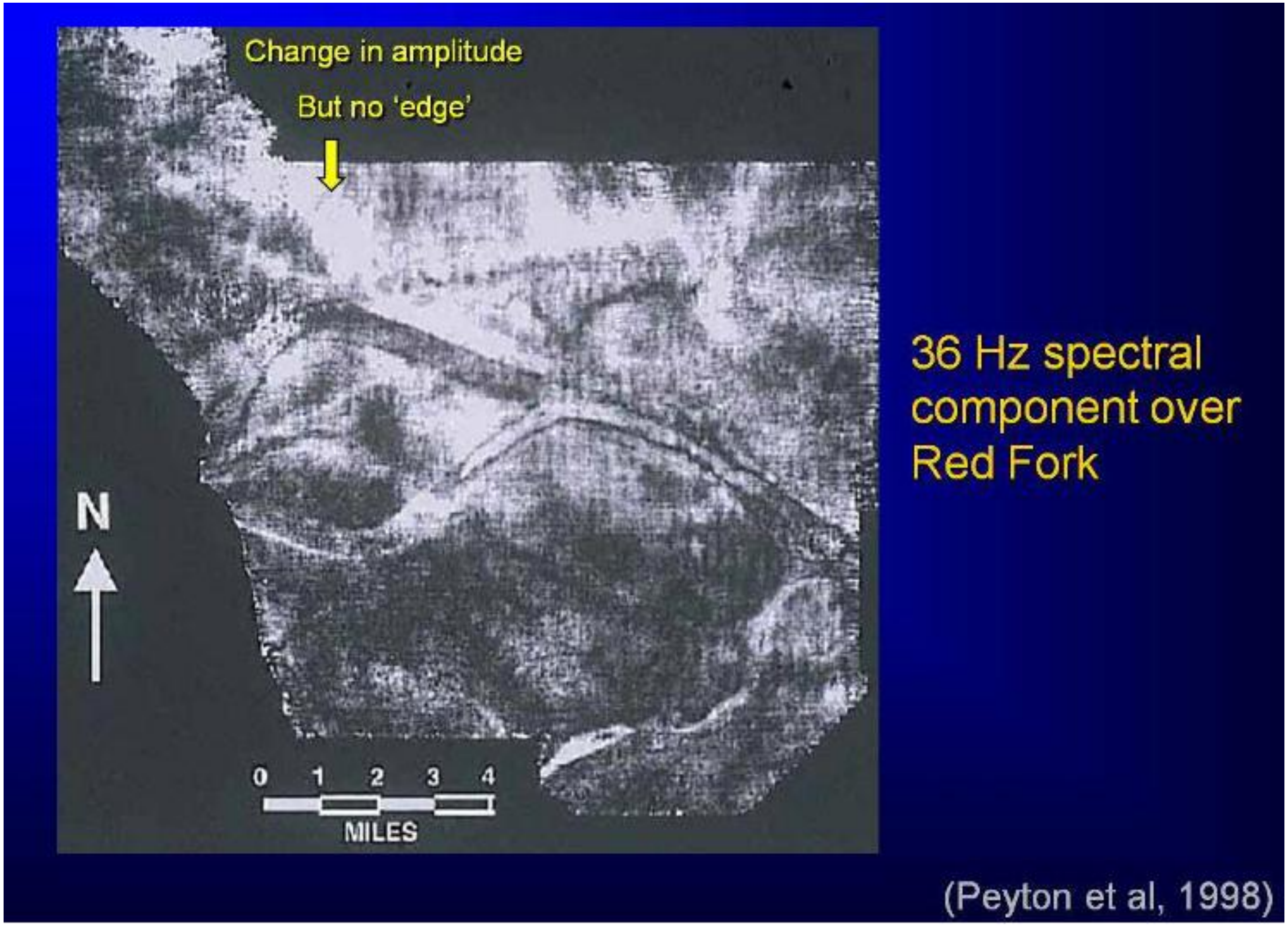

Courtesy Kurt Marfurt

SPECTRAL BALANCING

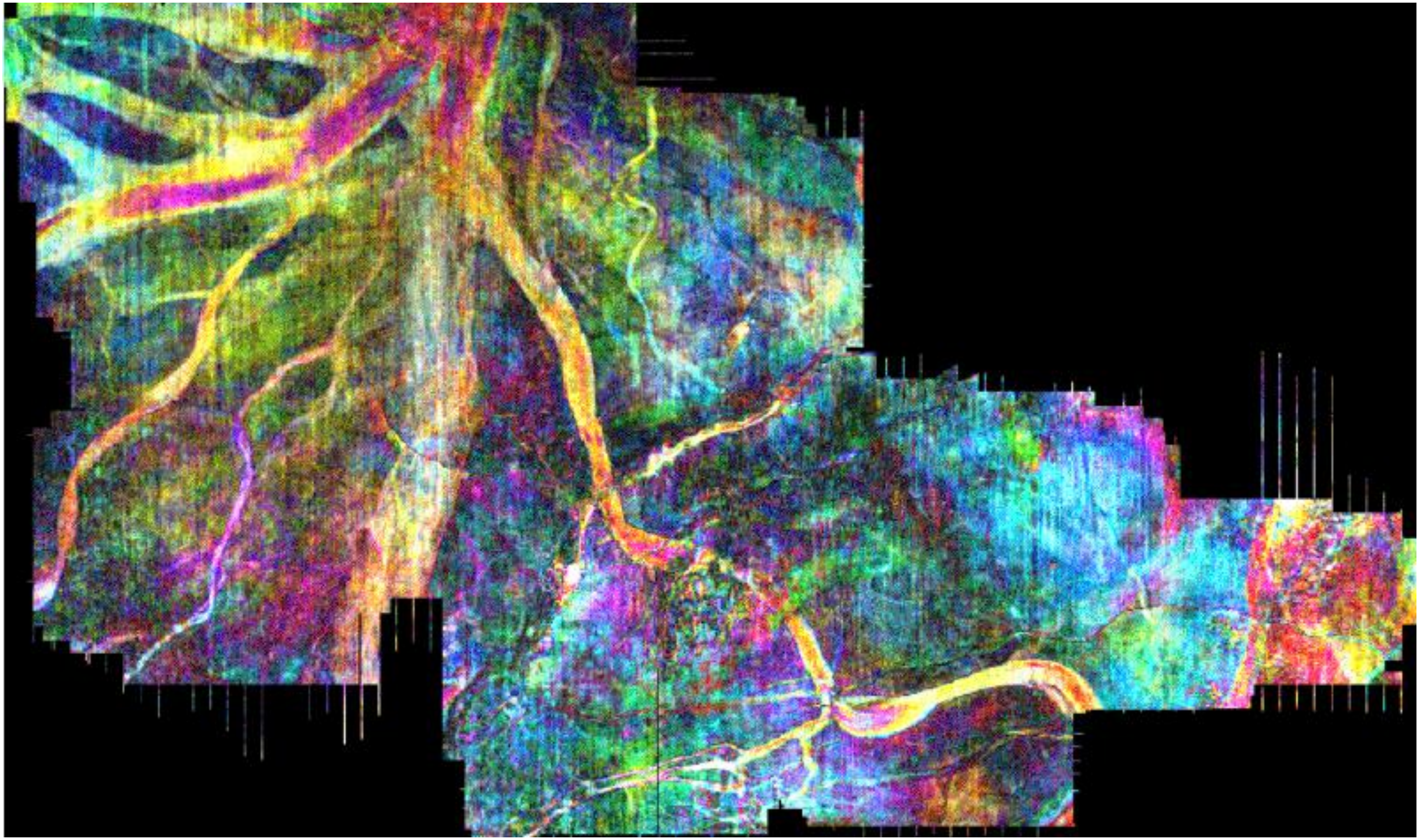

Courtesy Kurt Marfurt

SELECTIVE-Q SPECTRAL FILTERING

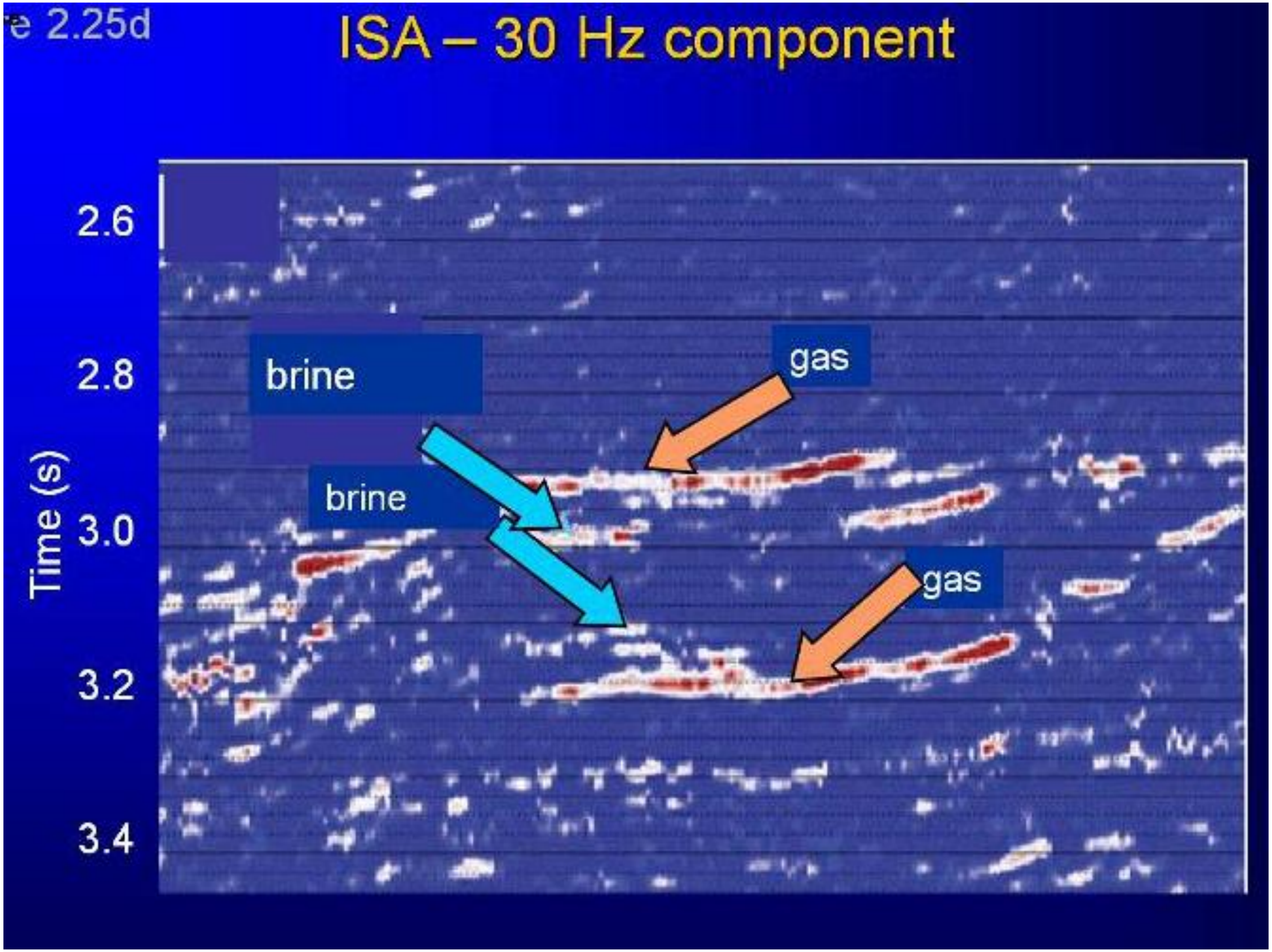

10Hz Brine – 30Hz Gas

Courtesy Kurt Marfurt, Gennadi Goloshubin

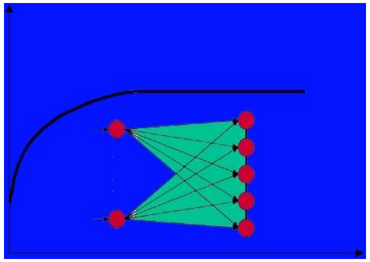

PROPERTY DISTRIBUTION ON SEISMIC VOLUME

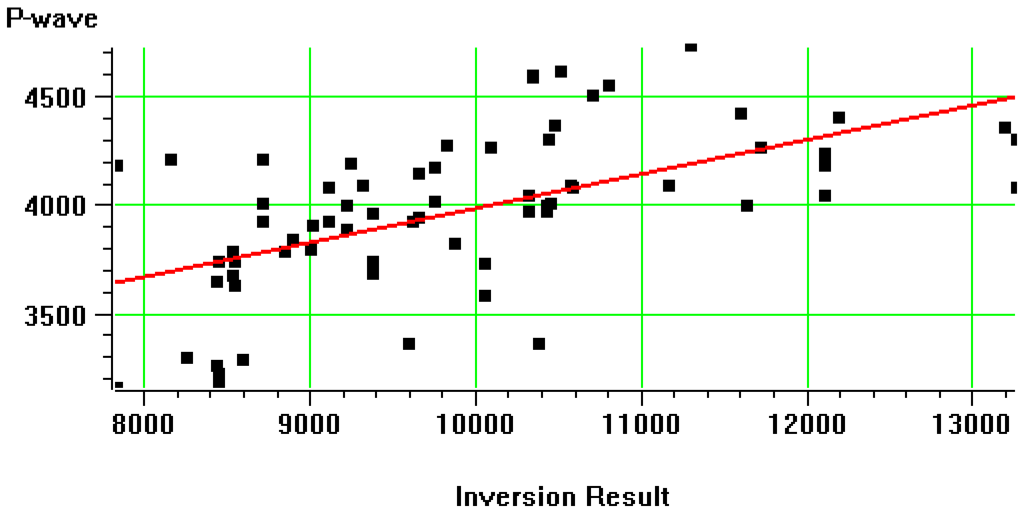

REGRESSION LINE

Courtesy Dan Hampson, Brian Russell Hampson-Russell / CGG

MULTIPLE ATTRIBUTES

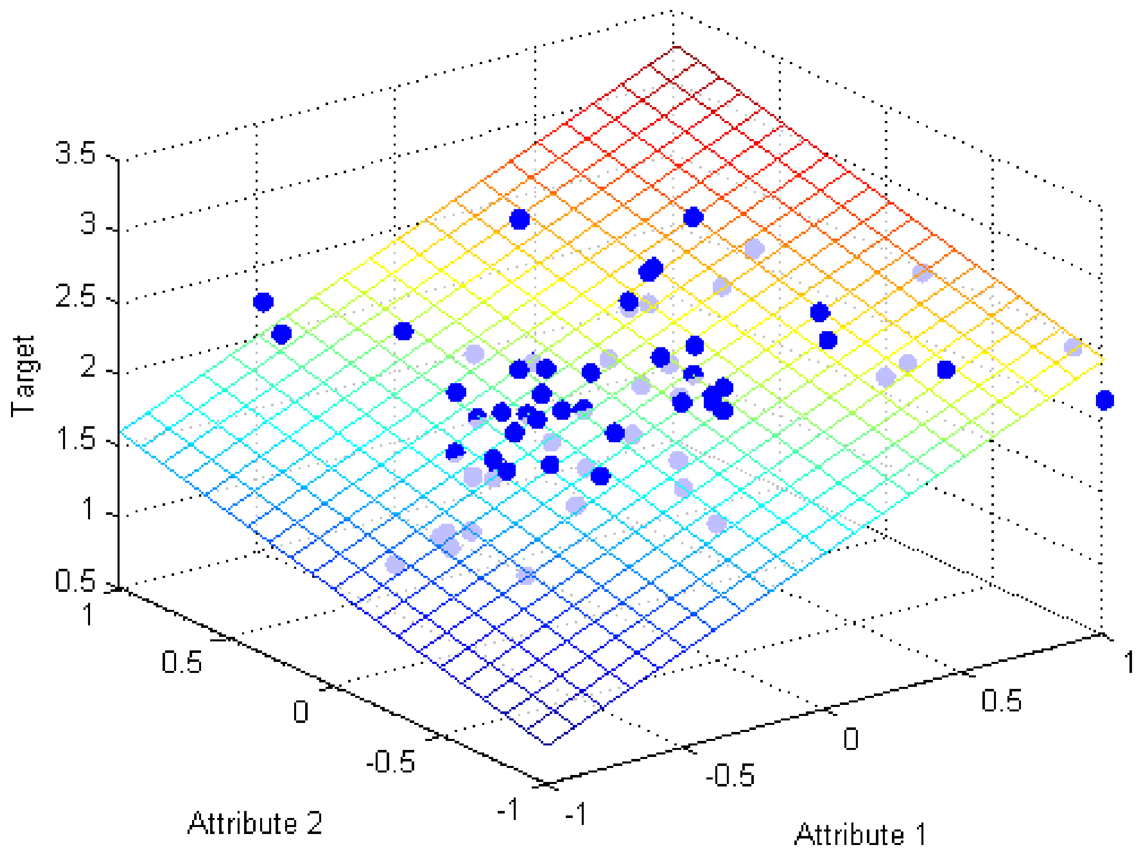

REGRESSION PLANE

Courtesy Dan Hampson, Brian Russell Hampson-Russell / CGG

MULTIATTRIBUTES ANALYSIS

This can be solved by least-squares minimization to give

$$W = \left[A^T A\right]^{-1} A^T P$$

As a detailed computation, note that:

$$\begin{bmatrix} w_0 \\ w_1 \\ w_2 \\ w_3 \end{bmatrix} = \left\{ \begin{bmatrix} 1 & 1 & \cdots & 1 \\ I_i & I_2 & \cdots & I_N \\ E_1 & E_2 & \cdots & E_N \\ F_1 & F_2 & \cdots & F_N \end{bmatrix} \begin{bmatrix} 1 & I_1 & E_1 & F_1 \\ 1 & I_2 & E_2 & F_2 \\ \vdots & \vdots & \vdots & \vdots \\ 1 & I_N & E_N & F_N \end{bmatrix} \right\}^{-1} \begin{bmatrix} 1 & 1 & \cdots & 1 \\ I_1 & I_2 & \cdots & I_N \\ E_1 & E_2 & \cdots & E_N \\ F_1 & F_2 & \cdots & F_N \end{bmatrix} \begin{bmatrix} \phi_1 \\ \phi_2 \\ \vdots \\ \phi_N \end{bmatrix}$$

or:

$$\begin{bmatrix} w_0 \\ w_1 \\ w_2 \\ w_3 \end{bmatrix} = \begin{bmatrix} N & \Sigma I_i & \Sigma E_i & \Sigma F_i \\ \Sigma I_i & \Sigma I_i^2 & \Sigma I_i E_i & \Sigma I_i F_i \\ \Sigma E_i & \Sigma E_i I_i & \Sigma E_i^2 & \Sigma E_i F_i \\ \Sigma F_i & \Sigma F_i I_i & \Sigma F_i E_i & \Sigma F_i^2 \end{bmatrix}^{-1} \begin{bmatrix} \Sigma \phi_i \\ \Sigma I_i \phi_i \\ \Sigma E_i \phi_i \\ \Sigma F_i \phi_i \end{bmatrix}$$

These coefficients minimize the total prediction error:

$$\mathrm{E}^2 = \frac{1}{\mathrm{N}} \sum_{\mathrm{i}=1}^{\mathrm{N}} (\varphi_{\mathrm{i}} - \mathrm{w}_0 - \mathrm{w}_1 * \mathrm{I}_{\mathrm{i}} - \mathrm{w}_2 * \mathrm{E}_{\mathrm{i}} - \mathrm{w}_3 * \mathrm{F}_{\mathrm{i}})^2$$

MULTIREGRESSION WITH PROBABILISTIC NEURAL NETWORKS (PNN)

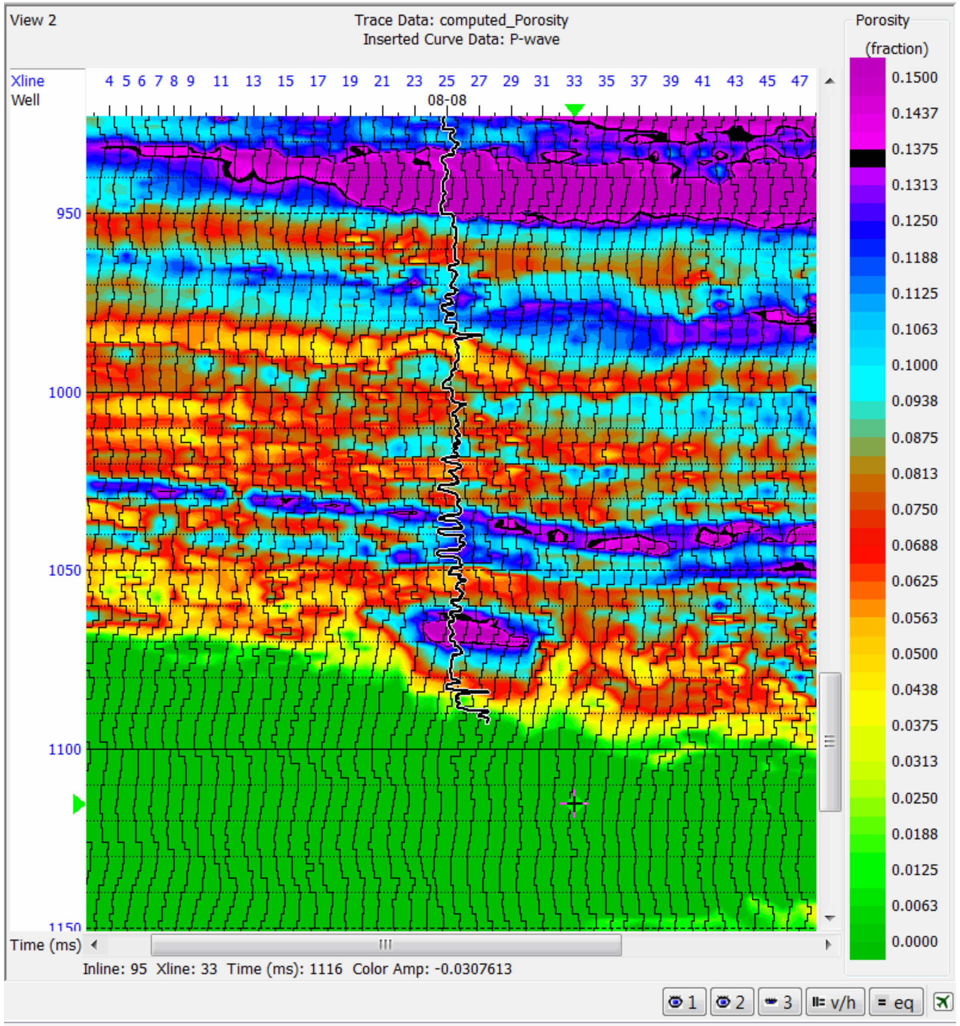

OPTIMAL RESULTS CAN BE REACHED WITH PNN. ABOVE A CALCULATION OF POROSITY THROUGH SEISMIC ATTRIBUTES

Courtesy Dan Hampson, Brian Russell Hampson-Russell / CGG

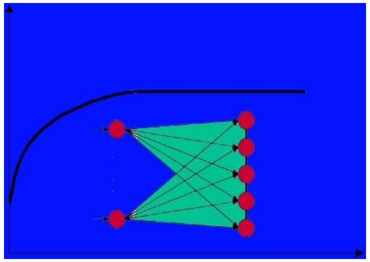

RESEARCH AREA

MICRO – MACROSYSTEMS INTEGRATION

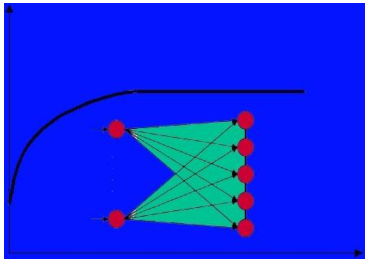

A BASELINE MODEL FOR ANOMALY INDENTIFICATION AND SEISMIC ATTRIBUTES CORRELATION

Following the Aki-Richards linearization we introduce the Electrical-Weighted Density into the Acoustic Impedance expression and into the Wiggins et al. variant equation for the Reflectivity.
Considering that the weighting factor $\frac{\Delta\rho}{\rho}$ compares in all equations we get

this as a function of the Electrical-Weighted Density :

$$\rho_b = \rho_{ma} + (\rho_f - \rho_{ma})\, e^{\left(\frac{\mathrm{Ln} \frac{a\, R_w}{S_w^{\,n}\, R_t}}{m} \right)}$$

Further we will consider that for a simple case (Baseline pure Archie rock the parameters **a, n, m** can be expressed as numerical standard 1,2,2.
To simplify the model we will call the exponent of e (Ar_Mod) which means: Simple Archie Model.
Thus:

$$\boxed{\rho_b = \rho_{ma} + (\rho_f - \rho_{ma})\, e^{[Ar\_Mod]}}$$

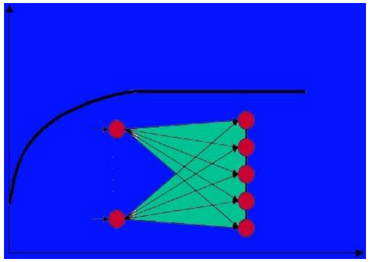

The Zero-Offset Reflectivity is therefore defined as:

$$R_p(0) = \frac{\Delta V_p}{V_p} + \frac{\left[\rho_{ma} + (\rho_f - \rho_{ma})\, e^{[Ar\_Mod]}\right]_2 - \left[\rho_{ma} + (\rho_f - \rho_{ma})\, e^{[Ar\_Mod]}\right]_1}{\dfrac{\left[\rho_{ma} + (\rho_f - \rho_{ma})\, e^{[Ar\_Mod]}\right]_2 + \left[\rho_{ma} + (\rho_f - \rho_{ma})\, e^{[Ar\_Mod]}\right]_1}{2}}$$

This is a Seismic-Electrical (S-E) Attribute and express reflectivity as a function of an electrical-weighted Density. The Ar_Mod represents the simple Archie rock model , as baseline for correlations with well-calibrated S-E Reflectivities.
However it is possible to calculate also Non-Archie Rocks
Models, Complex Lithology or Dual-Water models taking into account the porosity partitioning
In Carbonate and the Shale Resistivity component in clastic rocks.
At the same time we can use the E-Density (E-**r**) to calculate simply the Acoustic Impedance
and compare it with the conventional acoustic impedance from from inversion.

$$Z_e = V_p \left[\rho_{ma} + (\rho_f - \rho_{ma})\, e^{[Ar\_Mod]}\right]$$

This attribute can also be used to find anomalies related to shales in clastics or porosity type in carbonate.

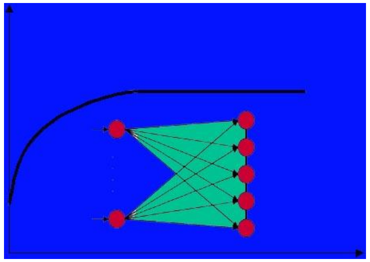

Resulting from this semplification the weighting coefficient is: $\frac{\Delta \rho}{\rho}$

of the Aki-Richards equation in form of Electrical-Weighted Density:

$$\rho = \frac{\left[\rho_{ma} + (\rho_f - \rho_{ma}) \, e^{[Ar\_Mod]} \right]_2 + \left[\rho_{ma} + (\rho_f - \rho_{ma}) \, e^{[Ar\_Mod]} \right]_1}{2}$$

$$\Delta\rho = \left[\rho_{ma} + (\rho_f - \rho_{ma}) \, e^{[Ar\_Mod]} \right]_2 - \left[\rho_{ma} + (\rho_f - \rho_{ma}) \, e^{[Ar\_Mod]} \right]_1$$

PARTIAL REFLECTIVITY EQUATION – DENSITY ELECTRO VARIANT

I first derive the partial Reflectivity for P and S waves where only the density component is and electro component while the velocity component is an elastic component:

$$R_p(0) = \frac{\Delta V_{p\text{-seis}}}{V_{Pave\text{-seis}}} + \frac{\left[\ \rho_{ma} + (\rho_f - \rho_{ma})\ e^{[Pexp]}\ \right]_2 - \left[\ \rho_{ma} + (\rho_f - \rho_{ma})\ e^{[Pexp]}\ \right]_1}{\dfrac{\left[\ \rho_{ma} + (\rho_f - \rho_{ma})\ e^{[Pexp]}\ \right]_2 + \left[\ \rho_{ma} + (\rho_f - \rho_{ma})\ e^{[Pexp]}\ \right]_1}{2}}$$

(8)

and:

(9)

$$R_s(0) = \frac{\Delta V_{s\text{-seis}}}{V_{Save\text{-seis}}} + \frac{\left[\ \rho_{ma} + (\rho_f - \rho_{ma})\ e^{[Pexp]}\ \right]_2 - \left[\ \rho_{ma} + (\rho_f - \rho_{ma})\ e^{[Pexp]}\ \right]_1}{\dfrac{\left[\ \rho_{ma} + (\rho_f - \rho_{ma})\ e^{[Pexp]}\ \right]_2 + \left[\ \rho_{ma} + (\rho_f - \rho_{ma})\ e^{[Pexp]}\ \right]_1}{2}}$$

Note: we have indetermination for τapp : this avoids the indetermination but neglects the **v** sensitivity.

The partial Reflectivity can be transformed in full electro reflectivity, by considering the slowness which is the inverse of velocity:

PARTIAL REFLECTIVITY EQUATION – DEVELOPMENT OF THE VELOCITY ELECTRO VARIANT

Note the presence of τapp that has to be determined with local measurements.

$$V_{Pe} = \frac{\dfrac{1}{\left[\tau_{ma} + (\tau_f - \tau_{ma})\, e^{[Pexp]}\right]_2} + \dfrac{1}{\left[\tau_{ma} + (\tau_f - \tau_{ma})\, e^{[Pexp]}\right]_1}}{2} \quad \mathbf{(10)}$$

$$\Delta V_{Pe} = \frac{1}{\left[\tau_{ma} + (\tau_f - \tau_{ma})\, e^{[Pexp]}\right]_2} - \frac{1}{\left[\tau_{ma} + (\tau_f - \tau_{ma})\, e^{[Pexp]}\right]_1} \quad \mathbf{(11)}$$

$$V_{Se} = \frac{\dfrac{1}{\left[\tau_{Sma} + (\tau_{Sf\text{-}app} - \tau_{Sma})\, e^{[Pexp]}\right]_2} + \dfrac{1}{\left[\tau_{Sma} + (\tau_{Sf\text{-}app} - \tau_{Sma})\, e^{[Pexp]}\right]_1}}{2} \quad \mathbf{(12)}$$

$$\Delta V_{Se} = \frac{1}{\left[\tau_{Sma} + (\tau_{Sf\text{-}app} - \tau_{Sma})\, e^{[Pexp]}\right]_2} - \frac{1}{\left[\tau_{Sma} + (\tau_{Sf\text{-}app} - \tau_{Sma})\, e^{[Pexp]}\right]_1} \quad \mathbf{(13)}$$

TOTAL ZERO OFFSET ELECTRO-REFLECTIVITY EQUATION

By substituting on the zero-offset reflectivity equation below only the electro-density, we get the partial reflectivity equation electro-density variant .

By substituting only the electro-velocity, we get the partial reflectivity equation electro– velocity variant .

By substituting the respective values of ΔV_{Pe} **,** V_{Pe} , $\Delta\rho_e$, ρ_e and the same for S waves in the P and S reflectivity equation below we can calculate the total zero offset electro-reflectivity.

$$R_{Pe}(0) = \frac{1}{2}\left(\frac{\Delta V_P}{V_P} + \frac{\Delta\rho_e}{\rho_e}\right)$$

$$R_{Se}(0) = \frac{1}{2}\left(\frac{\Delta V_S}{V_S} + \frac{\Delta\rho_e}{\rho_e}\right)$$

ELECTRO-ELASTIC ATTRIBUTES APPLIED TO THE TRIPLE POROSITY MODEL OF ROBERTO AGUILERA

$$m = \frac{-\log\left[\phi_{nc} + \dfrac{(1-\phi_{nc})^2}{\phi_2 + (1-\phi_2-\phi_{nc})/\phi_b^{-m_b}}\right]}{\log\phi}$$

Roberto Aguilera defines m in his triple porosity carbonate model as a function of
PHInc = Non connected Porosity relative to bulk volume
PHI2 = Fractures Porosity relative to bulk volume
PHIb = Matrix Porosity relative to matrix system
PHI = Total Porosity
mb = Cementation exponent for intercrystalline Porosity

$$\rho_{be} = \rho_{ma} - (\rho_m - \rho_f)\; 10^{\left\{\dfrac{-\mathrm{Log}\left(\phi_{nc} + \dfrac{(1-\phi_{nc})^2}{\phi_2 + (1-\phi_2-\phi_{nc})\,/\,\phi_b^{-m_b}}\right)}{m}\right\}}$$

Position:

$$\phi_{nc} = \eta\,\phi_b$$

$$\phi_2 = \iota\,\phi_b$$

$$m_b = \lambda\,m$$

(9)
$$\rho_{be} = \rho_{ma} - (\rho_m - \rho_f)\; 10^{\left\{ \frac{-\mathrm{Log}\left(\eta\,\phi_b + \frac{(1-\eta\,\phi_b)^2}{\iota\,\phi_b + (1-\iota\,\phi_b-\eta\,\phi_b)\,/\,\phi_b^{-\lambda m}} \right)}{m} \right\}}$$

$$TPexp = \left\{ \frac{-\mathrm{Log}\left(\eta\,\phi_b + \frac{(1-\eta\,\phi_b)^2}{\iota\,\phi_b + (1-\iota\,\phi_b-\eta\,\phi_b)\,/\,\phi_b^{-\lambda m}} \right)}{m} \right\}$$

$$R_p(0) = (1/2) * \left\{ \left(\frac{ \frac{1}{[\tau_{ma} + (\tau_f - \tau_{ma})\, 10^{TPexp(\eta, \iota, \lambda)}]_2} - \frac{1}{[\tau_{ma} + (\tau_f - \tau_{ma})\, 10^{TPexp(\eta, \iota, \lambda)}]_1} }{ \frac{ \frac{1}{[\tau_{ma} + (\tau_f - \tau_{ma})\, 10^{TPexp(\eta, \iota, \lambda)}]_2} + \frac{1}{[\tau_{ma} + (\tau_f - \tau_{ma})\, 10^{TPexp(\eta, \iota, \lambda)}]_1} }{2} } \right) + \left(\frac{ [\rho_{ma} + (\rho_f - \rho_{ma})\, 10^{TPexp(\eta, \iota, \lambda)}]_2 - [\rho_{ma} + (\rho_f - \rho_{ma})\, 10^{TPexp(\eta, \iota, \lambda)}]_1 }{ \frac{ [\rho_{ma} + (\rho_f - \rho_{ma})\, 10^{TPexp(\eta, \iota, \lambda)}]_2 + [\rho_{ma} + (\rho_f - \rho_{ma})\, 10^{TPexp(\eta, \iota, \lambda)}]_1 }{2} } \right) \right\}$$

Substitute the former algorithms to the basic function for zero-offset reflectivity:

$$R_p(0) = \frac{1}{2}\left(\frac{\Delta V_p}{V_p} + \frac{\Delta \rho}{\rho}\right)$$

APPLICATIONS

The former method (partial reflectivity) was tesetd, by producing a seismic model of the seismic impedance in the prestack inversion domain and a model of attributes variations to show the application of the electro- seimic (Pexp) attributes.

By superimposing the effect of AVO seismic attributes and Poisson ratio change the model was developed with a prestack inversion method to distribute the input of $\mathbf{r_{be}}$ in the $\mathbf{Z_{Pe}}$ algorithm.
A density variation volume in the 3D seismic cube was produced using zero-offset reflectivity attributes and curvature attributes. This showed an increased resolution and delineation of the higher Sw volume (red arrow).
The model shows the sensitivity to the variation in Sw on the electro-impedance.

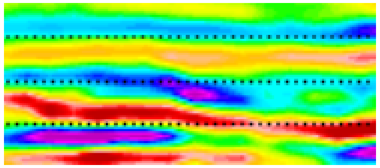

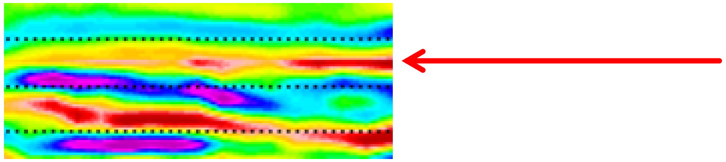

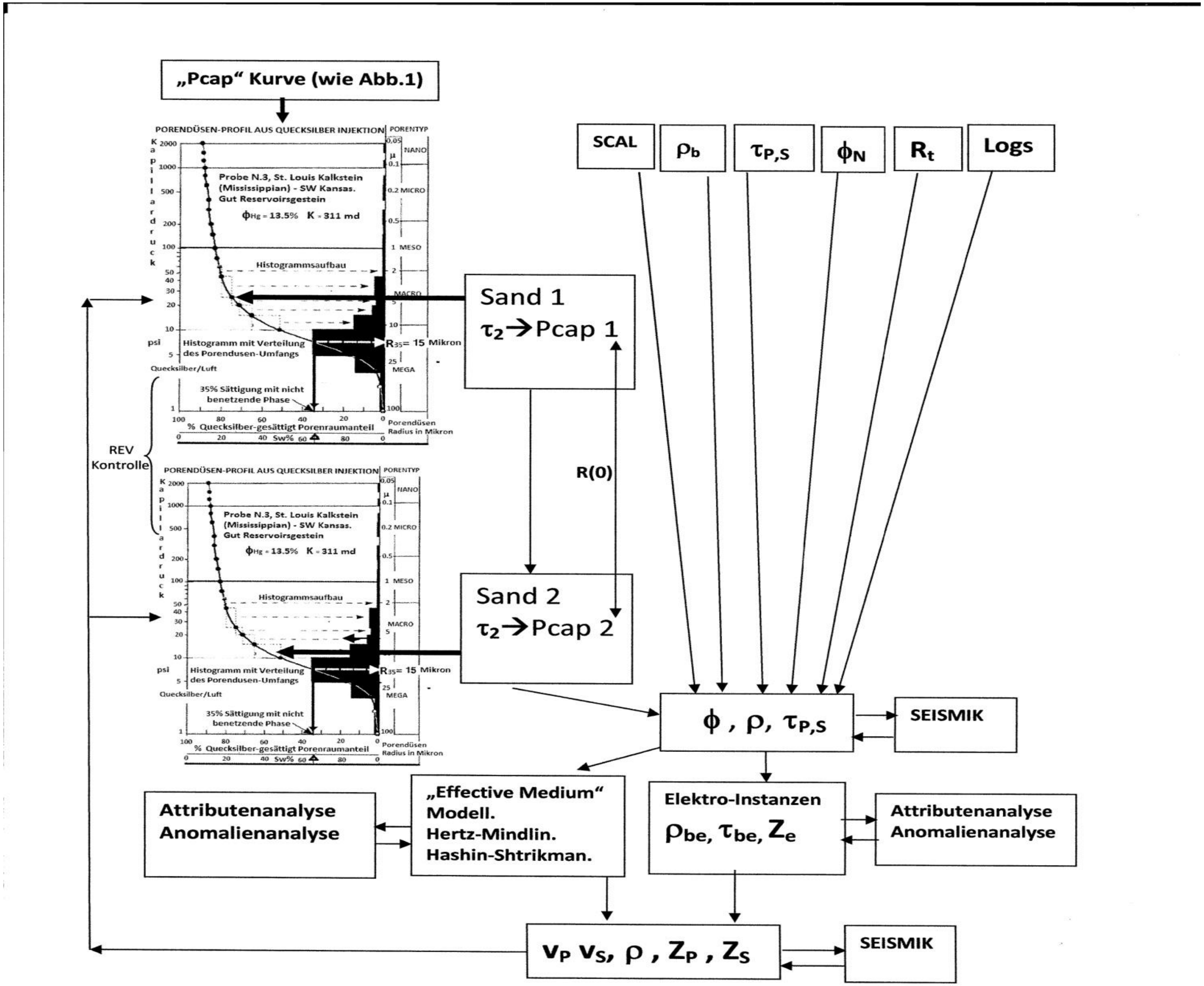
„Pcap“ Kurve (wie Abb.1)
PORENDÜSEN-PROFIL AUS QUECKSILBER INJEKTION
PORENTYP
Kapillardruck
Probe N.3, St. Louis Kalkstein (Mississippian) - SW Kansas. Gut Reservoirsgestein
ϕHg = 13.5% K = 311 md
Histogrammsaufbau
Histogramm mit Verteilung des Porendusen-Umfangs
R35= 15 Mikron
psi
Quecksilber/Luft
35% Sättigung mit nicht benetzende Phase
% Quecksilber-gesättigt Porenraumanteil
Sw%
Porendüsen Radius in Mikron
NANO
MICRO
MESO
MACRO
MEGA
REV
Kontrolle
SCAL
ρb
τP,S
ϕN
Rt
Logs
Sand 1
τ2→Pcap 1
R(0)
Sand 2
τ2→Pcap 2
ϕ , ρ, τP,S
SEISMIK
„Effective Medium“ Modell.
Hertz-Mindlin.
Hashin-Shtrikman.
Attributenanalyse
Anomalienanalyse
Elektro-Instanzen
ρbe, τbe, Ze
Attributenanalyse
Anomalienanalyse
vP vS, ρ , ZP , ZS
SEISMIK

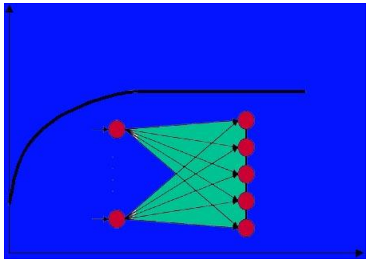

FUTURE PROJECTS FOR RENEWABLE ENERGY

DDS1

DEEP DIRECTIVITY SYSTEMS 1

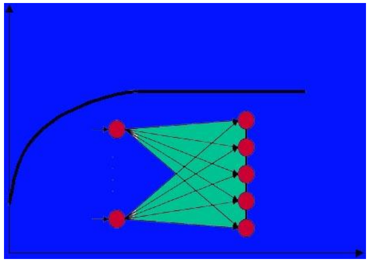

ITALY

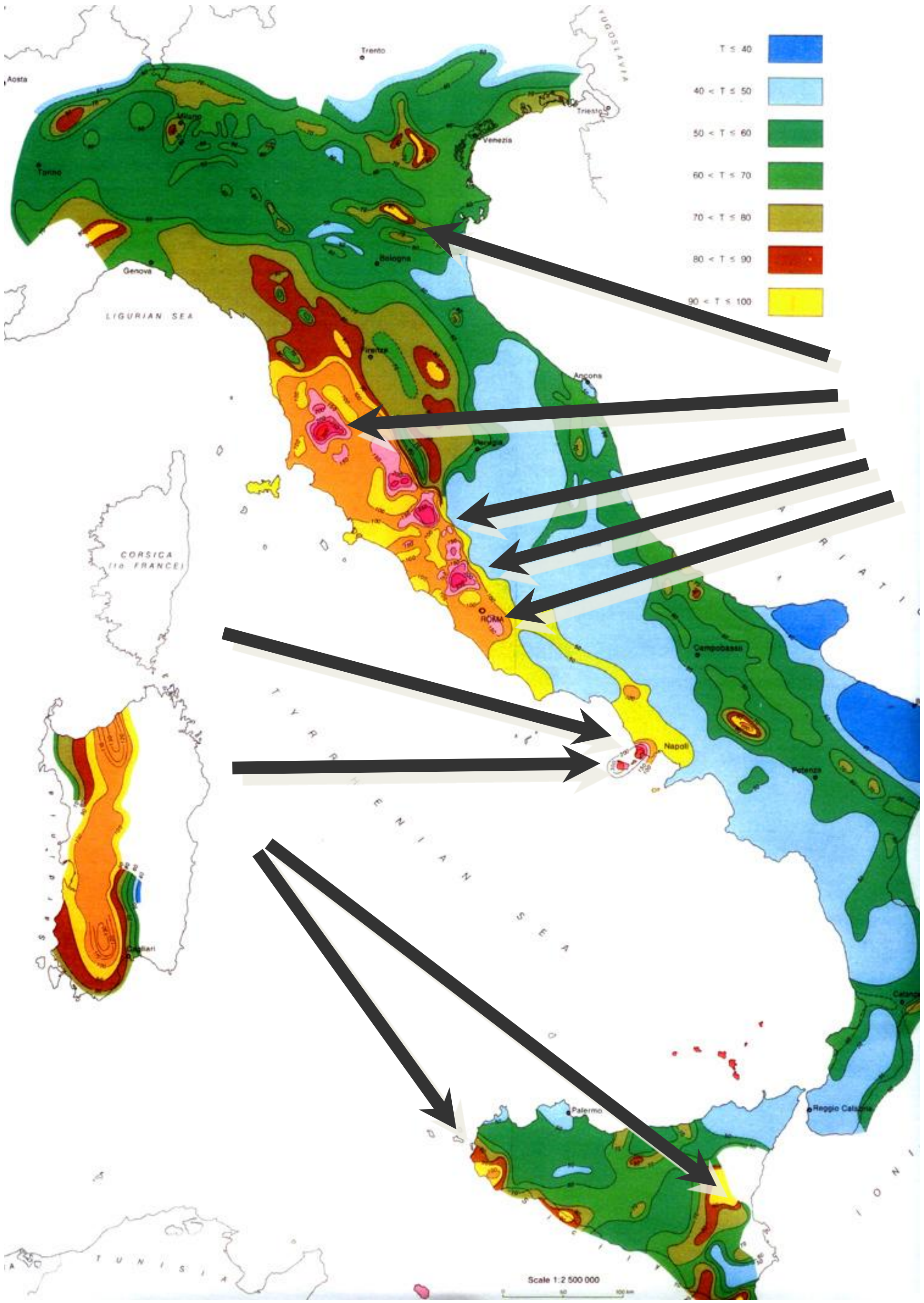

1. Montegrotto

2. Toscana

3. Lazio

4. Monti Albani

5. Napoli

6. Sicilia

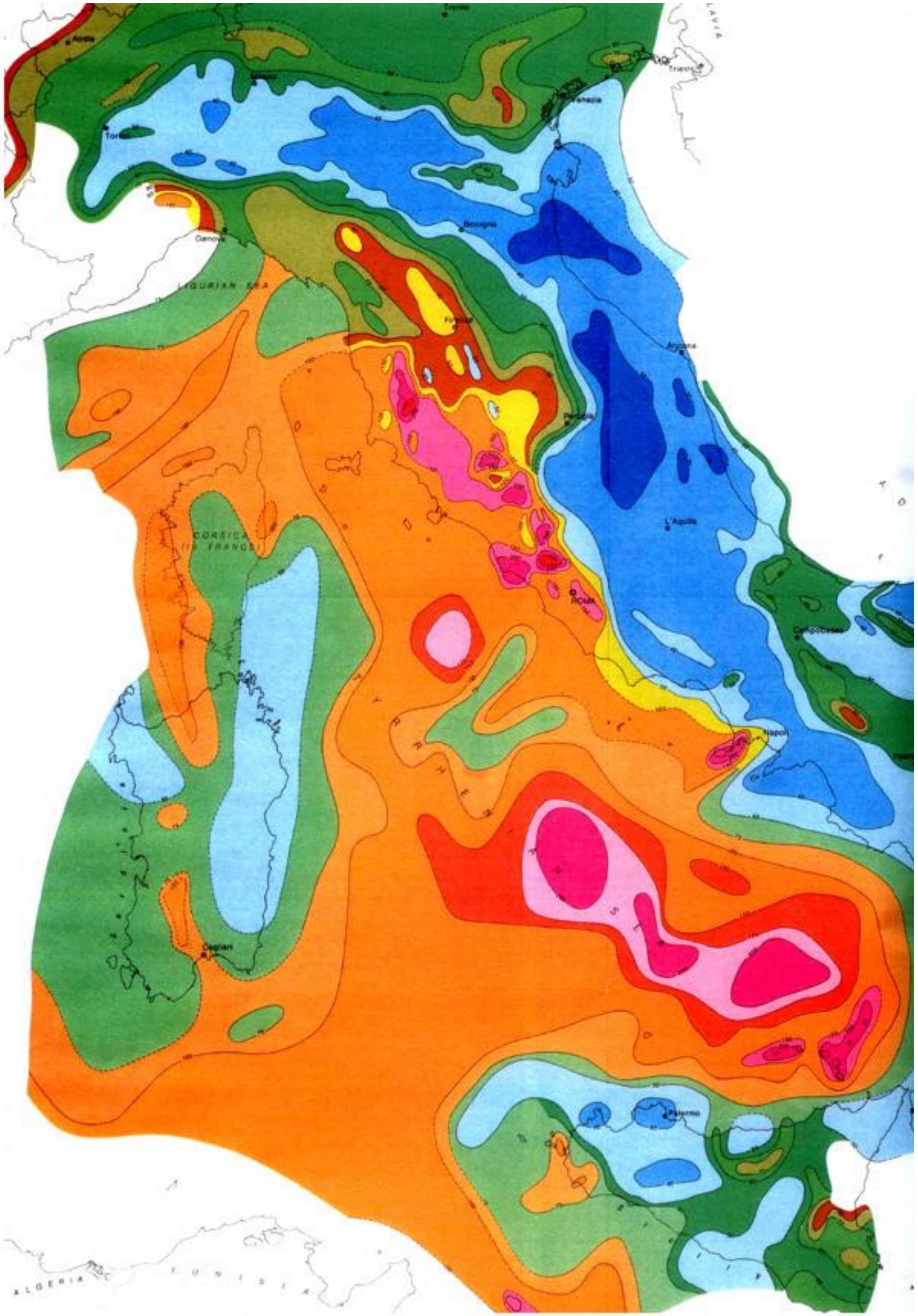

Aosta
Milano
Torino
Trieste
Venezia
Genova
Bologna
LIGURIAN SEA
Firenze
Ancona
Perugia
L'Aquila
CORSICA
(FRANCE)
ROMA
Campobasso
Napoli
Cagliari
Palermo
ALGERIA
TUNISIA

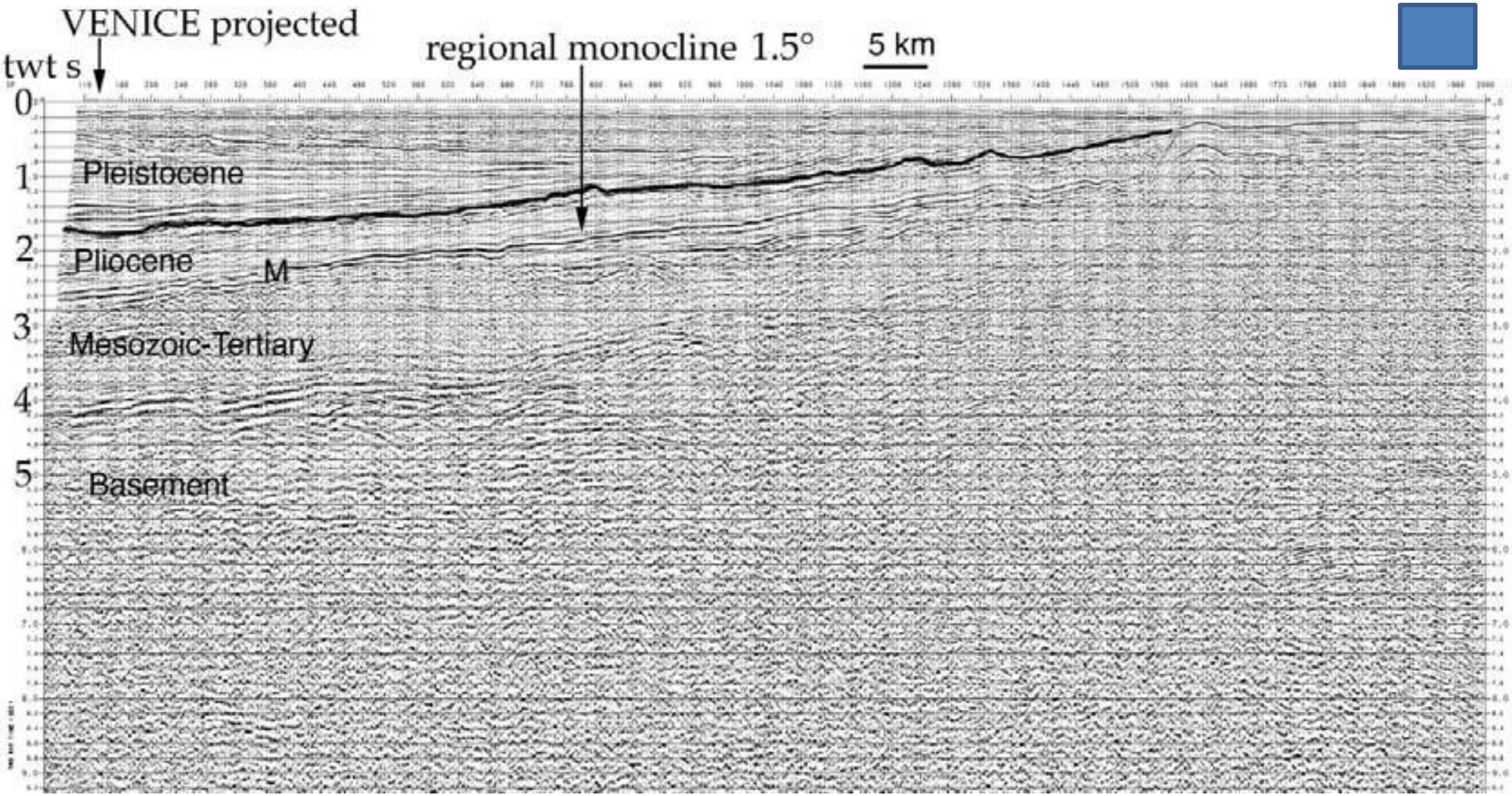
VENICE projected
twt s
regional monocline 1.5°
5 km
0
1
2
3
4
5
Pleistocene
Pliocene
M
Mesozoic-Tertiary
Basement

SEISMIC PROFILE – NS LAGUNA DI VENEZIA

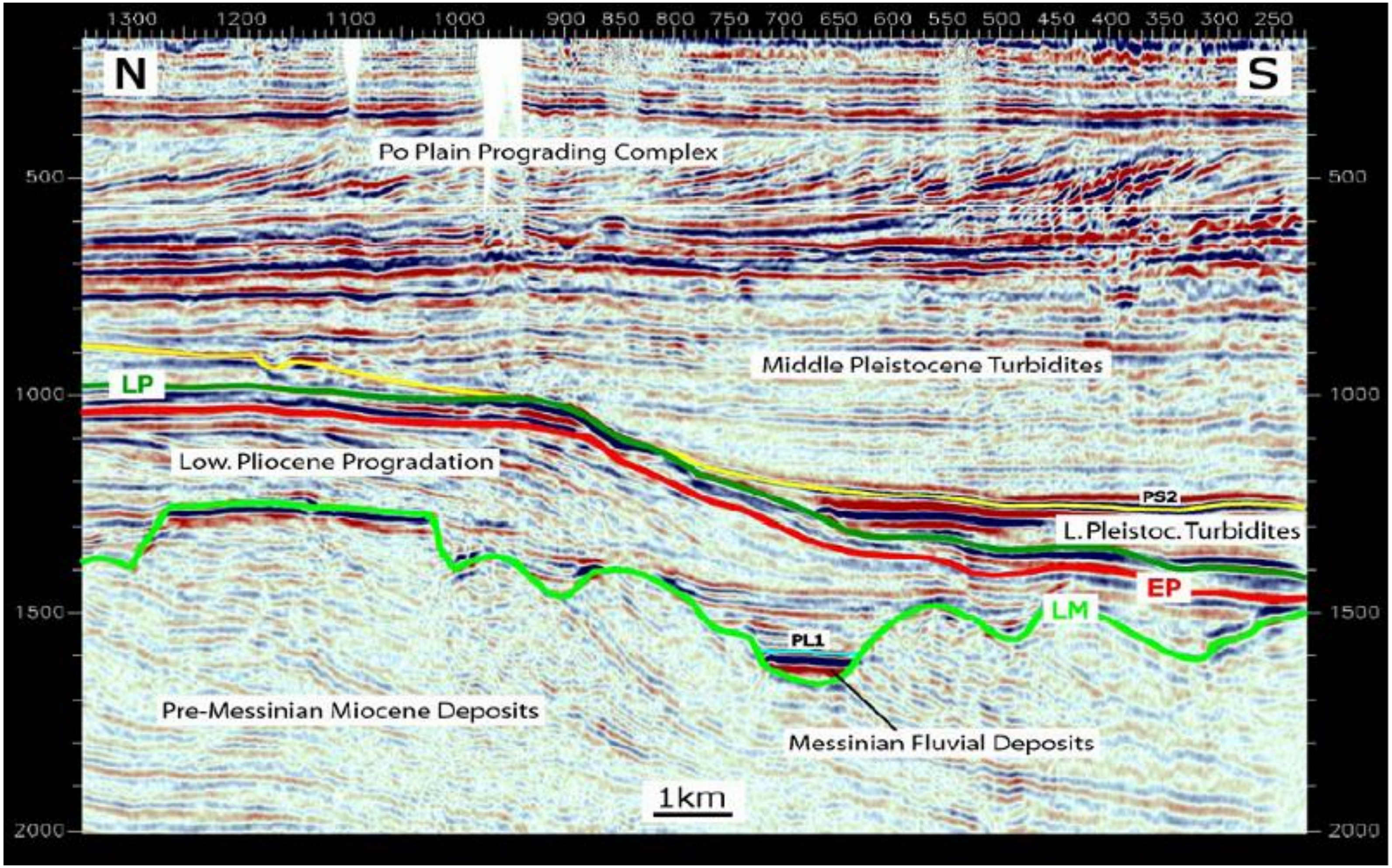

ISOBATS MAP IN FRIULI

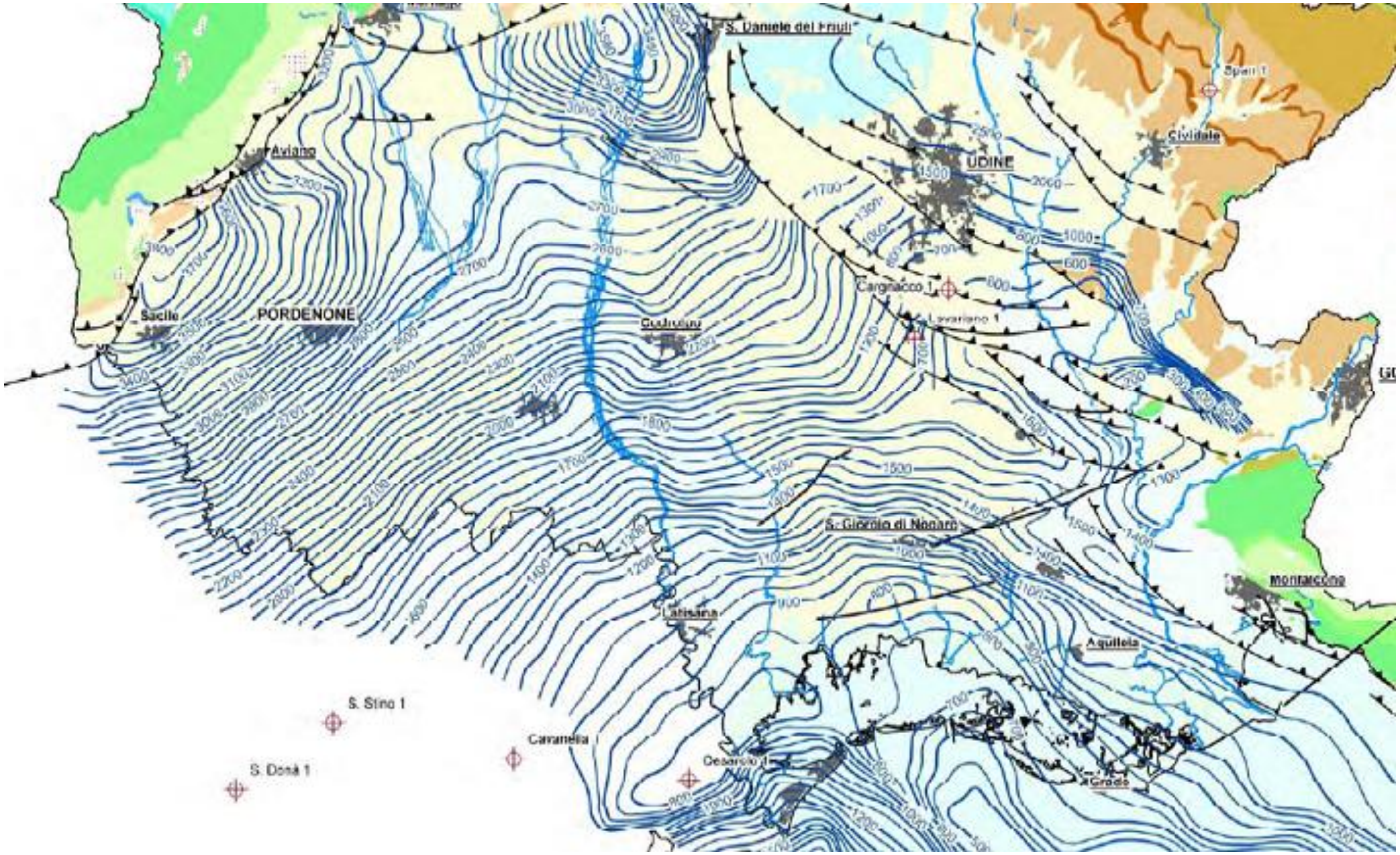

VENETO

1. **Italian Malm**

2. **DDS_1**

DDS_1

A. Possiamo circolare per 100 kilometri

B. 100 litri al secondo a 4000m di profondita´

C. tornare al punto di partenza

D. senza mai tornare in superficie

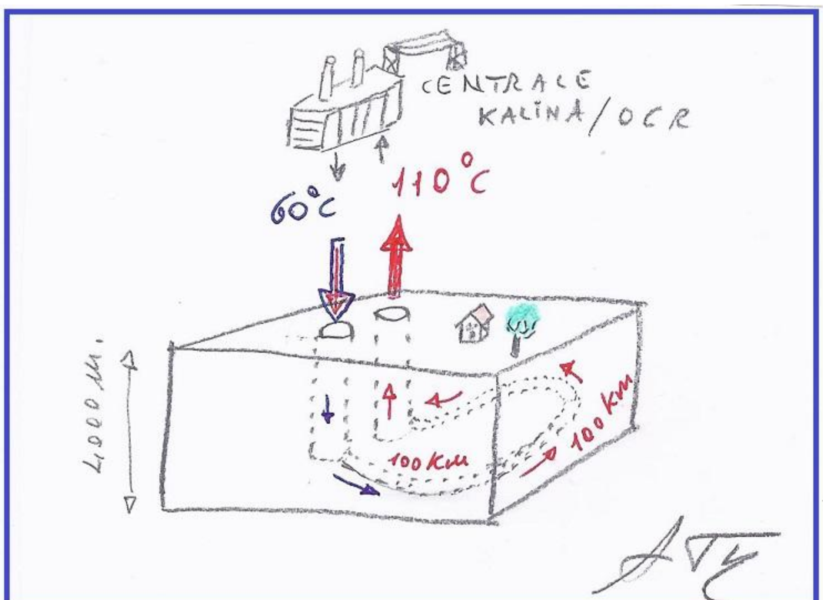

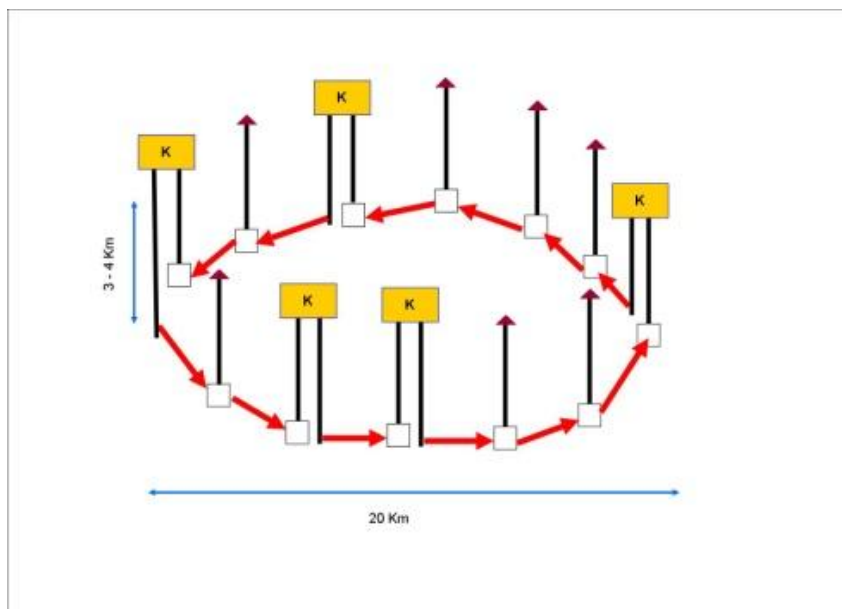

DDS1 PROJECTS DO NOT USE HYDRAULIC FRACTURING

BUT IF NECESSARY:

OBSERVATION ON THE USE OF FRAC-OPERATIONS TO CREATE THE FLOW-LINES FOR GEOTHERMAL HDR PROJECTS

-The risk to encounter unwanted heterogeneity influencing the Frac propagation increases with the distance

-The Frac Efficiency decreases with the distance (Tip effect decreasing and "Pipe-Viscosity" effect increases)

- The danger of vertical propagation and scree-out increases with distance

DDS uses Sync-Frac to avoid all these problems

DDS: A COMBINATION OF PRAGMATIC TECHNOLOGIES

DDS Methods are the result of the association of 4 optimized technologies:

1. CT DRILLING → **Horizontal Geosteering**
2. MULTILATERAL WELL TECHNOLOGY
2. OPTIM LUNG-CONNECT OPERATIONS → **TimeSync**
3. OPTIM THERMAL EFFICIENCY → **Pivot well**

CT - COILED TUBING DRILLING

→ Continuously improved technology
→ RPM up to 500 m/day
→ DOGLEG SEVERITY → High build up rate of up to 75 degree/100’

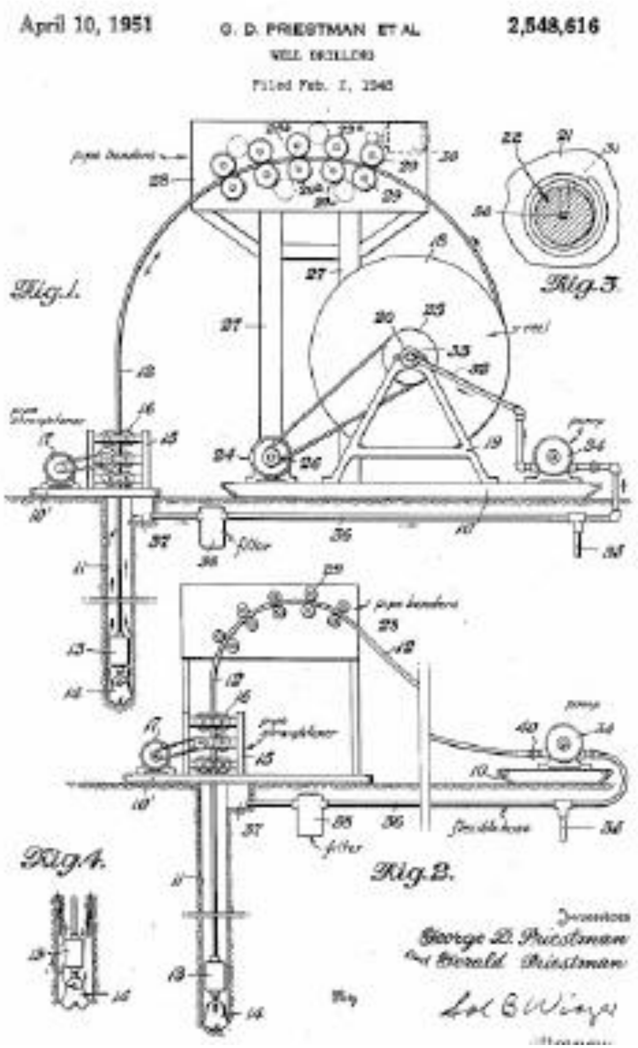

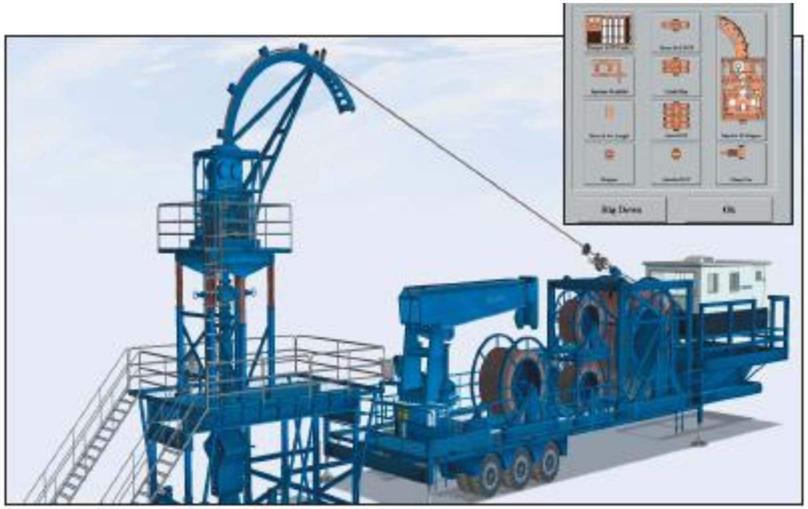

→ SIDETRACK

→ MULTILATERAL WELL TECHNOLOGY

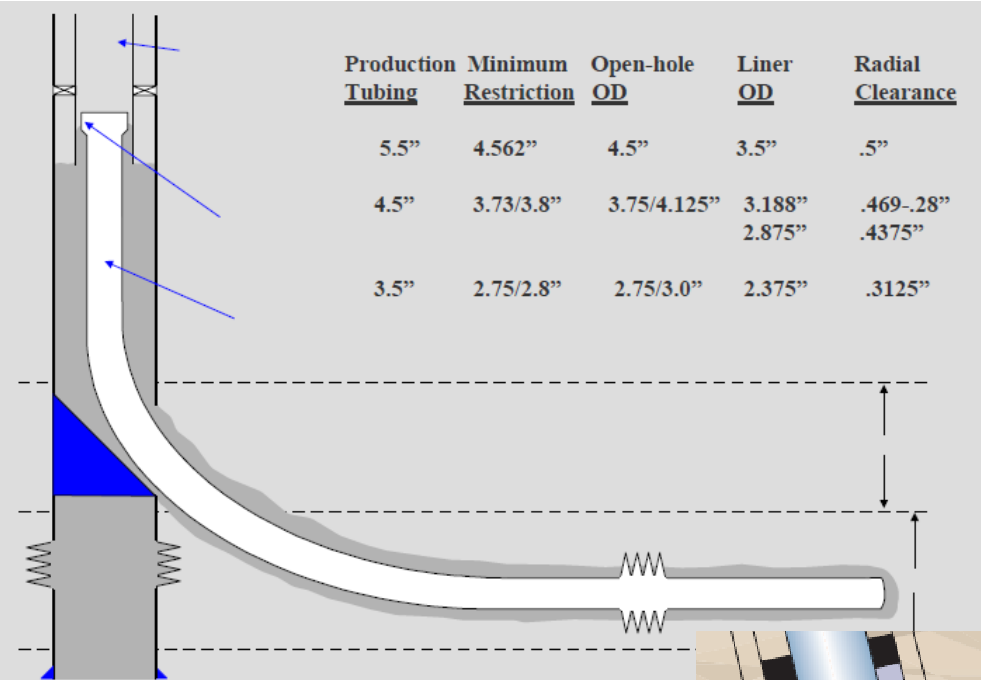

Production Tubing	Minimum Restriction	Open-hole OD	Liner OD	Radial Clearance
5.5”	4.562”	4.5”	3.5”	.5”
4.5”	3.73/3.8”	3.75/4.125”	3.188” 2.875”	.469-.28” .4375”
3.5”	2.75/2.8”	2.75/3.0”	2.375”	.3125”

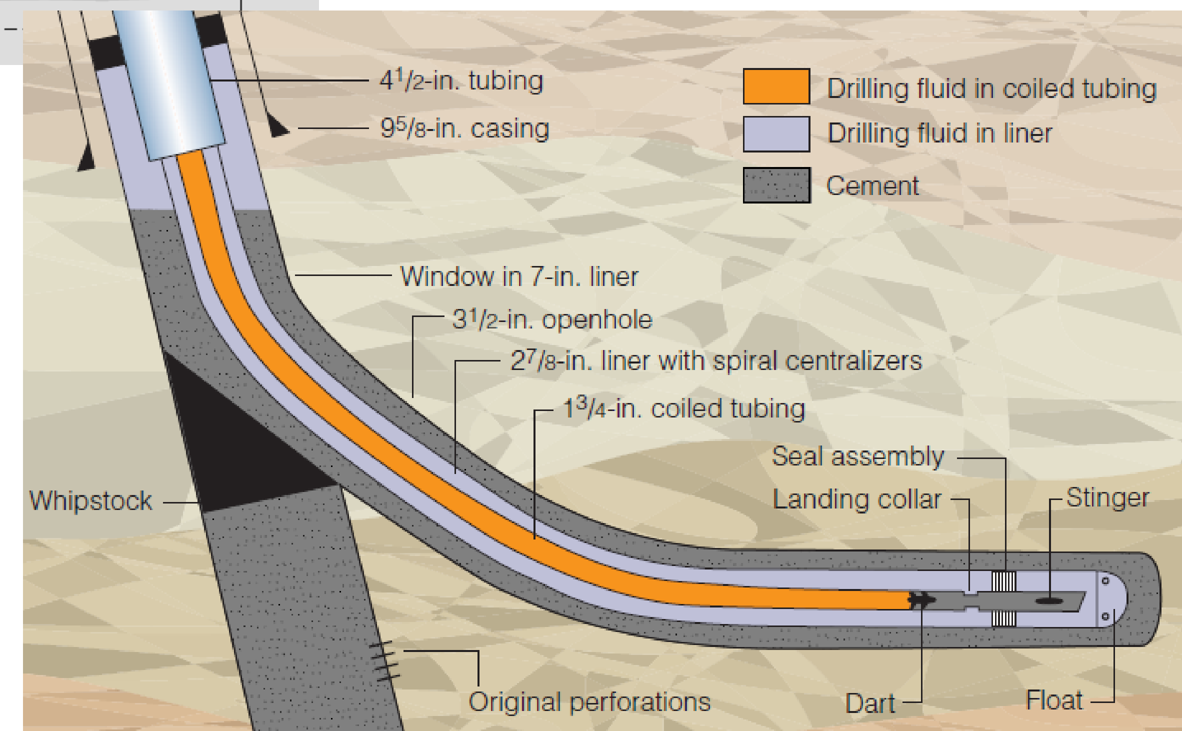

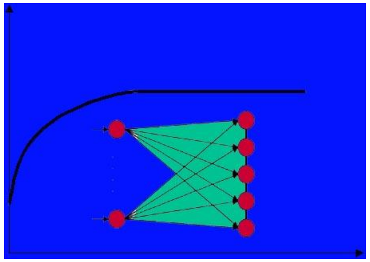

THE FEEDBACK LOOP CONCEPT

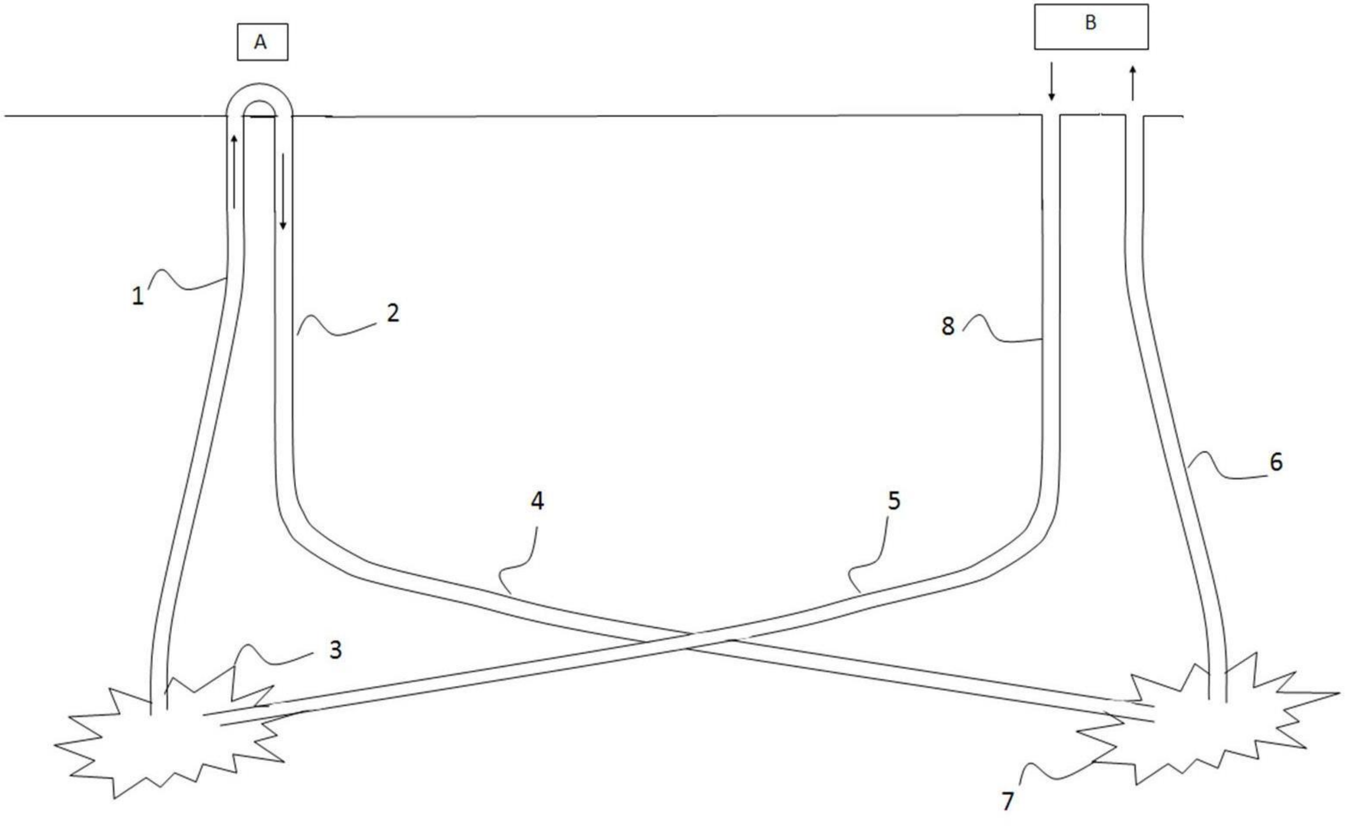

FIG. 3B

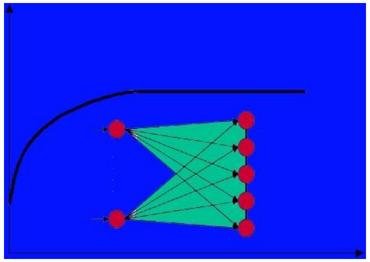

PIVOTING UNITS CONCEPT

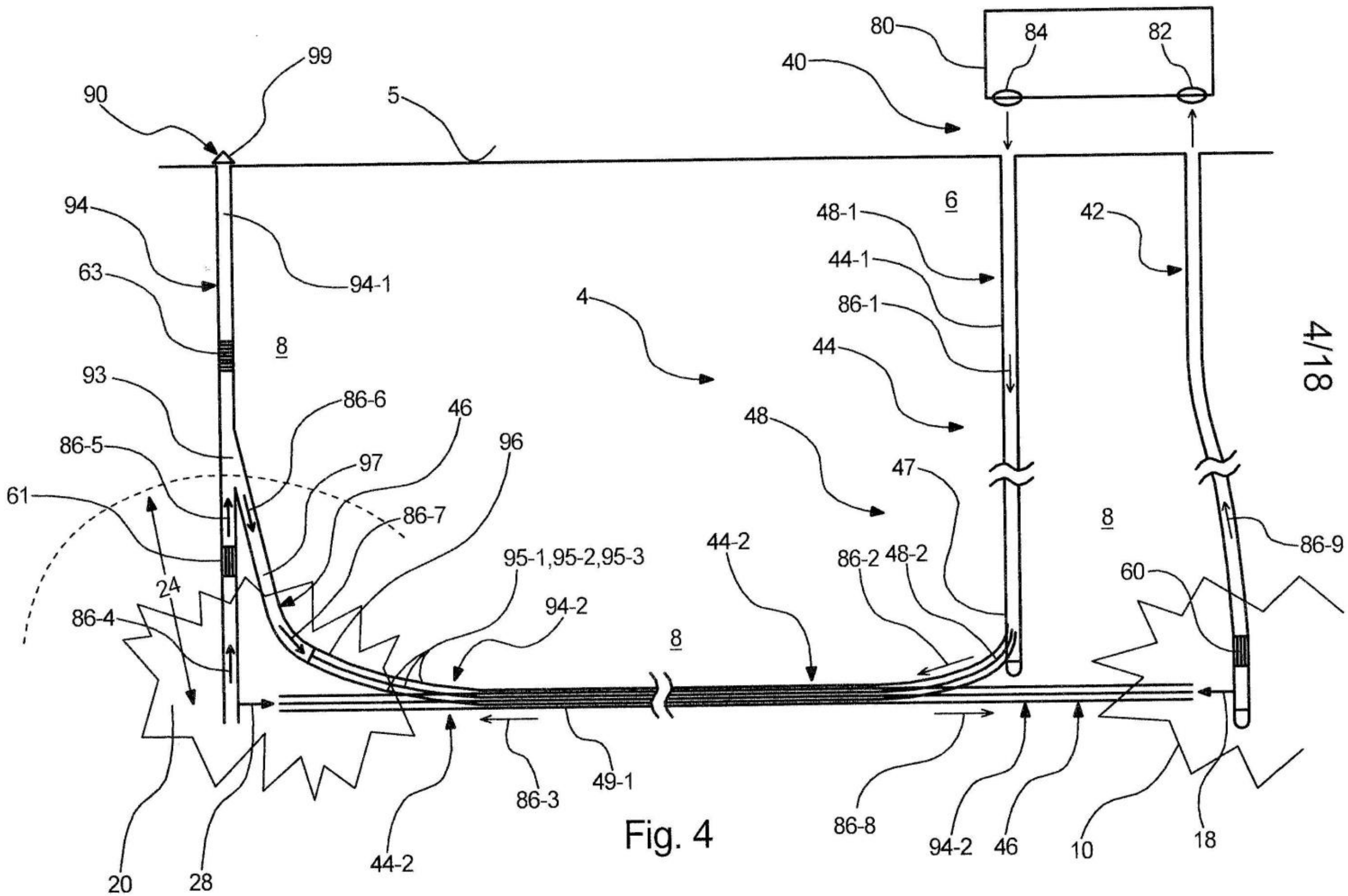

Fig. 4

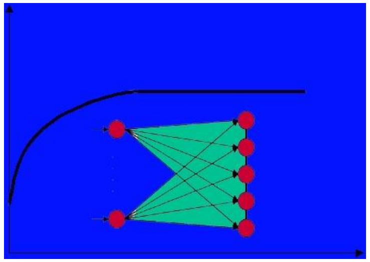

PIVOTING UNITS CONCEPT

1 Pivoting Unit = 3 Mwatt; 3 Pivoting Units = 9 MWatt
Enhanced Reservoir efficiency = 14 MWatt

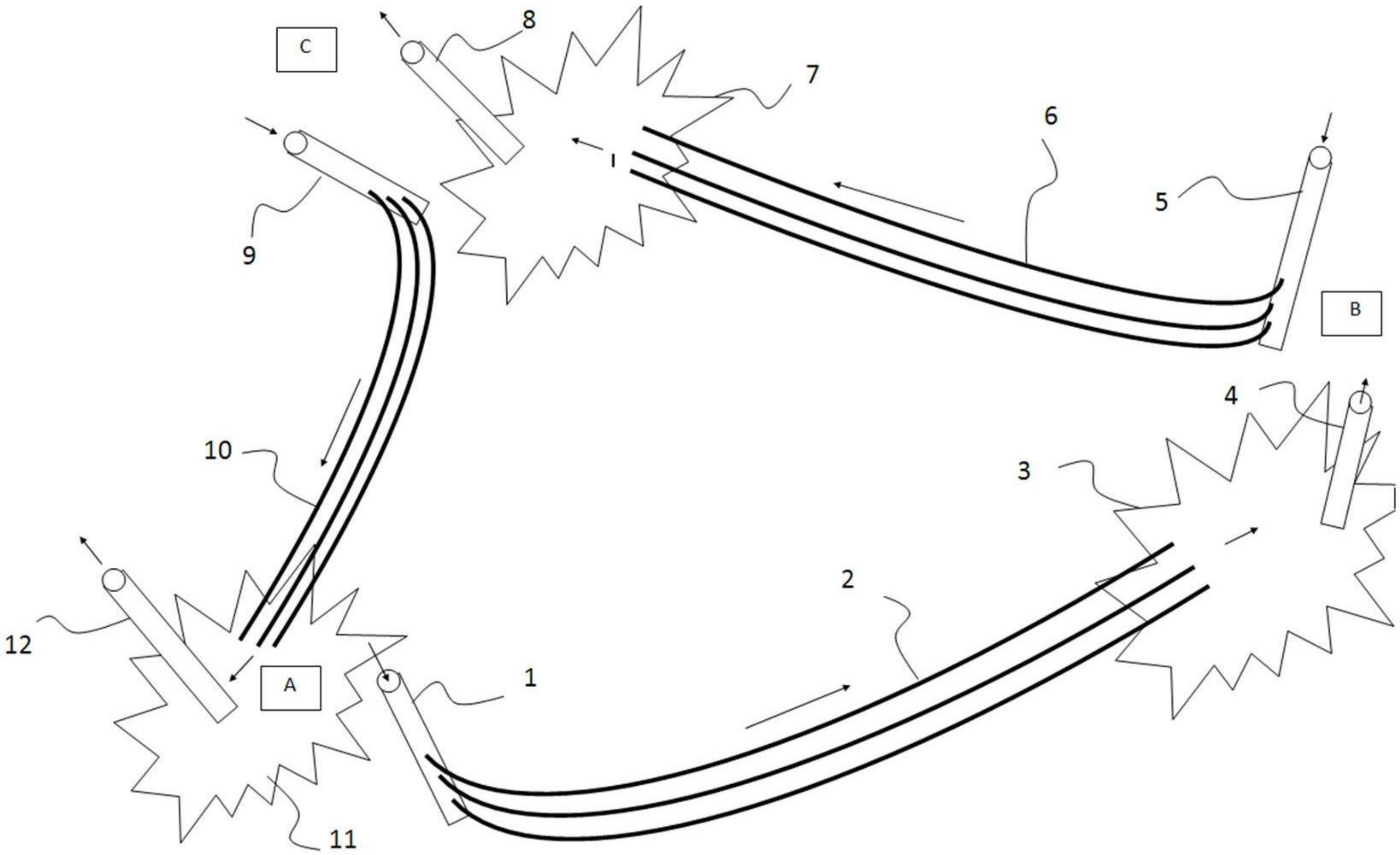

FIG. 3H

DDS

PARALLEL SYSTEMS

1 UNIT

Standard Flow-Rate: 200-400 Liters/Second

@120° C → 24 MWatt Electric Power

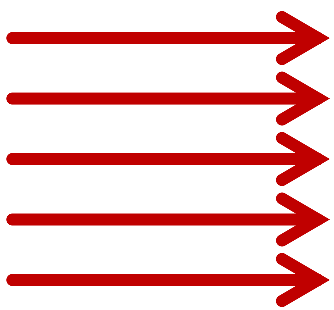

SERIAL SYSTEMS

12 UNITS

Standatd Flow-Rate: 100-150 Liters/Second

@ 120° C → 8 MWatt Electric Power

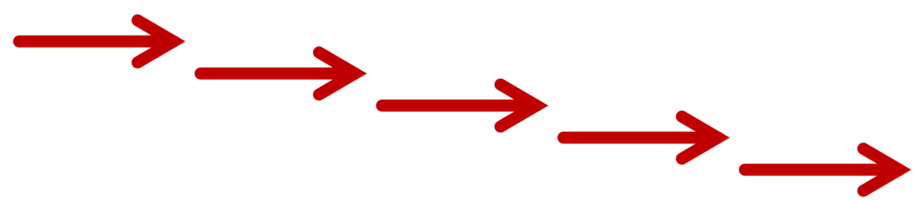

1 UNIT → 30 - 40 Km Flowlines

EXAMPLE OF A DDS INTERCITY SYSTEM THAT CAN SUPPLY 12 SMALL TOWNS WITH 80 MWatt POWER OR CAN BE REALIZED ALONG 2 HIGHWAYS FOR ELECTRIC CARS SUPPLY

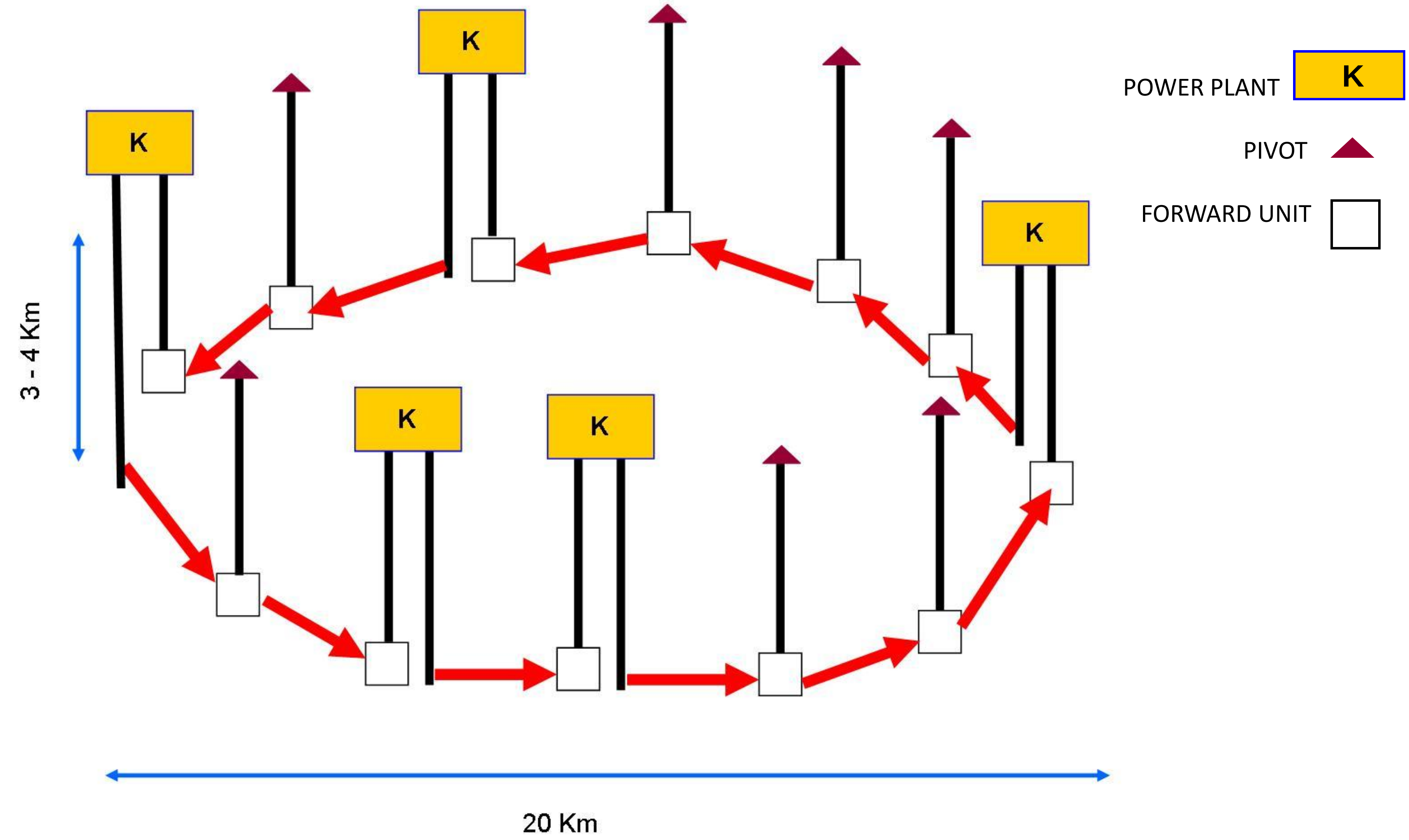

DDS

DDS (Deep Directivity Systems) is a new technology, the key for the future of the renewable energy.
A method for the universal development of geothermal projects not only in high geothermal gradient and favourable areas but in every part of the world.
With DDS the door to the future of the clean renewable energies is open.
Petrophysic-Consultants develops and supervises the operative phase of DDS projects.
www.Petrophysic-Consultants.com

Advantages of the DDS technology :

1. DDS is a standard method and a final turnkey product.
2. DDS is a final product and standard for every kind of formation.
3. DDS can be applied to old oil wells in depleted reservoirs to develop a geothermal project, saving drilling costs, adding value to old projects.
4. DDS can be applied to reactivate failed geothermal projects using the old wells and saving the drilling costs to produce a new successful geothermal project.
5. DDS can be theoretically planned for the desired efficiency and electrical power There is no theoretical limit to the maximal efficiency and output of the method.
6. DDS can be planned to for a working cycles of 10, 100, or more years. There is no theoretical limit for the efficiency and life time of a project.
7. DDS is ideal for the joint development in a cooperation between 2 , 3 or more bordering towns.
8. DDS can be applied in every formation except the exceptional presence of evaporites and karst carbonate.
9. DDS can be applied in every region of the world.
10. DDS can be expecially applied in volcanic areas defining the target and well path within a safety area from the volcanic system, reaching the maximum efficiency in the power production.
11. DDS can be both used for power production or for hot water/heathing systems.
12. DDS ensure the maximal efficiency compared with the other geothermal classical systems.
13. DDS ensure the minimum risk compared with other geothermal methods.

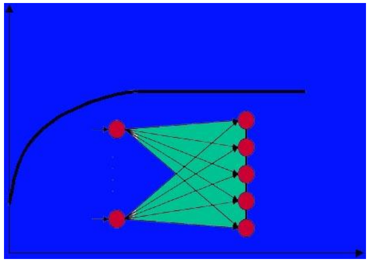

DDS

FUNDAMENTAL CONCEPT

Using these technologies, according to DDS concepts, it becomes possible to circulate water within predefined flow lines, in continuous flow and in a closed system, for more than 100 kilometers, while keeping most of or all the flow line system below a predefined depth.
This depth could be, for example 3000 m and more, so that the water flow is for most of the flow path length in a formation, the temperature of which is above 110 degrees Celsius, which is an ideal minimum temperature level enabling the production of electrical power.

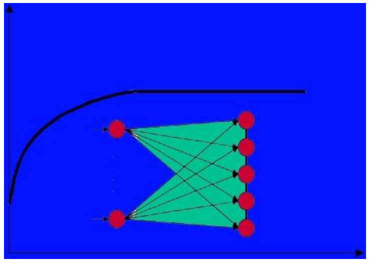

GeoNeurale / Wavefields new research fields

FWI

NN Algorithms Stochastic Seismic Inversion

Variographic analysis for log interpretation with Ecole Superiere des Mines Fontainebleau

MICRO/MACROSYSTEMS INTEGRATION

LINKS

TRAINING CENTER: www.GeoNeurale.com

INTERPRETATION, INVERSION,PROCESSING
OPERATIVE PROJECTS: www.Wavefields.eu

A Special Thanks to:

Luigi Beghi, Professor of Applied Mathematics at the University of Padova

For teaching basic concepts of Signal Analysis and Programming language at the early days when operating system was just a first MS DOS version

Robert Garotta, CGG Senior Vicepresident of Geophysical Methods

For the theory and philosophy of 3D Seismic Multicomponent

Gene Ballay, Senior Petrophysicist at Shell and Saudi Aramco

For the theory and philosophy of Carbonate Petrophysics

GeoNeurale

Am Nymphenbad 8
81245 München
T 089 8969 1118
F 089 8969 1117

www.GeoNeurale.com
www.Wavefields.eu